La Rivista del Nuovo Cimento
https://doi.org/10.1007/s40766-023-00045-6

REVIEW PAPER

Imperfections in natural diamond: the key to understanding diamond genesis and the mantle

Maxwell C. Day[1] · Martha G. Pamato[1] · Davide Novella[1] · Fabrizio Nestola[1]

Received: 1 June 2023 / Accepted: 17 July 2023

Abstract
Diamond has unique physical, thermal, electrical, and optical properties with respect to other minerals and related synthetic compounds that make it extremely valuable from an economic and industrial perspective. Natural diamond that forms in the upper mantle, transition zone, and lower mantle may encapsulate mantle minerals during growth and protect them from physical breakdown and chemical alteration upon ascent of the diamond to the surface via kimberlite eruption. Such mineral inclusions serve as the only direct means to study the deep Earth and provide critical information about the pressure, temperature, and redox conditions and the chemical and isotopic composition of the mantle. Natural diamonds show a wide range of ages and thus allow one to reconstruct the history of large-scale Earth processes, such as the formation and amalgamation of Earth's lithosphere, the onset and evolution of tectonic processes (e.g., Wilson cycles), and the recycling of C, H, and N between different primordial and crustal reservoirs. In this review, a detailed description of all types of imperfections (e.g., mineral and fluid inclusions and structural defects) and the methods by which such imperfections can be analyzed to elucidate aspects of Earth's complex geologic history is given.

Keywords Diamonds · Carbon · Mineral inclusions · Crystallographic defects · Nitrogen-vacancy defects · Carbon (re)cycling · Mantle geodynamics

1 Introduction

Diamond is a naturally occurring allotrope of carbon. Several unique physical, thermal, optical, and electrical properties arise from the cubic crystal structure of diamond consisting of covalently bonded carbon (C) atoms in tetrahedral coordination. Perhaps of most notoriety is the extreme hardness of diamond making it the ideal choice for

✉ Maxwell C. Day
maxwell.day@unipd.it

[1] Department of Geosciences, University of Padua, Via Giovanni Gradenigo, 6, 35131 Padua, PD, Italy

cutting and polishing applications and the ultra-wide band gap of diamond, a property required for use as semi- and superconductors. Over the last several decades, diamonds have received considerable attention in many scientific fields, such as theoretical and applied physics, quantum technologies, engineering, electronics, medicine, and materials science [1]. Consequently, many advances have been made in the synthesis of diamond, particularly via chemical-vapor deposition (CVD) and high-pressure high-temperature (HPHT) methods ([2] and references therein).

Natural diamonds form in a variety of geologic settings (Sect. 1.2); however, the majority of mined diamonds form in the deep Earth, in the lithospheric and sub-lithospheric mantle at depths of 120–800 km [3–7]. In these environments, diamonds precipitate due to reduction or oxidation or C-species (e.g., CO_2 and CH_4) in fluids and melts upon metasomatic (redox) reaction of such fluids with mantle rocks, such as meta-peridotites. After formation, diamonds may reside in the mantle for billions of years, during which they may undergo continued growth or dissolution depending on the type of fluids and the degree of pressure (P), temperature (T), and oxygen fugacity (f_{O2}) fluctuations they are subject to. An exceedingly small proportion of diamonds are eventually transported to the surface in melts via deep-seated volcanic systems called kimberlite pipes.

Crystallographically perfect and chemically pure diamond contains minimal information about the conditions and environments in which it formed. Fortunately, most natural diamonds contain different types of *imperfections* that record aspects of the complex history of diamond formation, growth, residence in the mantle, and transport to the surface. Imperfections such as crystallographic point-defects associated with nitrogen (N), hydrogen (H), and boron (B) impurities provide information about the residence temperature/time of diamond. The most informative imperfections are mineral and fluid inclusions which allow direct observation of the geochemical and mineralogical properties of the otherwise inaccessible deep Earth. Other mantle derivatives such as xenoliths or xenocrysts are susceptible to alteration and mechanical breakdown during transport to the surface. In contrast, diamond is chemically inert and physically robust providing the ideal time capsule to preserve inclusions and fluids associated with diamond formation in the mantle underlying different geographic regions (diamond are observed in six continents) over a wide range of geologic time.

The hierarchical organization of this review is shown in Fig. 1 where the topic of each chapter (1–5) is related to the following and preceding chapter by arrows. In Chapter 1, a brief introduction of the structure and composition of the mantle gleaned from diamond research is given in addition to an overview of the geologic setting of diamond formation. In Chapter 2, the economic and scientific value of diamond is explained based on its physical, thermal, optical, and electrical properties. Moreover, the nomenclature and classification schemes used in the geological study of diamonds are given based on properties, including textures, morphology, crystallinity, N-aggregation state, host (or parental) rock types, inclusion mineralogy, and geologic settings of formation. In Chapter 3, imperfections observed in natural diamond are discussed and divided into three groups:

(1) Intrinsic imperfections (e.g., edge dislocations due to plastic deformation).
(2) Extrinsic imperfections (e.g., N-, H- and B-related defects).

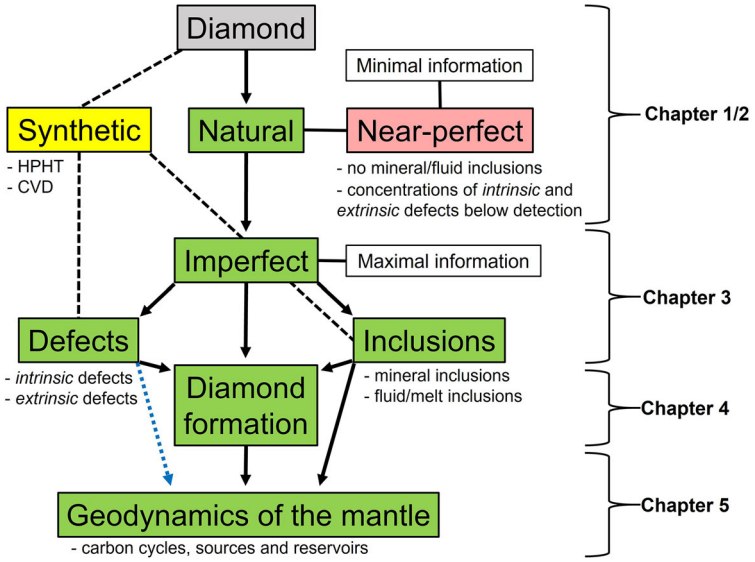

Fig. 1 Hierarchical organization of this review where arrows connecting green boxes indicate progression from one chapter to the next. Dashed black lines indicate studies that are not discussed (or discussed only briefly) in this review. Dashed blue arrow indicates an area of diamond research that has received relatively less attention, relating the structure and composition of defects (other than mineral and fluid inclusions) to diamond genesis and the geodynamics of carbon in the mantle

(3) Imperfections related to mineral, fluid, and melt inclusions.

In Chapter 4, different models for lithospheric and sub-lithospheric diamond formation at varying conditions (P, T, and f_{O2}) in the mantle are discussed using data from primarily (3). In Chapter 5, the imperfections observed in natural diamond, primarily mineral and fluid inclusions and isotopic data of C and N, are related to large-scale, deep Earth processes, such as (1) ancient and modern carbon (re)cycling in the mantle and its relation to the onset and evolution of different styles of plate tectonics in the Archean and Proterozoic, (2) evolution of recycled carbon reservoirs and associated C-bearing, diamond-forming fluids sources in the mantle through geologic time, and (3) mobilization and transport of diamond and associated fluids in the mantle, and the C-speciation for different types of diamond-forming fluids and melts.

The primary focus of this review is to relate the properties of imperfections in diamond to the structural and compositional evolution of the mantle through geologic time. For the purposes of brevity, we direct our review to monocrystalline, lithospheric, and sub-lithospheric diamonds. However, experimental data from other types of diamonds (e.g., fibrous and synthetic diamonds) are invoked where useful. Although there are numerous reviews on imperfections in diamond, particularly inclusions, and their relation to mantle geodynamics, few evaluate all types of imperfections. A notable exception is the recent *Review in Geochemistry and Mineralogy, ed. 88, Diamonds: Genesis, Mineralogy and Geochemistry* [8], much of which is reviewed in this paper.

1.1 Structure and composition of the mantle: insights from diamond

Since the work of Richard Dixon Oldham and Andrija Mohorovičić in the early twentieth century (e.g., [9, 10].), who provided evidence for the existence of a crust (with thickness of 6–70 km), mantle (down to 2900 km), and core (2900–6371 km), geophysical methods have remained the principal tool for investigating the structure of the Earth. Such methods rely on the behaviour of seismic waves as they propagate through mediums of different density but are inherently *indirect* as data (e.g., mineralogical composition of the mantle) can only be inferred rather than directly measured or observed. *Direct* methods involve the study of xenoliths or xenocrysts, rock fragments, or crystals from the upper mantle that have been transported to the surface by volcanism (kimberlites or lamproites) and/or tectonic exhumation. Xenoliths are predominately from the upper mantle and of peridotitic or eclogitic paragenesis containing mostly olivine, clinopyroxene, orthopyroxene, and garnet [11–14]. Thus far, mantle xenoliths from depths down to ~ 300 km have been described (e.g., [15–17]) but not from depths representative of the lower mantle. Furthermore, chemical alteration (e.g., recrystallization and isotopic re-equilibration) of xenoliths and xenocrysts due to interaction with volatile-rich fluids or melts associated with the kimberlitic system is common [12, 18–21]. Thus, caution must be used when making geochemical, petrogenetic, or geochronological inferences about mantle xenoliths.

Fortunately, one type of xenocryst, diamond, is particularly resistant to chemical and physical alteration and can preserve its chemical and isotopic composition and protect mineral and fluid inclusions that it may contain. Diamonds form in mantle environments at depths of 120–800 km [3, 5–7], have ages of ~ 69 Mya [22] to ~ 3.3–3.5 Ga [23–25], and have a large geographic distribution [26] which is continually expanding due to mining and exploration efforts. For these reasons, diamonds are the best window through which geologists can *directly* sample the deep Earth through geologic time. Thus far, the study of natural diamond and its inclusions has provided critical information about:

(1) The onset of Wilson cycles (plate tectonics) and processes related to subduction, continental collision, assembly, and crustal growth (e.g., [27–37]). For example, evolution of the Mesoarchean lithosphere by large-scale, sub-lithospheric magmatism (e.g., [38]).
(2) Mantle heterogeneity with respect to the pressure, temperature, redox conditions, and compositions of diamond-host lithologies (substrates) and fluids/melts (mediums) related to diamond formation (e.g., [39–52]).
(3) The nature and extent of carbon reservoirs in the transition zone and lower mantle (e.g., C in metallic Fe complexes and Fe-carbides, [53–55]) and fluxes between different recycled carbon and water (C–O–H fluid) reservoirs in the transition zone and lower mantle (e.g., [56–62]).
(4) Mechanisms of carbon (re)cycling in the mantle through processes involving lithospheric carbon, such as subduction of hydrous, carbonated oceanic lithosphere and intra-mantle processes, such as mantle-plume upwelling and mantle metasomatism (e.g., [47, 48, 62–69]).

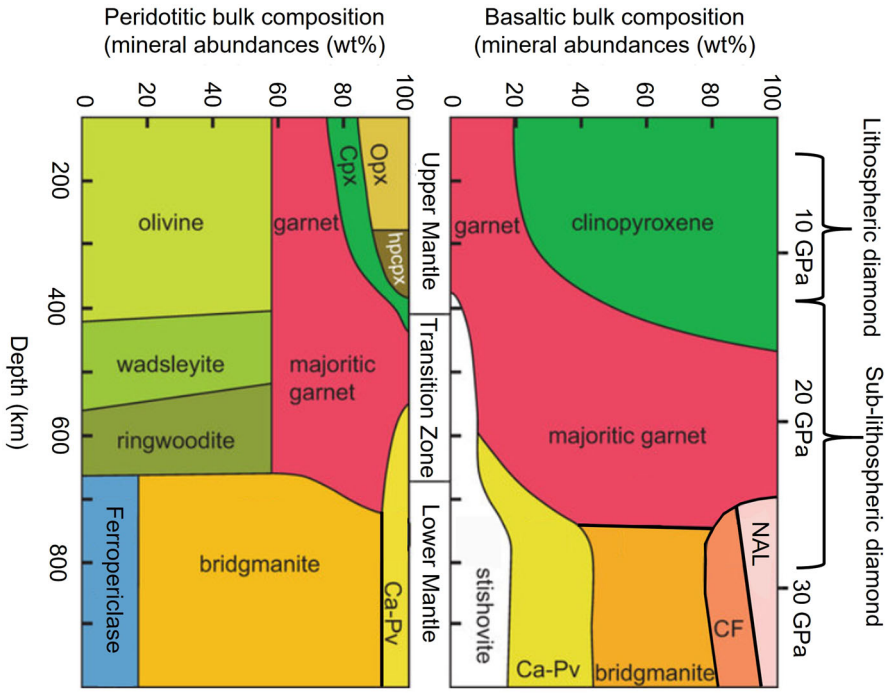

Fig. 2 Predicted mineralogy of the upper mantle, transition zone, and lower mantle as a function of depth and pressure for peridotitic and basaltic bulk compositions. Modified from Smith et al. [113] and calculated by Stixrude and Lithgow-Bertelloni [386]

Completed works regarding (1–4) often involve isotopic, major- and trace-element analysis of mineral inclusions in diamond coupled with geochronological (age of diamond or inclusion) and geothermobarometric (pressure and temperature of diamond formation) data and readers are referred to the above references if more detailed explanations are desired. High-pressure and high-temperature experiments coupled with geophysical data and modeling have generated much indirect evidence regarding the mineralogy of the Earth's interior. In Fig. 2, the mineral proportions expected for peridotitic and basaltic bulk compositions across P/T conditions representative of the upper mantle, transition zone, and lower mantle is shown [70]. Diamond formation from 120 to 800 km acts to effectively sample different mantle lithologies and helps one support theoretical or experimental assumptions about the geochemistry of the Earth's interior. As discussed in Sects. 3.3.1 and 3.3.2, there are major discrepancies between predicted and observed (in diamond) abundances of particular mantle minerals.

1.2 Geologic settings of diamond formation

On Earth, natural diamonds form in four distinct geologic settings; (1) the lithospheric mantle; (2) the sub-lithospheric mantle; (3) ultra-high-pressure metamorphic (UHPM)

terranes (orogenic belts); and (4) in meteorite impact sites. The source (provenance) and speciation of C, mineralogical (e.g., graphite) or molecular (e.g., CH_4), and the means by which carbon is subject to pressure and temperature (P/T) conditions conducive to formation of diamond, is different for each setting. Lithospheric diamonds form in the continental lithospheric mantle and sub-lithospheric diamonds form in the sub-lithospheric mantle, most commonly in the base of the upper mantle and transition zone [6]. Diamonds are transported to the surface in magmas associated with kimberlites, and to a lesser extent lamproites and lamprophyres, which are usually much younger (on average, 45 Ma to 1.2 Ga, [26]) than lithospheric diamonds, as old as ~ 3.5 Ga [23–25] and sub-lithospheric diamonds which are largely Mesoproterozoic [71]. UHPM diamonds form in much shallower environments in the lithosphere where orogenic processes produce the P/T conditions necessary to convert carbon, sourced from the crust (e.g., metasedimentary protoliths), to diamond [72]. Impact diamonds form due to a rapid increase in P and T from collisions (e.g., with meteorites, asteroids, and planetary bodies) involving carbon-bearing materials [73, 74].

As of today, ~ 6500 kimberlite occurrences have been discovered [75], ~ 1000 of which contain diamonds of sufficient size (microdiamonds, ≥ 0.85 mm) and abundance to warrant economic interest [76]; however, only ~ 1% of kimberlite deposits are mined. There are ~ 500 lamprophyre and lamproite occurrences, an increasingly small number of which are diamond producing [26, 77, 78].

Most diamondiferous kimberlites occur in the central regions of seismically stable, Archean and early Proterozoic cratons. A *craton* as defined by [36], are regions of the continental crust underlain by 150–200 km-thick lithospheric mantle that have been tectonically stable since 1 Ga. Below the nuclei of these cratons, the lithospheric mantle protrudes into the deeper convecting mantle to depths of 250–300 km, much deeper than other regions of surrounding continental or oceanic lithosphere (~ 110 km under the oceanic lithosphere) [79–82]. These features, called *lithospheric mantle keels* (Fig. 3), formed shortly after the onset of Archean plate tectonics. During the subduction of oceanic lithosphere, a layer of relatively hot (~ 200 °C hotter than current mantle temperatures) and buoyant [79], melt-depleted lithospheric mantle separates from the colder dense slab and is emplaced beneath the adjacent continental lithosphere where it cools to temperatures in the diamond stability field (900–1400 °C at lithospheric mantle pressure, [42]) and stabilizes the overlying cratonic lithosphere [83]. Formation of Paleo-Archean mantle keels and some of the oldest known diamonds (e.g., 3.5 Ga, Ekati mine, Slave Craton) occurred before the onset of plate tectonics, and thus, the mechanisms by which they form do not involve subduction; this is discussed in more detail in Chapter 5.

Lithospheric mantle keels are located below the graphite-diamond transition depth and may induce kimberlite magmatism in the mantle at depths greater than would be possible beneath younger (and thinner) lithosphere. The mantle keel is continually supplied with C-rich melts derived from the deeper convecting mantle and from the partial melting of the subducting lithospheric slab. Consequently, mantle keels are the ideal environment for diamond formation and transport via kimberlitic eruption. Clifford [84] recognized that most diamond-bearing kimberlites occur in stable cratonic nuclei overlying sections of relatively thick, melt-depleted lithospheric mantle or what are now called mantle keels, this correlation is referred to as *Clifford's Rule*.

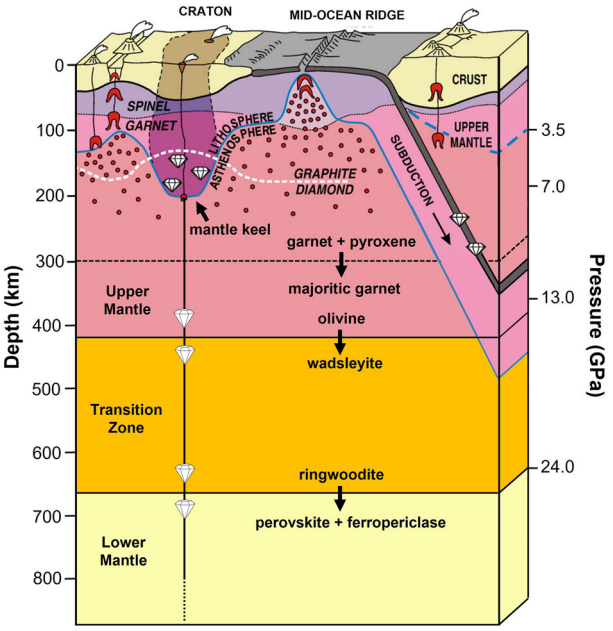

Fig. 3 A cross-section of the Earth's crust down to the lower mantle. Continental and oceanic crust is shown in beige and gray, respectively, and the upper mantle is separated into two mineralogical facies, spinel (purple) and garnet (pink), and the asthenosphere, transition zone, and lower mantle are shown in red, orange, and yellow, respectively. Small volume melts and upwelling magmatic systems are shown with dark red circles and larger U-shaped symbols. The area underlain by the cratonic mantle keel is shaded in gray; here, the cool cratonic lithosphere may extend to depths greater than 200 km and act to decrease the pressure (and depth) and which graphite transforms to diamond (white dashed line); this region is commonly referred to as the *diamond window*. Diamond (or diamond-forming fluids) may also form from partial melting and dehydration of subducted oceanic crust. Three major phase transitions are shown at ~ 300 km in the upper mantle, at ~ 410 km at the upper mantle-transition zone boundary and at ~ 660 km at the transition-zone-lower mantle boundary with black arrows. Modified from Stachel and Harris, [42]

Lithospheric diamonds form in mantle keel environments at depths of 120–200 km (average depth of 175 ± 15 km) and at an average temperature of 1160 ± 100 °C and pressure of 5–6 GPa [5, 43, 85]. Sub-lithospheric diamonds or *super-deep diamonds* (SDDs) form below the sub-continental lithospheric mantle (SCLM) in the convecting mantle at depths of ~ 300–800 km and at average temperatures and pressures of 1200–1500 °C and 9–11 GPa [6, 7, 86, 87]. However, the majority of SDDs form around the transition zone at 410–660 km [88].

2 Diamond: properties, description, and classification

Over the last 15 years, ~ 7400 articles about diamond were published in geology, mineralogy, geochemistry, geophysics, and mining-related journals, accumulating an average of ~ 500 citations per year. The diamond geology literature has a relatively high *data-density* and consequently, a complex and multi-faceted nomenclature has

emerged. An understanding of how different types of diamonds are described and classified is crucial before one attempts to familiarize themselves with the most recent scientific works on the processes and environments related to diamond genesis.

2.1 What is diamond and why is it valuable?

In diamond, each C atom forms four covalent bonds with neighboring C atoms to form C-tetrahedra. Tetrahedra link to form a relatively small unit cell that contains eight carbon atoms in cubic symmetry (space-group $Fd\,\bar{3}\,m$) in which all angles of the cell are 90° and all sides have a length of 3.567 Å [89]. The crystal structure of diamond can be simply described as two interpenetrating face-centered cubic lattices displaced with respect to one another along the body-diagonal of the cell by 1/4 the length of the diagonal. This displacement length is equal to the C–C bond length which is ~ 1.54 Å (Fig. 4) [89].

The behavior of carbon in the form of graphite, diamond, liquid, and vapor as a function pressure and temperature is well understood (Fig. 5). The structural description of diamond given above is based on observations made at room temperature. However, when subject to extremely high temperatures and/or pressures (P/T conditions in the diamond stability field, Fig. 5), the unit-cell parameters of diamond may vary as C–C bond lengths and angles change to equilibrate with the increased P/T conditions. Diamonds form in the deep mantle at extremely high pressures and temperatures and thus, are thermodynamically stable at such conditions compared to those at the surface (surface temperature and pressure (STP) = 20 °C and 0.10 MPa).

The thermodynamically stable allotrope of carbon at surface conditions is graphite and the famous slogan *diamonds are forever*, is not entirely true as diamonds are considered *metastable* at surface conditions. Although the rate at which diamond transforms to graphite at surface P/T conditions is almost zero, given enough time (on scales of billions of years), diamond will inevitably breakdown due to stochastic

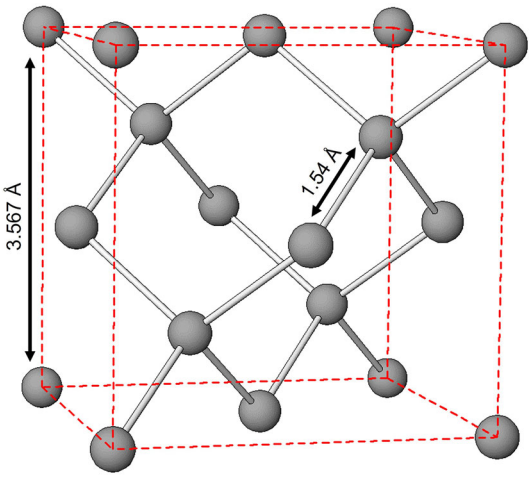

Fig. 4 Crystal structure of diamond in which all C atoms are in tetrahedral coordination and linked to one another by C–C bonds with lengths of 1.54 Å. Dashed red lines outline a single unit cell with edge lengths of 3.567. Structure generated from ATOMS V6.4 with data from Straumanis and Aka [89]

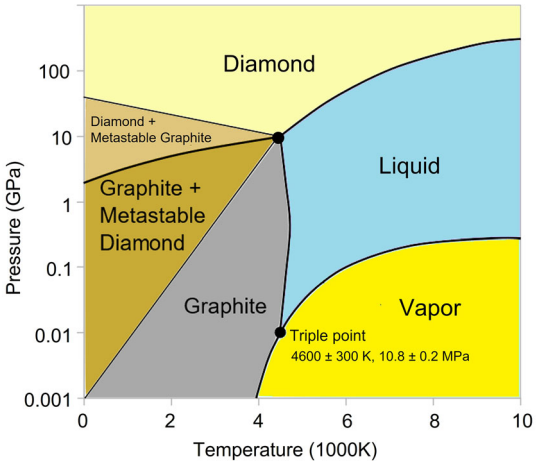

Fig. 5 Theoretical phase diagram of C as a function of pressure (GPa) and temperature (1000 K). Modified from Zazula [460]

processes. The diamond-to-graphite phase transition has a Gibb's free energy ($\Delta G^{\circ} = -2.9$ kJ mol^{-1}) [90] close to zero, as the thermodynamic stabilities of diamond and graphite at surface P/T conditions are similar; nevertheless, the reaction is exergonic and thus spontaneous. However, for this transformation to occur, a relatively large energy barrier (~ 370 kJ mol^{-1}) [90], related to the breaking of C–C bonds, must be overcome. Diamond in the presence of O_2 atmosphere may decompose to produce CO_2; this reaction is also spontaneous but more thermodynamically favored as $\Delta G^{\circ} = -397$ kJ mol^{-1} [90]. This was first shown by Antoine Lavoisier in 1772 who proved that diamonds were composed principally of carbon by showing that the same amount of CO_2 (per gram of material) is produced by burning diamond and graphite. It follows that, at surface P/T conditions, diamond is kinetically stable but thermodynamically unstable.

The diamond-to-graphite energy barrier is easily overcome by increasing temperature. However, the fast ascent (eruption) rates of kimberlitic systems, delivering diamonds from variable depths to the surface, prevent transformation of diamond to graphite until it reaches lower temperature environments near the surface. A significant increase in pressure is required to convert the diamond-to-graphite transformation from an exergonic-to-endergonic (non-spontaneous) reaction and eventually to convert metastable graphite to diamond (Fig. 5). Several studies suggest diamond may undergo additional phase transitions to body-centered cubic structures at extreme pressures (~ 1100 GPa) or melt to form a metallic fluid (liquid C) at extreme temperatures and pressures (~ 50,000 K and ~ 1000 GPa) [91]. However, natural diamonds form at pressures that do not exceed ~ 23 GPa [92], respectively, and thus, such phases are not considered here. Lonsdaleite, what is generally considered the hexagonal polymorph of diamond, is typically observed as inclusions in diamonds associated with meteorite impacts. However, recent work [93, 94] suggests that lonsdaleite is not a polymorph of diamond but instead a mixture of micro- to nano-scale cubic and hexagonal diamond layer stacking and graphitic domains.

Why are we interested in diamond? In general, people are interested in natural and synthetic diamond from (1) a scientific perspective and (2) an economic perspective. In this review, we will focus almost entirely on (1), but a brief description of how the utility and aesthetics of diamonds contribute to their value is warranted. The economic value of diamond is a function of its unique physical, optical, thermal, and electrical properties, each of which useful for particular applications. Here, a description of how these properties arise from aspects of the chemical and crystal structure of diamond is given.

2.1.1 Physical properties

It is generally accepted that diamond is the hardest mineral, and thus the most durable naturally occurring material. The extreme hardness of diamond makes it the ideal choice for abrasives (e.g., grinding, polishing, and drilling applications), cutting tools, and coatings to prevent mechanical wear or corrosion of computer (e.g., hard disks), mechanical (e.g., ball-bearings), or jewellery-related components. The extreme strength of diamond has even inspired several truss designs based on its cubic crystal structure.

The hardness of diamond is best explained in terms of elasticity, which describes how a mineral deforms reversibly (strains) in response to an applied pressure (stress). Stress and strain are linearly related during elastic deformation and non-linearly related during plastic (non-reversible) or brittle deformation, both of which may occur in diamond. The elasticity of minerals is related to the *bulk modulus,* K_{0T} (GPa), a measure of volume change in response to a compressive force. At room temperature, diamond has an extremely high bulk modulus, and harder and more rigid materials have a higher K_{0T} as they show a smaller volume change during compression. For diamond, $K_{0T} = 444.0\ (\pm 2)$ GPa [95], significantly larger than common rock-forming minerals, such as quartz ($K_{0T} = 37.0\ (\pm 0.3)$ GPa, [96]), olivine ($K_{0T} = 124.7\ (\pm 0.9)$ GPa, [97]), and plagioclase feldspars along the anorthite–albite join ($K_{0T} =$ ~ 52–82 GPa, [98]).

Although the superior hardness and incompressibility of diamond is often solely attributed to strong C–C bonds, it is actually the geometry of C–C bonds in the diamond lattice that results in such desirable properties. In diamond, all four valence electrons are involved in bonding via sp^3 orbital hybridization. In graphite each C atom is bonded to three other C atoms via sp^2-bonds to form graphene-type sheets. As only three valence electrons are involved in C–C bonding, the fourth becomes delocalized across the entirety of the sheet. Delocalized electrons contribute to bonding within the sheet and result in C–C bonds that are stronger than those in diamond. So why is diamond so hard (Moh's = 10) and graphite so soft (Moh's = 1–2)? In graphite, movement of delocalized electrons results in adjacent sheets with opposite dipoles and the consequent bonding of such sheets via Van der Waals dispersion forces. This type of bonding is relatively weak and predisposes graphite to breaking (cleaving) along planes parallel to each sheet. In diamond, all bonds are covalent and arranged, such that there are no orientations in diamond more or less susceptible to compression in response to an applied stress. Diamond contains the greatest number of atoms per unit-volume with an atomic density of 1.7×10^{23} atoms/cm^3 [90]. However, the

atomic packing fraction, a comparison between the volume of the unit cell and the sum volume of each atom in the unit cell, is low (34%) [90] compared to close-packed structures (74%) and the density of diamond (3.5 g/cm^3) is also relatively low, surpassed by common constituents of the crust, such as fayalite (4.39 g/cm^3), ferrosilite (3.95 g/cm^3), magnetite (5.15 g/cm^3), pyrite (5.01 g/cm^3), and spessartine (4.18 g/cm^3) [99].

2.1.2 Optical properties

Over the last 30 years, advances in the production of synthetic diamonds, specifically by chemical-vapor deposition (CVD diamonds), have allowed for the efficient production of high-quality diamond, free from the optical and structural defects that are often observed in other types of synthetic [e.g., high-pressure-high-temperature (HPHT) diamonds] or natural diamond [2]. Consequently, the optical applications of diamond have expanded and are used in X-ray windows, optical lenses, antireflection coatings, and attenuated total reflection (ATR) spectroscopic applications.

The aesthetic value of diamond is due to its optical properties, specifically those related to color and lustre. Natural diamonds can occur in many colors including, red, pink, purple, yellow, brown, blue, white, black, and, of course, colorless. Pure, perfect diamond is transparent from the UV (225 nm) to the far infrared spectrum and is thus colorless [100]. Chemical impurities (e.g., substitutional N, see Sect. 2.2.4), mineral inclusions, and structural defects (e.g., color centers) scatter visible light and impart color in diamond, some more desirable and rare than others. Type I diamonds contain N impurities which aggregate with site vacancies to different degrees and typically result in a yellow to brown or colorless diamond [101]. Type II diamonds contain no measurable amounts of N and may show pink, red or brown coloration due to structural defects (e.g., lattice dislocations). Type II diamonds may also contain B impurities which results in a light blue diamond, although extremely rare. Micro-inclusions of graphite and sulphides may result in dark-brown or black diamonds and fractures, and structural defects and micro-fluid inclusions may result in a cloudy or white appearance [101]. Diamond has a high refractive index (~ 2.418 at room temperature) and dispersion factor (0.044) in the visible spectrum [100]. These properties, in combination with reflection due to faceting, results in the adamantine luster of diamond and prismatic appearance that many gemologists refer to as *the diamond's fire*. Numerous treatments, including radiation exposure, HPHT and LPHT annealing, and surface coatings, are used to enhance the color of natural and synthetic diamonds, and a detailed review of these procedures is given by [102, 103] and [101].

Pristine, defect-free diamonds (and other materials with the diamond structure) have no dipole moment and thus no infrared active phonons that correspond to a fundamental lattice vibration (one-phonon absorption) [100, 101]. However, infrared light may excite two or more higher order lattice vibrations (anharmonic multiples of the fundamental lattice vibration) to produce IR-active two- and three-phonon absorption regions (~ 1500–4000 cm^{-1}) that are observed in the FTIR spectra of diamond. As is shown in Fig. 6, the intensity of each multiphonon absorption signal decreases with frequency. The introduction of lattice impurities, such as N, B, and H, results in absorption due to N(B)-C stretching and bending vibrational modes in the one-phonon region

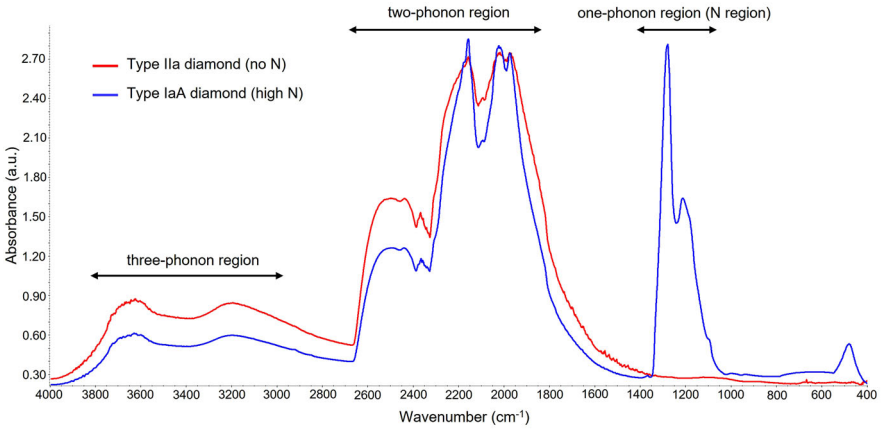

Fig. 6 FTIR spectrum of a *Type IIa* and a *Type I* diamond showing absorption in the three-phonon region (~ 3700 to 2650 cm^{-1}) and two-phonon region (~ 2650 to 1600 cm^{-1}) due to intrinsic lattice vibrations. The spectrum of the Type I diamond also shows absorption in the one-phonon region (~ 1400 to 1000 cm^{-1}) due to N defects

(Fig. 6) from ~ 1000 to 1400 cm^{-1} or at higher frequencies (e.g., 3107 cm^{-1}) for H-related stretching modes [101]. Analysis of IR signals in the one-phonon region is the principal means by which diamonds are classified by *type* (e.g., [104]) (Sect. 2.2.4).

2.1.3 Thermal and electrical properties

Natural diamond has an extremely high thermal conductivity of ~ 2000 W (mK) [105] due to the combination of strong covalent C–C bonds and a relatively low density compared to related cubic structures. This thermal conductivity is four-to-five times larger than the commonly used metal conductors, such as copper, silver, and gold. Diamond also has a very low coefficient of thermal expansion [reported as α (K^{-1})], that is the degree of volume change due to increasing temperature. For diamond, $\alpha = 0.267 \times 10^{-5}$ K^{-1}, which is significantly lower than any other mineral, for example, rock-forming silicates where $\alpha = \sim 3 \times 10^{-5}$ K^{-1} [95, 96, 98]. These properties have made diamond an attractive solution for heat-sink applications in electrical devices (e.g., high-voltage circuitry, laser diodes, transistors, and supercapacitors).

Diamond also has unique electrical properties most of which are related to its ultra-wide band gap (5.47 eV) between the valence and conduction bands [101] (Fig. 7). For non-metals, movement of electrons across the band gap into the conduction band is required to allow electrons to move freely throughout the crystal and act as charge carries to increase the electrical conductivity of the material. In electrical conductors, bands overlap, and electrical conductivity is high. In diamond, a relatively large excitation energy, 5.47 eV (i.e., temperatures in excess of 1000 °C or UV light where $\lambda < 0.23$ μm) [100] is required to allow electron transfer between bands, and thus, most diamonds are considered insulators. However, at lattice defects associated with specific impurities, specifically B and N, electron charge-transfer processes increase the overall electrical conductivity of the diamond, such that it acts as a semiconductor

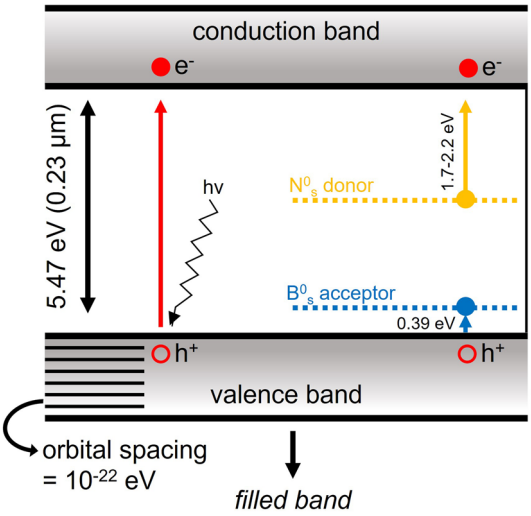

Fig. 7 The energy-level schematic of perfect (defect-free) diamond where the valence band is filled, and no electrons occupy the conduction band. Incident UV light (hv) with an energy $\geq$ 5.47 eV can excite electrons (e^-) from the valence band to the conduction band leaving behind a positively charged hole (h^+) in the valence band. To provide an example of donor-acceptor (charge-transfer) processes, a substitutional N atom with a neutral charge, $N^0{}_s$ is shown and may donate an electron (1.7–2.2 eV) to the conduction band to produce a positively charged, $N^+{}_s$ defect. A substitutional B atom with a neutral charge state, $B^0{}_s$ is shown and may accept an electron (0.39 eV) from the valence band to produce a positively charged hole (h^+) and a negatively charged, $B^-{}_s$ defect

as opposed to an insulator. In fact, as little as 1 ppm B is required to produce diamond semiconductors and HPHT polycrystalline diamond superconductors have been synthesized using different B-doping methods [106]. The electrical behavior of impurities also influences the color of diamond. For example, impurities such as N contain extra electrons with respect to C, and these electrons are not directly involved in N–C bonding (i.e., lone-pair electrons) and are donated to the conduction band with relatively smaller excitation energies (N donor = 1.7–2.2 eV) [101] (Fig. 7). Other atoms such as B may accept electrons from the conduction band (B acceptor = 0.39 eV) [101] (Fig. 7), and these *donor–acceptor* (charge-transfer) processes require absorbance of visible light and thus change the color of diamond.

2.2 Diamond description, nomenclature, and classification

There are several schemes used to describe and classify diamonds, each focusing on different properties of diamonds, e.g., textures, morphology, crystallinity, N-aggregation state, or geological features such as host (or parental) rock types, inclusion mineralogy, and geologic setting of formation. Each of these schemes has different applications for each sub-discipline of geological research. For example, if one is studying diamond dissolution features, classifying and describing diamonds based on secondary growth

morphologies and/or surface textures may be more useful and informative than classification based on the N-aggregation state. It is commonplace in geology to broadly classify diamonds as *lithospheric* or *sub-lithospheric* based on the depth at which they formed as this provides information about the geochemistry, mineralogy, and P/T conditions of the upper mantle (lithospheric diamonds) or transition zone and lower mantle (sub-lithospheric diamonds).

The earliest detailed recording of diamond classification dates to third century BC India, where the value of diamond was determined by its color and assigned a name corresponding to a social class; for example, colorless diamond was considered most valuable and associated with aristocracy. Since the early 1900s, experimental work has been conducted relating the color, lustre, and luminescence of diamond to the absorption of visible, UV, and infrared light. In the 1950s, the Gemological Institute of America developed a classification scheme to grade the quality of diamond based on *The Four C's*; color, clarity, cut, and carat (mass). In the following sections, classification schemes based on different criteria commonly used in the geological research of diamond will be described.

2.2.1 Primary morphologies and surface features of monocrystalline diamond

The journey of natural diamond from the deep Earth, where nucleation and primary growth occurs, to the surface via kimberlitic eruption is chemically and physically complex. Fortunately, natural diamonds have an exceptionally wide variety of morphologies and external (surface) and internal features which provide information about the types of fluids/melts and mechanisms related to diamond formation and growth and those that may cause physical or chemical breakdown (e.g., dissolution) of the diamond during transport to the surface. Such features can be broadly classified as *primary* or *secondary* and, in this section, and the following, a description of the common primary and secondary growth morphologies and textures observed in natural diamonds is given.

Primary morphologies represent the initial growth phase(s) of diamond which is controlled by the cubic symmetry of the diamond crystal structure (Sect. 2.1). As first postulated by Haüy and Bravais in the mid-nineteenth century, crystal faces tend to be parallel with planes that have a relatively high density of lattice points (or crystallographic sites) [107]. These faces grow relatively slowly and are expressed in the morphology of the crystal as the faster growing faces *grow-out* of the crystal [108]. This is the case for the (111) octahedral face of diamond which grows relatively slowly, consequently, most monocrystalline diamonds have an octahedral habit [108] (Fig. 8a). However, the growth rate of diamond faces is also influenced by the P/T conditions, fluid composition, speciation (and availability) of C in the growth medium, and crystallographic defects, and numerous monocrystalline diamond morphologies are observed [109]. Cubic diamonds are less common than octahedral diamonds and are typically referred to as *cuboid* as they are often poorly developed with rounded edges and irregular, straited faces [110]. Where both growth forms are operative during growth, cubo-octahedral diamonds may form (Fig. 8b), in some cases, such morphologies are not immediately recognized by external examination but are easily revealed by analysis of internal growth structure via cathodoluminescence (CL). If intergrown

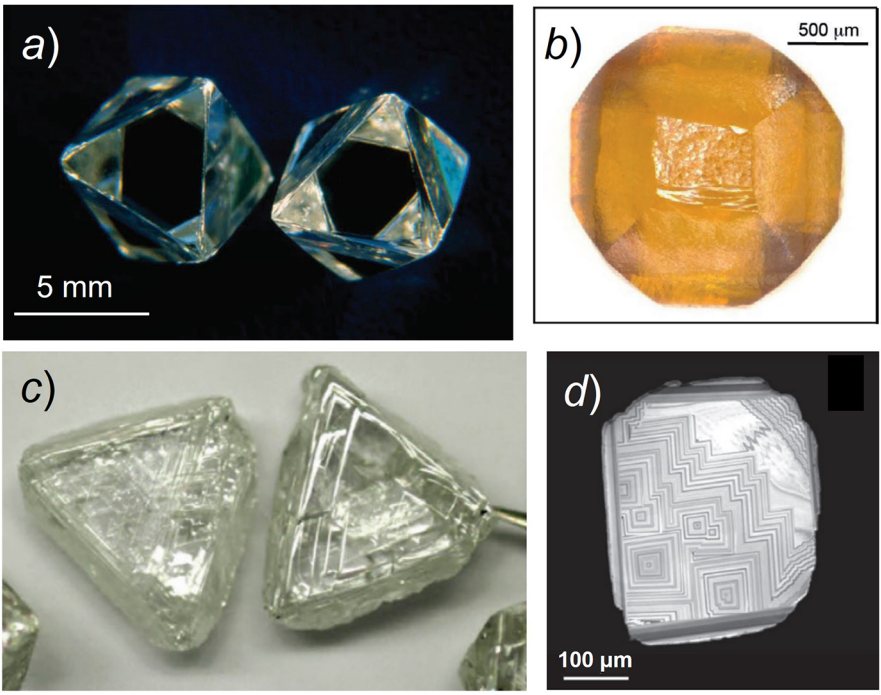

Fig. 8 A **a** two well-formed, equant octahedral diamonds, **b** cubo-octahedral or *cuboid* diamond, **c** set of macles showing rounded edges suggestive of dissolution and/or resorption (tweezer tip for scale), and **d** cathodoluminescence (CL) image of complex, non-concentric growth zonation patterns suggesting a complex growth history that likely involved several discrete crystals (for each growth center) before they became intergrown to form this octahedral diamond. Modified from Harris et al. [108], image **a** from Thomas Hunn Co., **b** from Dmitry Zedgenizov (Sobolev Institute of Geology and Mineralogy), **c** from Anetta Banas (University of Alberta), and **d** from Zhang [461]

monocrystalline diamond crystals are aligned along crystallographic directions, they are referred to as *twinned diamonds*, and if they are not aligned, they are referred to as *diamond aggregates* [108]. Contact twinning, described by the spinal-twin law, is most common and referred to as *macles* when observed in diamond (Fig. 8c). Macles form from faceted growth on the [111] face, and in some cases, multiple macles may become intergrown to form unique diamond morphologies (e.g., Star of David diamonds) [108]. Monocrystalline diamonds that do not exhibit an external crystallographic habit are termed *irregular diamonds* [108] (not to be confused with irregular diamonds described in Sect. 3.2). Such irregularity is due to dissolution or fracturing, or in some cases a combination of both and is related to physical damage during eruption or dissolution [111].

Octahedral diamonds exhibit three main types of surface features; *triangular plates*, *imbricated surfaces,* and *pyramids* [108]. Triangular plates grow on the octahedral faces of diamond and the size of each triangle decreases in the direction of growth [112]. Imbricated surfaces are produced when the growth of triangular plates is

disrupted, and pyramids are formed where triangular plates do not cover the entirety of the basal octahedral face [108]. As well-formed cubic and cubo-octahedral diamonds are relatively rare, attributing their surface features to primary or secondary growth features is difficult and will not be discussed here.

Investigations of the internal features in diamond via analytical methods such as cathodoluminescence and X-ray tomography are particularly useful for understanding the role of impurities such as N on the episodic growth and deformation of diamond. Diamonds often show concentric and/or non-concentric (polyconcentric) growth zonation (Fig. 8d), where each zone may show significant compositional differences (N and B content) and ages (> billions of years). Diamonds also often show deformation features, such as lattice dislocations, stacking faults, and plastic deformation features) which provide information about mantle annealing times and temperatures (e.g., [53, 113]). Specific features associated with plastic deformation will be discussed in Sect. 3.2, and readers are referred to [108] for a complete review of primary morphologies and related features.

2.2.2 Secondary morphologies and surface features of monocrystalline diamond

Secondary morphologies of monocrystalline diamond are formed primarily by dissolution in a corrosive fluid or kimberlitic melt. Moore and Lang [114] were the first to show that dodecahedral diamonds are produced by dissolution of octahedral diamonds. Dissolution of octahedral diamonds involves reduction of each octahedral face to a vertex, which appears as a triple point between three rounded rhombic faces. A linear feature, called the *medial line*, occurs across the diagonal of each rhombic face [108]. If one assumes the medial line represents the intersection of two crystal faces, the secondary growth morphology has 24 faces and is best described as a *tetrahexadron* (THH) [115] (Fig. 9a). If the medial line is not considered representative of the intersection of two crystal faces, the diamond has 12 faces and is best described as a dodecahedron [115] (Fig. 9b). Regardless of how one describes the secondary growth morphology, in almost all cases, increasing degrees of dissolution result in more rounded diamonds.

Surficial dissolution features on octahedral diamonds include *shield-shaped* and *serrate laminae*, *trigons,* and *hexagons* [108]. Shield-shaped and serrate laminae are produced from dissolution of triangular plates and imbricated surfaces, respectively. Trigons are arguably the most commonly observed and best understood dissolution feature in octahedral diamonds. Trigons are produced by crystallographically controlled dissolution etching and their orientation is a function of temperature and f_{O2} [116]. *Positive trigons* (Fig. 9c) are triangular pits with the same orientation as the octahedral face on which they occur, and *negative trigons* (Fig. 9d) are rotated 180° with respect to the octahedral face [117]. X-ray topography experiments suggest that trigons form on areas of the octahedral face predisposed to etching due to the presence of structural dislocations or plastic deformation lines [118–120]. The dissolution conditions responsible for the formation of positive and negative trigons are likely different; at boundary conditions, a positive and negative contribution to trigon formation results in *hexagons*, six-sided pits that develop on the octahedral faces [121]. Cuboid diamonds contain tetragons rather than trigons and are similarly divided into positive

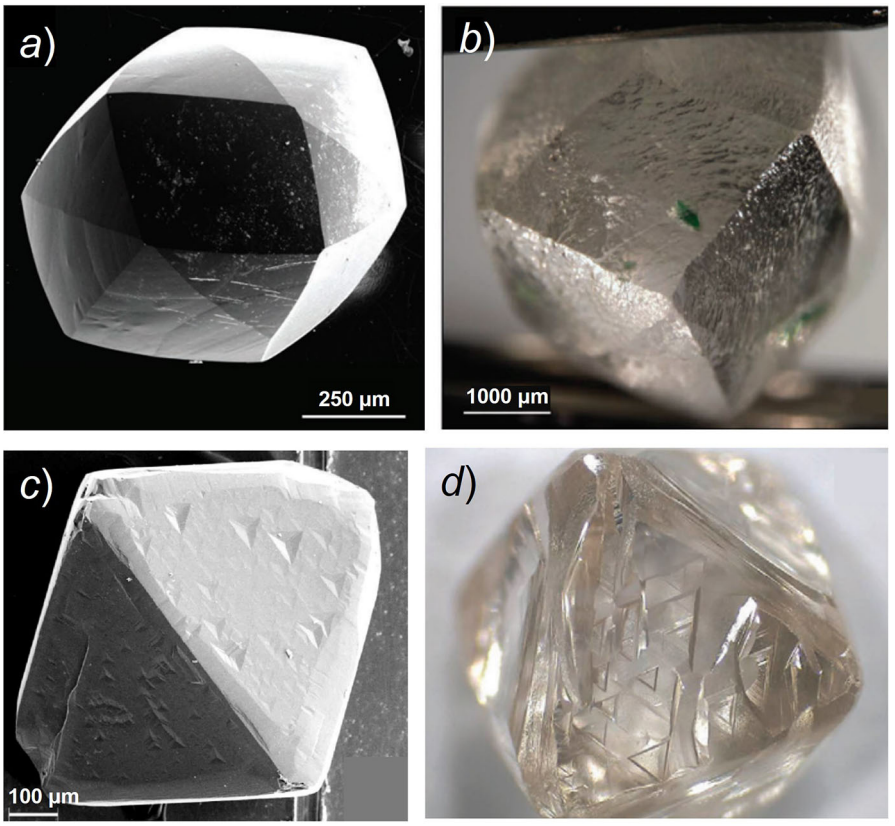

Fig. 9 A **a** back-scattered electron (BSE) image of a tetrahexahedroid (THH) diamond, **b** vertex of a dodecahedroid diamond, adjoined by three rhombi produced by dissolution of an octahedral face to produce dodecahedroids and eventually rounded THH morphologies with progressive dissolution, **c** BSE images of an octahedral diamond with positive trigons, and **d** octahedral diamond with negative trigons. **a**, **b**, and **d** modified from Harris et al. [108], image (**a**) from Yana Fedortchouk, **b** from Karen Smit, and **d** from Evan Smith (GIA). **c** modified from Khokhryakov and Palyanov [462]

and negative tetragons based on their orientation about the cube edge [122]. In general, dissolution of diamonds to form dodecahedral or THH morphologies is accompanied by the formation of additional surface dissolution features, such as *terraces*, *hillocks*, *plastic deformation lines and planes*, *corrosion sculptures*, *shallow depressions*, *ruts*, *micro-disks*, and *frostings*. A review of these features is given by [108].

2.2.3 Polycrystalline diamond aggregates and fibrous diamonds

In this paper, we review work on primarily monocrystalline diamond for the purposes of brevity. However, polycrystalline diamond aggregates (PDAs) and fibrous diamonds and their mineral and fluid inclusions contain a wealth of information regarding the composition of fluids associated with diamond formation. Consequently, they are described here briefly and invoked in later discussion when useful.

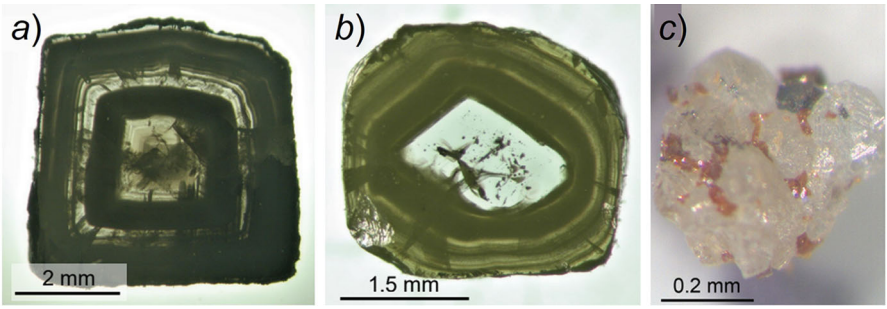

Fig. 10 A **a** polished cross-section of a *fully fibrous*, cuboid diamond showing concentric growth zonation due to variation in the density of micro-fluid inclusions, **b** polished cross-section of a *coated* diamond showing a non-fibrous, monocrystalline octahedral core surrounding by a zoned coat of fibrous diamond, and **c** polycrystalline diamond aggregate (PDA) intergrown with orange silicate minerals. **a** and **b** Modified from Weiss et al. [52] and **c** modified from Mikhail et al. [127]

Fibrous diamonds consist of parallel fibers that may or may not comprise the entirety of the diamond (fully fibrous, Fig. 10a) or grow over non-fibrous monocrystalline diamonds to produce *coated diamonds* (Fig. 10b). Fully fibrous diamonds are cuboid and consist of fibers closely aligned to the diamond axis [123]. Coated diamonds commonly consist of an inner monocrystalline octahedral core and a fibrous overgrowth in which fibers are oriented perpendicular to the octahedral faces [52, 123]. In some cases, octahedral monocrystalline growth may occur over a fibrous cuboid core. Although poorly understood, the boundary between monocrystalline and fibrous growth in coated diamond likely represents major changes in the growth conditions. Fortunately, fibrous diamond is particularly well suited for incorporation and preservation of fluid and melt microinclusions which are central to recent works aimed at understanding the composition and redox state of fluids related to diamond formation (see [52] and references therein).

Polycrystalline diamond aggregates (PDAs) are rocks (mantle xenoliths) in which the dominant mineral is diamond (Fig. 10c) [124]. Following classical petrographic nomenclature, they are best described as *diamondite* [125]. However, akin to much of the geologic nomenclature, it is still commonplace to use rock names that originate from industry. For example, PDAs may be classified as *boart* if they are not gem quality but still economically viable for use in cutting or abrasive tools. Boart may be classified as *stewartite* or *framesite* based on the presence or absence of magnetic minerals, respectively [124]. Carbonados comprise another groups of PDAs and are typically black in color, contain a strange suite of minerals inclusions with crustal and metasedimentary provenance, and occur in Mid-proterozoic metaconglomerates from only a handful of localities [124]. PDAs form by rapid nucleation and growth from C supersaturated fluids [126] resulting in syngenetic intergrowths of diamonds with other minerals, a feature not typical of monocrystalline diamond. In general, PDAs are δ^{13}C-depleted, δ^{15}N-enriched, have high N concentrations, and have variable N-aggregation states compared to monocrystalline diamonds [127]. Whereas slow-growing, zoned, monocrystalline diamonds provide information about the evolution of the diamond-

forming environment through time, PDAs provide similar information corresponding to short moments in time when PDAs formed and/or grew.

2.2.4 Diamond type classification: aggregation state of nitrogen and boron

As described above, substitutional impurities, specifically N, B and H, can significantly alter the optical, thermal, and electrical properties of the diamond in which they occur. Thus, a classification scheme in which diamonds are grouped based on presence of impurity-related defects is extremely useful in the geological, gemological, and crystallographic study of diamond. This was first realized by Robertson [128] who developed the *Type Classification* of diamonds based on the concentration and aggregation state of N and B atoms which substitute for C atoms in the diamond lattice. At the broadest classification level, diamonds that contain measurable amounts of N are *Type I* and those that contain no measurable N are *Type II*. The N concentration of diamond is typically measured using Fourier-transform infrared (FTIR) spectroscopy, as the detection limit of N using this technique is ~ 10 at.ppm, and the definition of Type II diamond is often expanded to include all diamonds with < 10 at.ppm N [129]. Although other techniques [e.g., secondary-ion mass spectrometry (SIMS)] offer lower detection limits for N (e.g., [130]), further type classification, based on the aggregation state of N, requires interpretable signal intensity in the IR spectra which may not possible for diamonds with N contents < 10 at.ppm.

Type I diamonds are further classified based on the aggregation state of N, a description of how one or more N atoms are arranged in the diamond lattice. During early stages of diamond formation, N substitution results in singular, isolated N defects, called *C-centers*. With increasing residence time/temperature, C-centers rapidly aggregate to form N dimers, which consist of two neighboring substitutional N atoms, these defects are called *A-centers*. Eventually, A-centers aggregate to form defects that consist of four N atoms surrounding a carbon-vacancy called *B-centers*. Type I diamonds are subdivided into the following groups based on the occurrence of these defect centers;

Type Ia: diamonds that contain aggregated N defects, specifically A- and B-centers in concentrations detectable via FTIR spectroscopy. The normalized ratio of A- and B-centers, $\%B = [100 \times B_c/(B_c + A_c)]$ where A_c and B_c are the measured concentrations of A and B-centers in the diamond, is used to further subdivide Type Ia diamonds. If %B < 10%, the diamond is *Type IaA*; if %B > 90%, the diamond is *Type IaB*; and if 10% < %B < 90%, the diamond is *Type IaAB*.

Type Ib: diamonds that often contain lower concentrations of N than Type Ia diamonds where the majority of N occurs as C-centers.

Type II diamonds are also subdivided into *Type IIa* and *Type IIb* diamonds. Type IIa diamonds are the purest variety of natural diamond and contain little-to-no measurable concentration of substitutional N or B. Type IIb diamonds also do not contain appreciable amounts of N but contain B, which results in their striking blue color [101]. Each diamond type and the associated defect configurations, as described above, are shown in Fig. 11. The C-, A-, and B-centers are the most common defects observed in diamond; however, there are almost countless varieties of defects involving different impurities (elements) in different configurations with different charge states

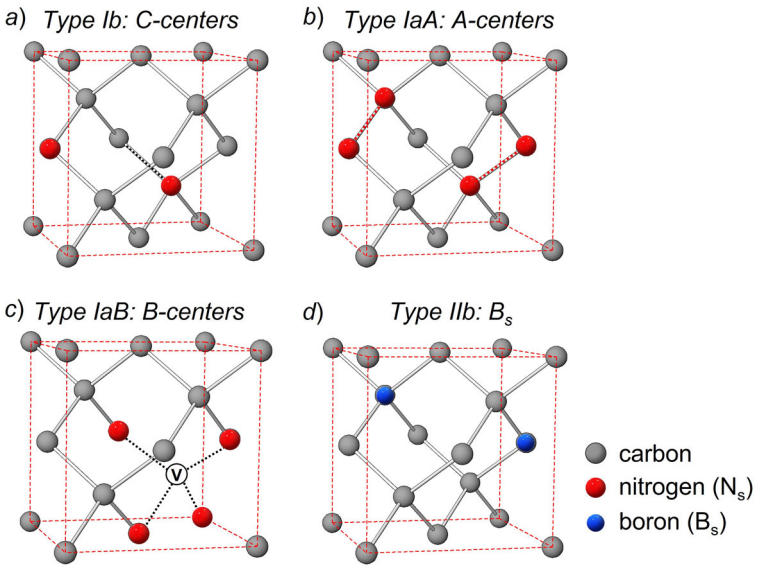

Fig. 11 Structural configuration of **a** *C-centers* which consist of single, N_S atoms that form three identical N–C bonds and a fourth, significantly longer, N–C bond shown with the dashed black line, **b** *A-centers* which consist of two adjacent N_S atoms which are not bonded to one another as shown with the red dashed line, **c** *B-centers* which consist of four N_S atoms around a C-vacancy; here, dashed black lines do not indicate bonds and simply serve as a visual guide, and **d** singular B_S atoms that form three identical B-C bonds and one slightly shorter (98% shorter than a C–C bond) B–C bond. Structures generated from ATOMS V6.4 with data from Straumanis and Aka [89]

(e.g., [131, 132]). In Sect. 3.1.1, a detailed discussion of the some of the less common defects, including those that belong to the VN_xH_y family will be discussed.

2.2.5 Classification of lithospheric and sub-lithospheric diamond based on inclusion parageneses

As discussed in Sect. 1.2, it is commonplace to classify natural diamond as lithospheric or sub-lithospheric based on the geologic setting in which they form. Lithospheric diamonds typically show well-formed octahedral and cubo-octahedral morphologies. Sub-lithospheric (super-deep) diamonds are poorly formed, irregularly shaped, and often have several growth centers with non-concentric zonation due to repeated cycles of dissolution and re-growth in the convecting mantle [6, 108]. The irregular morphology of SDDs may also be due to fracturing during brecciation at shallow (lower temperature) environments in the kimberlite system [111]; despite the plasticity of diamond at temperatures > 900 °C, Shirey [133] has shown that deep-seated earthquakes may also result in brittle fracturing of SDDs in the mantle.

One may further classify lithospheric diamond based on the associated mineral assemblage. Lithospheric diamonds have one, or a mix, of the following parageneses; *peridotitic*, *eclogitic,* and to a much lesser extent, *websteritic*. Following Stachel [134], these parageneses are characterized by the following mineral assemblages:

Peridotitic: Cr-pyrope, forsterite, enstatite, Cr-diopside, Mg-chromite, and Fe–Ni sulphides. These diamonds can be further subdivided as *harzburgites*, *lherzolites*, and *wehrlites* based on the occurrence of clinopyroxene and the major-element composition (Cr and Ca) of garnet [135–137]. However, the presence of particular inclusions, such as Fe–Ni sulphides, cannot be used to determine paragenesis in the absence of other inclusion minerals.

Eclogitic: grossular–almandine–pyrope, omphacite and other Na-rich clinopyroxene, and Fe-sulphides.

Websteritic: almandine–pyrope, diopside–augite, enstatite.

Strict chemical definitions of each of the above parageneses, which is based primarily on the Mg# of olivine, clinopyroxene, and orthopyroxene, the Al_2O_3 content of clinopyroxene and the CaO and Cr_2O_3 content of garnet, is given by [42, 137–139].

Peridotitic substrates (mantle meta-peridotites), associated with peridotitic diamonds, likely formed in the hotter, Archean mantle due to extreme degrees of primary melt depletion associated with mantle-plume activity [30, 140–142]. However, the mechanisms of emplacement into the sub-cratonic lithosphere during collision and subduction remain unclear. Eclogitic substrates are thought to represent material derived from hydrothermal alteration, dehydration, and partial melting of subducted oceanic lithosphere [13, 143, 144]. This is supported by oxygen isotope compositions inconsistent with the mantle [13, 145, 146], sulfur (S) isotope compositions in accord altered oceanic crust and sediments exposed to the O_2-poor Archean atmosphere [35, 147–150], and negative and positive Eu anomalies in garnet and clinopyroxene suggesting fractional crystallization processes in a relatively low pressure, crustal setting [144]. Several aspects regarding the formation of lithospheric diamonds and their inclusions are discussed in Sect. 3.3.1.

Like lithospheric diamonds, SDDs are commonly grouped based on inclusion paragenesis: *meta-peridotitic* (e.g., meta-harzburgitic) or *meta-basaltic* (and meta-pyroxenitic). The basis for this paragenetic division is given in Sect. 3.3.2 where mineral inclusions in SDDs are described in more detail. For now, we provide a general classification of SDDs (following [129]) based on the geologic setting and depth in which they form:

Upper mantle and transition zone: these diamonds form in meta-basaltic-to-meta-pyroxenitic substrates at depths of 250–660 km and often contain inclusions of majoritic garnet and other silicates [6].

Lower mantle: these diamonds form in meta-peridotitic substrates and may contain inclusions of bridgmanite, CaSi-perovskite, and ferropericlase [6, 88, 92, 151]. Only if inclusions of bridgmanite were observed, could one unequivocally assign a formation depth of > 660 km. If this is not the case in SDDs, distinguishing between transition zone and lower mantles origins is difficult. This is the case for the famous *Cullinan-like, Large, Inclusion Poor, Pure, Irregular, and Resorbed* (CLIPPIR) diamonds [54] which are interpreted to form between depths of 360–750 km in the deep metal-saturated mantle (see Sect. 4.3).

Approximately 98% of studied diamonds are lithospheric (2% are SDDs) and 64.8%, 32.8%, and 2.4% are peridotitic, eclogitic, and websteritic, respectively [42]. For peridotitic diamonds, 81% are harzburgitic, 18% are lherzolitic, and 1% are wehrlitic [134]. However, geophysical estimates by Garber [152] suggest that the

cratonic lithosphere consists of $\leq$ 20% eclogite which is thus overrepresented by lithospheric diamonds. This may be due to selective incorporation of eclogite by the kimberlitic magma or more likely due to the relatively low preservation potential of peridotite compared to eclogite or other more complicated explanations as discussed in Chapter 6. Fluids associated with diamond formation and kimberlitic magmatism that are CO_2-rich react with olivine to form magnesite to reduce the cohesivity of the rock and predispose peridotite xenoliths to disaggregation during kimberlite eruption [47, 153, 154]. Many other types of alteration (metasomatic oxidization and hydration, recrystallization, and re-equilibration) may affect the xenoliths during residence in the mantle and ascent to the surface, and in many cases, reliable identification of *parental-rock* type is impossible. For such cases, classification based on the *host-rock* type is useful. Lithospheric and sub-lithospheric diamonds are found in four principal rock types, following the recent nomenclature revisions of Pearson [155], they are as follows:

[1] *Kimberlites* (*or Group I kimberlites*): ultramafic, potassic (K/Na > 1) igneous rocks that are rich in volatiles, particularly CO_2 (6.6 ± 3.3 wt% for $n = 307$, [155]), and contain primarily forsterite, pyrope, Cr-diopside, enstatite, phlogopite, chromite, serpentine, and carbonates. Isotopic compositions of Sr, Nd, Hf, and Pb suggest equilibration in the convecting mantle [156].

[2] *Carbonate-rich olivine lamproite* (CROL) (*or Group II kimberlites/orangeites*): ultrapotassic (K/Na > 3), peralkaline ([K + Na]/Al > 1), micaceous igneous rocks that are rich in volatiles, particularly H_2O and CO_2 (5.8 ± 4.0 wt% for $n = 38$, [155]) and contain primarily olivine, phlogopite, diopside, Ti-aegirine, spinel, chromite, magnetite and perovskite [157]. Isotopic compositions of Sr, Nd, Hf, and Pb suggest equilibration in metasomatized lithospheric mantle [156]. CROL lithologies are divided into *evolved* and *unevolved* groups by Mitchell [158] with higher SiO_2 and Al_2O_3 contents and lower MgO and CaO in the former and higher MgO and lower SiO_2 contents in the latter with respect to kimberlites [155]. In general, CROLs have higher CO_2 and CaO contents than olivine lamproites (hence the name, carbonate-rich olivine lamproite).

[3] *Olivine lamproites*: ultrapotassic, peralkaline, (sub)volcanic rocks that are depleted with respect to CaO, Al_2O_3, Na_2O and enriched in K_2O, MgO and incompatible elements. Lamproites contain Ti-phlogopite, Ti–K-richterite, Mg-olivine, diopside, leucite, and sanidine. They do not contain plagioclase or alkali-feldspar, melilite, monticellite, Ti-garnet or any feldspathoid other than leucite [157]. The K_2O content and K_2O/Ti_2O (0.8 to > 2) is like that observed in unevolved CROLs, but the CO_2 content (0.37 ± 0.24 wt% for $n = 91$, [155]) is significantly lower than in kimberlites and CROLs.

[4] *Lamprophyres*: mafic-to-ultramafic, ultrapotassic igneous rocks enriched in MgO, Na_2O, and K_2O that contain olivine, phlogopite, pargasite, Mg-hornblende, clinopyroxene, melilite, plagioclase, alkali-feldspar, feldspathoids, carbonates, monticellite, and perovskite [159]. Lamprophyres, like unevolved CROLs, are compositionally similar to kimberlites but contain higher Al_2O_3, FeO, and TiO_2 contents and lower SiO_2/Al_2O_3 and MgO/CaO ratios [155].

For the purposes of this review, we refer to such rocks as kimberlites, lamproites or lamprophyres, and in most cases as simply kimberlites to simplify description of

magmatic and eruptive systems responsible for the transport of diamond to the surface. In general, kimberlitic, lamproitic, and lamprophyric deposits are highly texturally and mineralogically variable depending on what part of the deposit (e.g., crater-, diatreme-, and hypabyssal-facies) is exposed and thus being examined, i.e., the degree of exhumation and erosion of the kimberlite pipe. Approximately 30% of kimberlites are diamondiferous, significantly more common than lamproites and lamprophyres all of which are significantly younger (on average 45 Ma to 1.2 Ga, [26]) than the diamonds they host and the Archean cratons they intrude. The youngest known kimberlite pipe located in Igwisi, Tanzania, erupted ~ 12,000 years ago [160].

3 Imperfections in natural diamond

Here, we define an *imperfection* in a hypothetical single crystal of diamond, D_c, as any substitutional atoms in D_c that are not carbon, any interstitial atoms in D_c including carbon, any mineral, melt or fluid inclusion in D_c, and/or any crystallographic feature of D_c that is not strictly given by the space-group symmetry, $Fd\,\bar{3}\,m$. Imperfections can be classified as *intrinsic* and *extrinsic* as follows:

Intrinsic: imperfections related to site vacancies, edge dislocations, plastic deformations, or interstitial carbon atoms. Intrinsic imperfections do not involve atoms other than carbon.

Extrinsic: imperfections related to impurities (e.g., N, H, and B).

Intrinsic and extrinsic imperfections influence the properties of diamond (Chapter 2) and can be grouped as *point-defects* and/or *extended-defects*. Point-defects describe imperfections that occur at a discrete location in the diamond crystal structure, typically displacing < 10 atoms (across 1 to 2 unit-cells) from their ideal positions in a perfect crystal of diamond. Examples of intrinsic point-defects in diamond include site vacancies (V) and interstitial carbon (C_i) atoms that occupy a position *off-center* with respect to the lattice point. The most common extrinsic point defect is single substitutional nitrogen (N_s) or interstitial nitrogen (N_i). Extended defects describe imperfections that consist of larger scale aggregates of impurities vacancies and/or edge dislocations. Lattice dislocations and loops (see below) are common examples of intrinsic extended-defects. The most common type of extrinsic extended-defect are *platelets*, planar features that consist of complex aggregations of N_s and C_i around vacancies.

Inclusions of any mineral, melt, or fluid may be regarded as a type of extrinsic extended-defect. However, as they may form under conditions unrelated to that of diamond formation and independent from crystallographic influence of the diamond (e.g., protogenetic inclusions), we discuss inclusions in a separate Sect. 3.3. There are an extremely large number of different imperfections in diamond, and in the following sections, we focus on those that are the most informative with regards to diamond genesis, growth, and residence in the mantle.

3.1 N, H, and B impurities and vacancies: point-defects

The most common impurities in natural diamond are N, H, B, Si, Ni, and Al [131] and trace concentrations of > 40 different elements have been measured in synthetic HPHT and CVD diamonds. Nitrogen is the most abundant impurity in natural diamond, the highest concentration is 3833 at.ppm [161], it is also arguably the most important, as it is the basis for the *Type* classification (Sect. 2.2.4) and allows for calculation of residence temperature or time. The median N content for peridotitic and eclogitic diamond is ~ 109 and ~ 454 at.ppm, respectively [134], and 24% and 10% of peridotitic and eclogitic diamonds are Type II, respectively [43], and thus contain no N or N at concentrations below detection. Most lithospheric diamonds are Type IaAB and IaA and, thus, have poorly aggregated N (< 50%B). Sub-lithospheric diamonds have significantly lower average N contents, ~ 70% are Type II, and > 90% have < 100 at.ppm N. However, when observed in sufficient concentrations, N defects show high degrees of aggregation (87% have > 50%B) in sub-lithospheric diamonds [6].

Nitrogen has five valence electrons, one more than carbon, and thus, N_s atoms produce areas of local strain in the diamond lattice. The incorporation of N_s (C-center, Fig. 10a Sect. 2.2.4) in its neutral charge state (N_s^0) results in three N–C bonds with neighboring C atoms and *lone-pair* electrons on N_s. The uncoupled electron of the fourth C (the *dangling bond*) forms a fourth weaker, longer (~ 26–32% longer than the other N–C bonds) N–C bond [162]. The extra, uncoupled (lone-pair) electron of the N_s forms a donor energy level in the band gap (1.7–2.2 eV below the conduction band at low N concentrations) which can be excited across the band gap and donated to the conduction band by visible light with energy $\geq$ 2.2 eV producing the characteristic yellow color of *Type Ib* diamonds (Fig. 7) [101]. For this reason, the N_s^0 defect is referred to as a *deep donor*, and once the uncoupled electron is donated, a N_s^+ defect is formed with four identical N–C bonds [101]. Free electrons in the conduction band may be trapped by other N_s^0 or B_s^0 defects to form N_s^- and B_s^- defects, respectively [101]. A large number of defects involving N_s (e.g., N_2, NV, N_4V, etc.) and N_i (e.g., N_i, N_{2i}) have been observed by various spectroscopic methods and are described in detail by [131].

Hydrogen is ubiquitous in natural diamond and plays a crucial role in the nitrogen aggregation processes and in the synthesis of CVD diamond. Nuclear reaction analyses have shown that the H content of diamonds is between 500 and 3500 at.ppm [163] and ion-beam analyses suggest that atomic H could reach concentrations of 1 at wt% [164]. Compared to nitrogen, there is much less work on H-related defects in diamond and the assignment of such defects to specific vibrational modes and IR absorption frequencies remains largely speculative. However, recent quantum mechanical investigations have shown that interstitial hydrogen may occur as singular H or dimeric H_2 in diamond (e.g., [165]). Interstitial H atoms in the neutral, negative, or positive charge states may occupy a *bond-centered-* (BC), *anti-bonding-* (AB), *tetrahedral-* (T), *hexagonal-* (H), and/or *C-site* in diamond (Fig. 12) where the bond-centered site has been shown to be energetically favorable regardless of charge state [165, 166]. Interstitial H_2 dimers may comprise (a) both H atoms passivating a broken C–C bond, (b) both H atoms at T-sites, (c) one H atom at the BC-site and one at the AB-site, and (d) one H atom

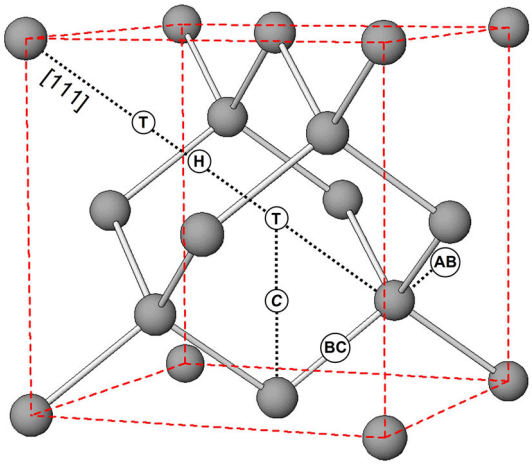

Fig. 12 The crystallographic positions of interstitial H and H_2 dimers in the crystal structure of diamond. Interstitial H atoms in the neutral, negative, or positive charge states may occupy a *bond-centered-* (BC), *anti-bonding-* (AB), *tetrahedral-* (T), *hexagonal-* (H) and/or *C-site*. Interstitial H_2 dimers may comprise (1) both H atoms passivating a broken C–C bond, (2) both H atoms at T-sites, (3) one H atom at the BC-site and one at the AB-site, and (4) one H atom at the T-site and one at the H-site. Structure generated from ATOMS V6.4 with data from Straumanis and Aka [89]

at the T-site and one at the H-site, (c) is the most energetically favorable [165–168]. However, no definitive assignment of IR absorption features to interstitial H has been made for natural diamonds. H concentrations measured using bulk techniques (e.g. nuclear reaction analysis) are typically higher than H concentrations estimated using spectroscopic data, suggesting large quantities of H in diamond are IR-inactive and thus occupy positions with null (or negligible) dipole moments. It is likely that the majority of optically-active H is involved in the passivation of defects related to N, B and vacancies, apart from perhaps CVD diamonds where H_2 is used as the primary source gas. In any defect in which dangling bonds on carbon are formed, H passivation by formation of C–H bonds stabilizes the defect and may prevent further H and N aggregation.

Boron is extremely rare in diamond and typically reported at concentrations ≤ 0.5 at.ppm; however, some diamonds (e.g., the Hope Diamond) have B contents in the 1–10 at.ppm range [169]. Boron has three valence electrons, one less than carbon and thus acts as an electron *acceptor*. The substitution of C for B creates electron holes in the band gap which can accept electrons from the valence band from donor impurities such as N (Fig. 7). These electron holes can move throughout the crystal and increase its conductivity, and akin to vacancy-nitrogen defects, B_s^0 defects have been shown to trap H in *p*- and *n*-type semiconductor CVD diamonds [170, 171]. A growing number of defects, primarily associated with N, H, and vacancies, have been assigned to signals detectable via UV–visible, FTIR, Raman, electron paramagnetic resonance (EPR), and cathodoluminescence (CL) spectroscopy [131] and even more have been described based on density-functional theory (DFT) and associated first-principals simulations of FTIR and Raman spectra [132, 172–176].

3.1.1 FTIR spectroscopy: vacancy-nitrogen–hydrogen point-defects

Selected vacancy-nitrogen–hydrogen defects in diamond are listed in Table 1. Most of these defects have yet to be recognized in experiment, others have been described by DFT calculations but have simulated intensities below of the detection limit of any current spectroscopic techniques and/or are obscured by other more intense peaks (e.g., [173, 177]). The most common and well-understood defect families observed in natural diamond are N_x ($x = 1$–2), VN_x ($x = 1$–4), and VN_xH_y [$x = 1$–3 and $y = 1$–(4–x)] defects [177]. Absorption of IR light occurs at frequencies associated with C–H, and N–H stretching and bending vibrations, each of which may correspond to several different vibrational modes. Additional properties, such as isotopic composition (e.g., ^{14}N vs. ^{15}N), charge state, and the quantum spin-state, influences the position of peaks in the IR. Detailed descriptions of N-, H-, and vacancy-related defects and their corresponding signal observed in the IR are given by [131, 178–180].

The concentrations of the most common defects: C-centers (N_s), A-centers (N_2), and B-centers (VN_4) can be calculated, specifically the concentration of A- and B-centers ($[N_A]$ and $[N_B]$) and %B to group diamonds according to the *Type classification* system (Sect. 2.2.4). However, most natural diamonds contain detectable amounts of both A- and B-centers, and thus, the corresponding signal in the one-phonon region of the FTIR spectrum must be deconvoluted before %B can be calculated, and a

Table 1 Selected vacancy-nitrogen–hydrogen defects that may occur in diamond

V, N_x and H_y	$V_{1\text{-}2}$	N_x ($x = 1$–2)	H_y ($y = 1$–2)
	V	N (C-center)	H (interstitial)
	V_2	N_2 (A-center)	H_2 (interstitial)
VH_y, VN_x and NH_y	VH_y ($y = 1$–4)	VN_x ($x = 1$–4)	NH_y ($y = 1$)
	VH	VN	NH
	VH_2	VN_2	
	VH_3	VN_3 (N3-center)	
	VH_4	VN_4 (B-center)	
VN_xH_y	VNH_y ($y = 1$–3)	VN_xH ($x = 1$–4)	VN_xH_y ($x = 2$, $y = 2$)
	VNH	VNH	VN_2H_2
	VNH_2	VN_2H	
	VNH_3	VN_3H	
		VN_4H	

Although not specified in this table, each defect may occur in neutral, positive, and negative charge states, different quantum spin-states and with different isotopic compositions, all of which may shift the position (cm^{-1}) of corresponding band in the FTIR spectrum (e.g., [177]). This table does not contain all possible vacancy-nitrogen–hydrogen defects; readers are referred to [131, 177, 180] and references therein for description of other defects

Type can be assigned to the diamond. It is important to note that most calculations do not involve C-centers as it is assumed that all C-centers aggregate to A-centers before any of the A-centers aggregate to B-centers [181, 182], and this is typically the case in natural diamonds. Deconvolution involves (1) normalizing spectra to a specific sample thickness by scaling absorption to a specific value at a particular peak in two-phonon region (*i.e.,* at 1992 cm^{-1}), (2) least-squares fitting of the spectra to a normalized Type IIa reference spectra to a produce a *corrected spectra*, and (3) least-squares fitting of the one-phonon region to reference spectra of A- and B-centers using a pseudo-Voigt function [183]. Deconvolution is typically conducted using the CAXBD97n Excel spreadsheet (David Fisher, Da Beers Technologies, Maidenhead), the QUIDDIT program [183], or the DiaMap software [184]. After deconvolution and the production of corrected spectra, $[N_B]$ and $[N_A]$ (and thus %B), are easily calculated using the known absorption coefficients for each defect center.

The N-aggregation sequence C → A → B behaves according to a second-order rate equation [182, 185] and is significantly more sensitive to temperature than time [181]. Therefore, the calculated N-aggregation state of a diamond with known formation and exhumation ages can be used as a geothermometer. The calculated temperature represents a *model temperature* in the mantle where the diamond resided after growth because temperature fluctuations can be not calculated as an average as N-aggregation rate and temperature are not linearly correlated over time. This geothermometer (see [186]) allows one to produce plots of total N content vs. %IaB in which isochrons can be plotted for different ages and ranges of residence temperatures (e.g., Figure 13a) or for temperature vs. time plots in which the N-aggregation state (degree of C → A or A → B) may be plotted (Fig. 13b). According to the second-order rate equation [182, 185], it would take a diamond with 1000 at.ppm N, 10 Ma at 950 °C (or 0.1 Ma at 1050 °C) for 10% of the N to aggregate to C-centers and ~ 100 Ma at 1150 °C (or billions of years at ~ 1000 °C) for 1–2% of the N to aggregate to B-centers.

The general deconvolution routine described above also involves fitting peaks associated with D-centers (due to platelets, see Sect. 3.2) and the 3107 cm^{-1} peak (Fig. 14) (referred to here as the H' peak) due to C–H stretching associated with the VN_3H defect [187]. Early studies attributed the H' peak to N–H stretching, but this was later discounted as substitution of $^{14}N_s$ for $^{15}N_s$ does not result in peak shifting and, thus, the H' peak must be due to C–H stretching [188]. The H' peak and the corresponding C–H bending peak at 1405 cm^{-1}, is ubiquitous in *Type Ia* diamonds and can be extremely intense, with absorption values larger than peaks due to intrinsic lattice vibrations in the two-phonon region. Although > 90 peaks observed in IR (and UV–vis) spectra have been associated with H-related defects (e.g., [131, 178, 180]), the peak at 3107 cm^{-1} is arguably the only H-related peak that has been definitively assigned to a specific defect configuration [187]. Consequently, the H' peak has become the topic of many recent works related to H diffusion (see, [180] and references therein), chemical kinetics of VNH defects [101], H passivation and trapping (e.g., [189]), and the calculation of H concentrations in diamond via FTIR spectroscopy. From a geological perspective, studies of the H' peak and H-related defects in diamond may provide crucial information about the role of H species (e.g., CH_4, H_2O, H_2, etc.) in fluids and melts related to diamond formation and about the sources and cycling of H and H_2O in the upper and lower mantle through time (e.g., [92]). The VN_3H defect consists of an

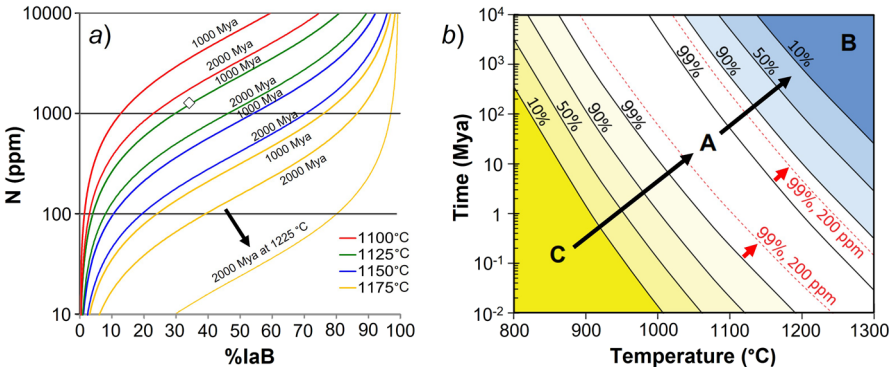

Fig. 13 **a** A plot of total N content (ppm) as a function of %IaB showing mantle residence isotherms for temperatures of 1100 °C (red), 1125 °C (green), 1150 °C (blue), and 1175 °C (orange) each of which for residence times of 1000 and 2000 Mya. To emphasize the relatively strong effect of residence temperature compared to time on N-aggregation, an additional isotherm is plotted for 1225 °C and 2000 Mya (shown with black arrow). A single diamond composition has been plotted (white diamond) as an example. **b** A plot of time (Mya) as a function of temperature (°C) showing the progression of N-aggregation from C-centers (yellow area) to A-centers (white area) and eventually to B-centers (blue area) shown with the black arrows. Differences in aggregation state are defined as the percent of N in A-centers (e.g., 99 to 10%) and are calculated (and shown with black lines) for N concentrations of 1000 at.ppm. Red dashed lines are calculated for 99% A-centers at N concentrations of 200 at.ppm to demonstrate that diamonds with lower N concentrations require higher temperatures or longer times to reach the same degree of N-aggregation compared to those with higher N concentrations; such temperature and time differences are shown with red arrows; **a** generated with the *DiaMap software* [184]. See Weiss et al. [52] (Fig. 2) for details regarding the parameters used in the calculation for **b** which is modified from Weiss et al. [52]

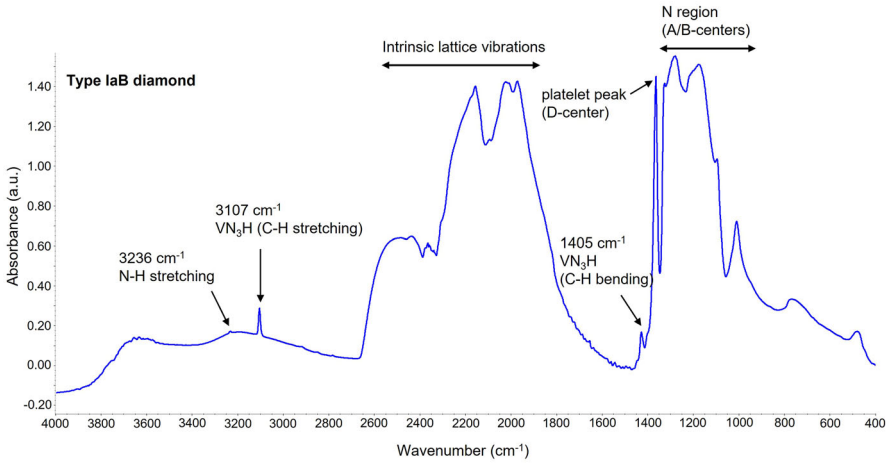

Fig. 14 The FTIR spectra of a *Type IaB* diamond showing absorption in the one-phonon, N-region due to A- and B-centers, the platelet peak at ~ 1378 cm^{-1} (D-center), absorption in the two-phonon region due to intrinsic lattice vibrations, the 3017 cm^{-1} (H' peak) and 1405 cm^{-1} peaks due to C–H stretching and bending, respectively, associated with the VN_3H defect, and the 3236 cm^{-1} peak which has yet to be definitively assigned a defect configuration but may be due to N–H stretching

N3-center, three N_s around a vacancy, in which H forms a C–H bond to passivate the dangling bonds of the fourth C [187]. It follows that trapping of a H atom by an N3-center (VN_3) may be the dominant mechanism by which VN_3H defects are produced [180]. However, it has been shown both theoretically and experimentally (in HPHT) diamonds that VNH defects may trap A-centers (N_2) to produce VN_3H defects [187, 190]. Regardless of the aggregation sequence responsible for the formation of VN_3H defects, it is evident that H plays an important role in quenching N aggregation. This relationship has been evaluated in detail through comparison of peak intensities and defect concentrations by [180, 187, 191, 192].

Other relatively intense peaks in the IR that have been assigned to H-related defects include the 2786 cm^{-1} and 3236 cm^{-1} peaks (Fig. 14). The intensity of the 2786 cm^{-1} peak shows some correlation with the 3107 cm^{-1} peak and has been attributed to an overtone of the 1405 cm^{-1} C–H bending mode of the VN_3H defect [180, 187]. Other peaks observed at 4167 cm^{-1}, 4496 cm^{-1}, 5555 cm^{-1}, 5880 cm^{-1}, and 6070 cm^{-1} also have intensities that correlate with that of the 3107 cm^{-1} peak and are attributed to various overtone and combination bands of the VN_3H defect. The 3236 cm^{-1} peak is most commonly observed in Type IaB diamonds and often not observed in diamonds with low N content [178]. The intensity of the 3236 cm^{-1} peak shows no correlation with the intensity of the 3107 cm^{-1} peak and thus has been attributed to N–H stretching as opposed to C–H stretching [179, 180, 188]. If this was the case, one would also expect a N–H bending mode at ~ 1600 cm^{-1} which has not been observed. An inverse correlation between the intensity of the 3236 cm^{-1} peak and the D-center (platelet) peak has been observed and Gu et al.[173] suggests that this peak may be associated with N–H stretching associated with a platelet-centered VN_4H defect. This defect would form by H trapping by a B-center (VN_4) and has important implications for platelets acting as H reservoirs in diamond as discussed in Sect. 3.2.

3.2 N and H impurities and vacancies: extended-defects

All extended-defects are inherently related to combinations of intrinsic and extrinsic point-defects. For example, irradiation can eject a C atom from its site to produce C_i and vacancies which migrate and coalesce with increasing mantle residence time and temperature. These areas of aggregated point-defects (interstitials and vacancies) are relatively susceptible to plastic deformation (shear stress) that may result in mechanical twinning and edge dislocations depending on the temperature. In response to increasing shear stress, edge dislocations will propagate through the diamond structure (Fig. 15a–c). Due to the cubic symmetry of diamond, two sets of dislocations may occur along [111] slip planes parallel to the octahedral face, *shuffle* and *glides* sets [193–195]. Shuffle and glide sets describe edge dislocations along planes in which C–C bonds of the same and different indices are broken, respectively (Fig. 16) [196]. As is the case with N_s and B_s, dislocations involve breaking of C–C bonds and the formation of dangling bonds which may act to trap other impurities such as H. This structural description of dislocations in diamond masks a wealth of complexity and readers are referred to the above references for a more detailed description. Edge dislocations propagate and combine to form dislocation loops and mosaic networks

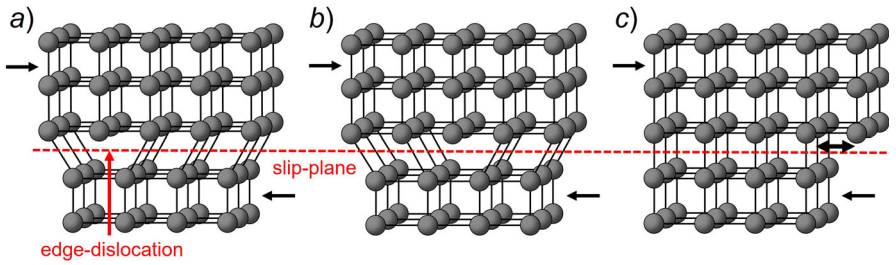

Fig. 15 The propagation of **a** an edge dislocation due to shear stress (black arrows) along a slip plane from the left side of a simplified cubic lattice to **b** a central position and eventually **c** through the lattice where the net slip distance is shown with a double-ended arrow

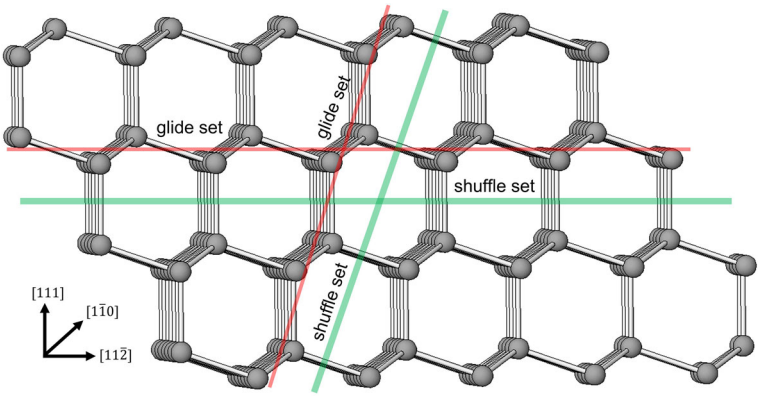

Fig. 16 The two types of dislocation sets that commonly occur in diamond, the *shuffle sets* (along planes shown in green) and the *glide sets* (along planes shown in red) in which the C–C bonds of the same and different crystallographic indices are broken, respectively. Structure generated from ATOMS V6.4 with data from Straumanis and Aka, [89]

which are characteristic internal features in Type IIa and IIb diamonds, often observed via CL spectroscopy (e.g., [53, 113]). In Type I diamonds, N impurities increase the yield strength of diamond and primary growth features are often preserved even where there is evidence of plastic deformation.

Platelets are the most common type of extended-defect observed in natural diamond and consist of thin regions of C_i, N_s and vacancies that occur in the [100] plane [180, 197, 198]; however, recent works suggests that platelets consist primarily of C_i [199]. Platelets, commonly referred to as the D-center, give rise to a characteristic peak in the IR (the B' peak) observed at 1358–1378 cm^{-1} (Fig. 14) [135] where the exact peak position and width varies as a function of platelet shape (short or elongate), size (diameter), and density [192, 200]. For example, Goss et al. [197] showed that increasing platelet size is accompanied by a downward frequency shift of the B' peak. It is now widely accepted that platelet formation is related to the production and accumulation of C_i as a biproduct of various N-aggregation sequences. As described

in Sect. 2.2.4, N_s defects (C-centers) aggregate with other N_s defects and vacancies to produce A- and B-centers. The first and simplest mechanisms proposed for production of C_i and platelets involves the combination of two A-centers (N_2) (1) to form a B-center (VN_4) as follows:

$$N_2 + N_2 \rightarrow VN_4 + \mathbf{C_i}. \tag{1}$$

Additional aggregation sequences [(2) and (3)] may produce C_i but requires one to assume A-centers migrate as dissociated N_s (rather than N_2) as suggested by [201, 202], e.g., $N_2 \rightarrow N_s + N_s$ (dissociation of A-center)

$$N_s + N_s + N_2 \rightarrow VN_4 + \mathbf{C_i} \tag{2}$$

or

$$N_s + N_2 = VN_3(\text{N3-center}) + \mathbf{C_i}. \tag{3}$$

However, ab-initio calculations by Goss et al. [197] suggest that these aggregation processes alone are not sufficiently fast to produce platelets observed in some experiments and propose a growth mechanism related to the formation of dislocations and subsequent production of mobile VN_2 defects that combine with A-centers to produce C_i. FTIR studies suggest that these aggregation sequences [and (2)] are responsible for platelet formation and growth as there is a linear correlation between the intensity of the B-center peak (and $[N_B]$) and the B' peak. Such diamonds are referred to as *regular diamonds* [199]. In other diamonds, referred to as *irregular diamonds*, there is minimal correlation between the intensity of the B-center and B' peaks as platelets degrade with increasing residence time and temperature [199]. Speich et al. [192, 199] have shown that degradation proceeds according to a first-order rate equation and have proposed methods to calculate the degree of platelet degradation and annealing temperature of irregular diamond during residence in the mantle. Platelet compositions with considerable H contents have been observed [173], particularly in degraded platelets, suggesting that H incorporation may quench platelet growth [180]. By taking into account the aggregation and degradation rate of platelets and the $[N_B]$ of the diamond, methods to reconstruct the thermal history of the diamond during residency in the mantle have been developed [192, 199].

3.3 Mineral, fluid, and melt inclusions

Inclusions are the most informative imperfection in natural diamond. Since the earliest rigorous analytical work on inclusions in the 1960s (e.g., [135, 203]), the study of inclusions in diamond have driven continued development of models for diamond formation from C-bearing fluids in cratonic mantle keels and the deeper convecting mantle [6, 42, 88, 134, 204–206].

Approximately 1% of diamonds contain minerals inclusions [42] which can be grouped as *protogenetic*, *syngenetic,* and *epigenetic* based on whether they crystallized before, during, or after diamond formation, respectively. For decades, classical

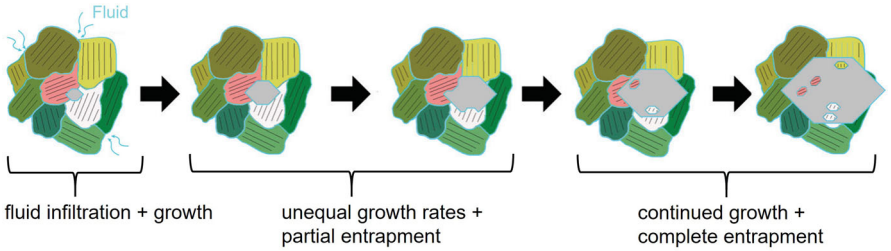

Fig. 17 A schematic showing the infiltration of diamond-forming C–O–H fluids into a cumulate mantle substrate and the subsequent growth of a diamond at the grain boundary of pre-existing mineral grains. With continued growth, diamond faces grow at unequal rates and begin to partially surround mineral grains until they are completely entrapped by the diamond. Note how mineral inclusions have the same morphology as the diamond and retain their original crystallographic orientation (shown with blue lines in each inclusion). Modified from Angel et al. [219]

thermobarometric work was conducted under the assumption that all inclusions grew syngenetically with their host diamond (formed from the same chemical reaction) and, in some cases, were later altered by epigenetic processes [108]. This was assumed based on the encapsulating diamond imposing its morphology on the inclusion minerals which typically appear octahedral and cubo-octahedral regardless of their crystal symmetry [207–209].

However, relatively recently, it was shown that inclusions may be protogenetic and form before their host diamond [210, 211], such inclusions represent minerals that comprise mantle lithologies into which diamond-forming fluids infiltrate and react (metasomatize) and are included during diamond growth, as shown in Fig. 17. This has been shown for several common inclusion minerals with diamond-like morphologies such as olivine, clinopyroxene, garnet, and magnesiochromite [210, 212–216]. These types of analyses often rely on *Crystallographic Orientation Relationships* (CORs), which describe the orientation relationship between (1) individual inclusion minerals, and (2) between the inclusion minerals and their host mineral (diamond) [217–219]. The above description masks a wealth of complexity, and in some cases, syngenetic inclusions may form from distinct processes (different chemical reactions) than their host diamonds (i.e., synchronous inclusions, [212]). Accurate determination of syngenesis or protogenesis has major implications for interpretations of geobarometric and geochronological data and readers are referred to the following references for a detailed explanation of syngenetic, protogenetic, and epigenetic inclusions [210, 212, 215, 219, 220].

3.3.1 Mineral inclusions in lithospheric diamonds

Most mineral inclusions in lithospheric diamonds appear as cubo-octahedral, range in size from nanometers to hundreds of microns and may occur as single crystals and/or crystal aggregates and/or polycrystalline material of the same or different minerals. Inclusions often act as loci for plastic or brittle deformation (Sect. 3.2), often observed as graphitized fractures around inclusions.

Of the mineral inclusions characterized in lithospheric diamonds by Stachel and Harris [42] and Pamato et al. [221], 32% are garnet, [$(Mg,Fe,Ca)_3(Al,Cr)_2Si_3O_{12}$]; 16% are olivine, [$(Mg,Fe)_2SiO_4$]; 16% are Cr-spinel, [$(Mg,Fe)(Cr,Fe,Al)_2O_4$]; 15% sulphides, primarily pyrrhotite (FeS) with subordinate pentlandite [$(Fe,Ni)_9S_8$] and chalcopyrite ($CuFeS_2$); 13% clinopyroxene, [$(Ca,Na,Mg,Fe,Al)_2Si_2O_6$]; 7% orthopyroxene [$(Mg,Fe,Ca)_2Si_2O_6$]; ~ 1% rutile, ($TiO_2$), and coesite, ($SiO_2$). While the mineral inclusions listed above are the most abundant, many other mineral inclusions have been observed in lithospheric diamonds (e.g., ilmenite, phlogopite, zircon, and calcite), although typically comprise < 1% of inclusions [134].

The most common mineral inclusions in lithospheric diamond are in accord with the mineralogical bulk composition of the upper mantle, largely meta-peridotitic (i.e., pyrolitic). However, inspection of Fig. 2 reveals major differences between the abundance of mineral inclusions in lithospheric diamond (as listed above) and those expected for the dominant upper mantle lithologies (e.g., meta-harzburgitic, meta-lherzolitic, and meta-basaltic rocks) some of which may be due to the fact that inclusions in diamonds of all parageneses are included above. When considering individual parageneses, the abundance of some mineral inclusions in diamond are in accord with the predicted abundance of that mineral for the corresponding mantle lithology. For example, ~ 12% of observed inclusions in peridotitic (harzburgitic, lherzolitic, and wehrlitic) diamonds are orthopyroxene [42] and primitive mantle peridotite is predicted to comprise ~ 15% orthopyroxene (Fig. 2); this small overestimation may be explained by the instability of orthopyroxene in peridotitic assemblages at depths > 280 km [70]. For other inclusions, namely olivine and garnet, observed abundances of inclusions in diamonds of known paragenesis are significantly different than those predicted for the corresponding mantle lithology. For example, 62% and 16% of inclusions are garnet and olivine in peridotitic diamonds, respectively [42], and primitive mantle peridotite is predicted to comprise ~ 17% garnet and ~ 58% olivine (Fig. 2) [70]. If one assumes entrapment of minerals by diamond occurs randomly, then peridotitic diamond-forming substrates must be enriched in Cr-spinel, sulphides, and garnet and depleted in olivine. Otherwise, one must assume the mode by which minerals are entrapped by diamond is non-random. Common mineral inclusions in peridotitic diamonds are shown in Fig. 18.

As discussed in Sect. 2.2.5, peridotitic diamond substrates are typically melt-depleted and eclogitic diamond substrates are sourced from slab environments in subduction settings. A deeper understanding is gleaned by comparison of major- and trace-element data from inclusions in diamond, representative of the diamond substrate, and mantle xenoliths, representative of the cratonic lithospheric mantle. Analysis of garnet peridotite xenoliths shows the proportion of harzburgite to lherzolite is 18:82%, effectively the inverse determined from peridotitic inclusions in diamonds suggesting that harzburgite may serve as the primary diamond substrate in the cratonic mantle [134]. In general, major-element geochemistry of Mg/Fe^{2+} in olivine, Cr/Al and Na/Ti enrichment in garnet, cpx and opx, and REE trends of peridotitic substrates and mantle xenoliths supports the preference for diamond formation in melt-depleted peridotitic (harzburgitic) substrates followed by episodic metasomatic events involving re-enrichment of depleted peridotitic substrates and diamond formation. Moreover, similar Mg# ($Mg/[Mg + Fe^{2+}] \times 100$) of olivine inclusions in

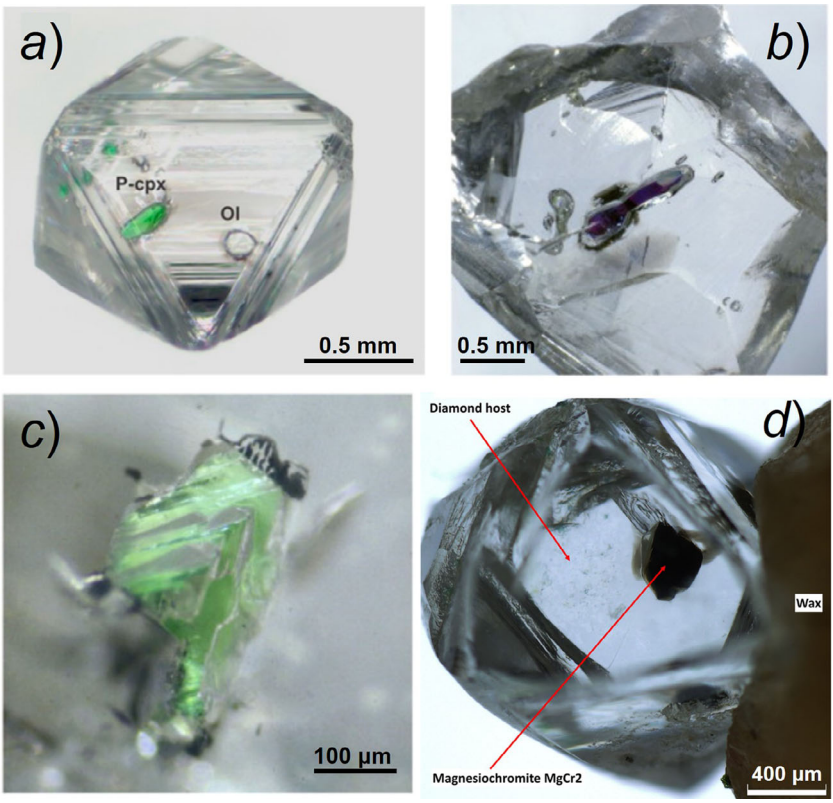

Fig. 18 Mineral inclusions in peridotitic lithospheric diamonds, **a** clinopyroxene and olivine in an octahedral diamond, **b** Cr-pyrope garnet, **c** clinopyroxene, and **d** magnesiochromite. Modified from **a** Kalugina and Zedgenizov [463], **b** Stachel and Harris, [42], taken by Anetta Banas (University of Alberta), **c** Stachel and Harris, [42], taken by J.W. Harris **d** Nestola et al. [214]

diamond and outside the diamond in the associated xenolith suggests that the diamond substrate is the primary control on the crystal chemistry of inclusions in diamond as opposed to the diamond-forming fluid or melt [134].

Eclogitic diamonds are characterized by predominately garnet and clinopyroxene inclusions (Fig. 19) with the addition of orthopyroxene for websteritic diamonds [42]. In general, picritic–basaltic rocks from subducted oceanic crust are considered the dominant protolith of diamondiferous eclogite xenoliths [13, 222] and evidence for this from inclusions in diamond is discussed in Sect. 2.2.5. The lithologic diversity of the subducted oceanic crust is reflected in the variable major- and trace-element compositions of inclusions observed in eclogitic diamonds. In general, eclogitic mineral assemblages are representative of the more mafic Archean-to-early Proterozoic oceanic crust. The Na, Ca, and Mg# of garnet inclusions in eclogitic diamonds suggest involvement of different igneous protoliths, such as clinopyroxene gabbroic cumulates (High Ca and Mg# in garnets) and olivine (± orthopyroxene) cumulates, and extrusive protoliths, such as ocean-floor basalts (low Ca garnets) [13, 42, 143, 223]. The bulk

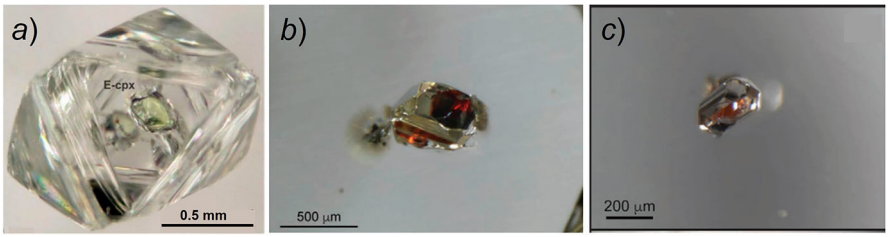

Fig. 19 Mineral inclusions in eclogitic lithospheric diamonds, **a** clinopyroxene in an octahedral diamond, **b** orange eclogitic garnet, and **c** orange and red eclogitic garnet. Modified from **a** Kalugina and Zedgenizov, [463] and **b**, **c** Harris et al. [108], images **b**, **c** from Karen Smit

rock REE pattern of inclusions in eclogitic diamonds is in accord with a primarily basaltic protolith and depletions in LREEs (but similar HREE values with respect to N-MORB) suggest partial melting and dehydration of the slab during subduction [42, 224, 225]. For detailed descriptions of the major- and trace-element and isotopic compositions and petrogenetic interpretations of individual mineral inclusions in lithospheric diamonds, readers are referred to [42, 134, 144].

3.3.2 Mineral inclusions in sub-lithospheric diamonds

Compared to lithospheric diamonds, the study of sub-lithospheric diamonds and their mineral inclusions has developed much more recently and hypotheses for the formation of mineral inclusions in SDDs are still strongly debated. Thus, a more detailed description, of the common mineral inclusions in SDDs, compared to that given above for lithospheric diamonds, is given below. As shown in Sect. 2.2.5, SDDs can be approximately grouped based on their mineral inclusions and the corresponding depths of formation. Based on the global database given by Walter et al. [6], inclusions observed in SDDs are 42% ferropericlase, $(Mg_{1–0.51}Fe_{0–0.49})O$ (or (magnesio)wustite, $(Fe_{1–0.51}Mg_{0–0.49})O$); 32% majoritic garnet, $Mg_3(MgSi)(SiO_4)_3$ or Na-majorite garnet, $(Na_2Mg)Si_2(SiO_4)_3$; 8% breyite, $CaSiO_3$; 8% enstatite (or former bridgmanite), $MgSiO_3$; 6% clinopyroxene, $XY(Si,Al)_2O_6$; 4% olivine (or former wadsleyite or ringwoodite), $(Mg,Fe)_2SiO_4$; and > 1% coesite (or former stishovite), SiO_2; calcium ferrite structured phase (CF), XY_2O_4 (X = K, Na, Ca, Mg; Y = Al, Si); new aluminous phase (NAL), $AX_2Y_6O_{12}$ (A = K, Na, Ca; X = Mg, Fe; Y = Al, Si) and many other inclusions at abundances < 1% such as jeffbenite ($Mg_3Al_2Si_3O_{12}$) [6, 226]. Like inclusions in lithospheric diamonds, inclusion minerals in SDDs are predicted in the modal mineralogy of meta-peridotitic and meta-basaltic lithologies at depths corresponding to the transition zone and lower mantle. However, they are observed in abundances inconsistent with the abundances of phases assumed to comprise these mantle lithologies (Fig. 2) (see [70]). It follows that either the deeper mantle is geochemical distinct or heterogenous with respect to its modal mineralogy or, more likely, that particular phases are preferentially included (or preserved) by SDDs [6, 227, 228]. Nevertheless, SDDs are commonly assigned meta-peridotitic (i.e., pyrolytic assemblages) and

meta-basaltic (i.e., MORB assemblages) parageneses where the former contains high-Cr majoritic garnet, low-Ti $CaSiO_3$, and low-Al, high Mg# $MgSiO_3$ and the latter contains low-Cr majoritic garnet, high-Ti $CaSiO_3$, high-Al, low Mg# $MgSiO_3$, and CF and NAL phases [6, 70, 88].

Ferropericlase, or more accurately, periclase, MgO (as defined by the International Mineralogical Association, IMA) forms a solid solution with wustite (FeO), and is often observed as iridescent inclusions in almost exclusively SDDs and are the most widely used indicator for a sub-lithospheric origin (Fig. 20d). Ferropericlase is stable at all pressures in the lithosphere and mantle and its composition (i.e., Mg#) is not dependent on temperature, and thus, ferropericlase cannot be used as a single-mineral barometer or thermometer [3, 66, 228–231]. The Mg# of ferropericlase inclusions ranges from 0.15 to 0.95; of the observed ferropericlase inclusions, 0.4% (one inclusion) have Mg# = 0.94, 60.2% have 0.90 < Mg# < 0.80, 36.1% have 0.79 < Mg# < 0.51, and 3.3% have 0.49 < Mg# < 0.12 [6]. This is in stark contrast with the much more restricted range of Mg#, 0.83 to 0.95 (*i.e.,* Fe-poor), of ferropericlase synthesized from lower mantle assemblages [6, 232–236].

To explain this discrepancy, Lorenzon et al. [237] analyzed 57 ferropericlase inclusions in 37 diamonds and showed that there are two populations of ferropericlase,

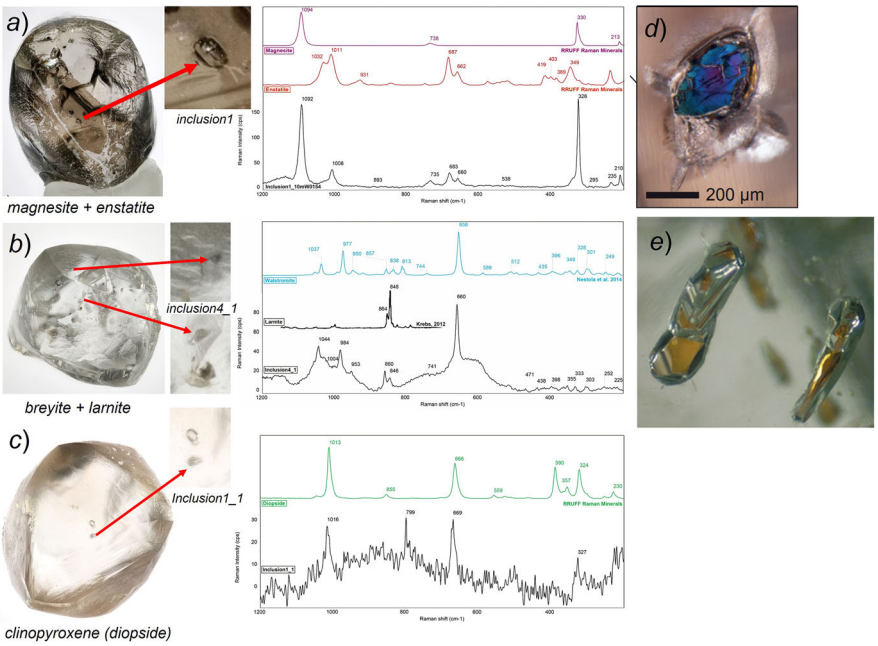

Fig. 20 Examples of sub-lithospheric diamonds that contain different inclusions, **a** a composite inclusion of magnesite and enstatite, **b** two composite inclusions of breyite (walstromite) and larnite, and **c** an inclusion of clinopyroxene (diopside), the Raman spectra for **a**–**c** are shown in black and the reference spectra used to identify these phases are shown above in color. **d** An iridescent inclusion of ferropericlase, and **e** an orange inclusion of majoritic garnet. Modified from **d** Smith et al. [464] and **e** from Anetta Banas (University of Alberta), taken by J.W. Harris (University of Glasgow)

one relatively Fe-rich and Mg-poor (Mg# < 0.70) (magnesiowustite), and a second that is Fe-poor and Mg-rich (Mg# > 0.80). Evaluation of the *Crystallographic Orientation Relations* (CORs) (see Sect. 3.3) of these inclusions showed that low Mg# ferropericlase have a non-random orientation with respect the host diamond indicating a *potential* syngenetic origin (co-crystallization of ferropericlase and diamond). Higher Mg# ferropericlase have a random crystallographic orientation with respect to the host diamond indicating a protogenetic origin (crystallization before diamond formation). To explain these observations, Lorenzon et al. [237] proposed a dual origin for ferropericlase involving potentially syngenetic growth of low Mg# (Fe-rich) ferropericlase and diamond in the upper mantle where diamond formation is likely associated with fluids derived from subducted slab materials and entrapment of protogenetic (pre-existing) high Mg# ferropericlase in the lower mantle. An upper mantle, subduction-related origin for low Mg# ferropericlase is supported by the Fe^{3+} contents and calculated f_{O2} (based on $Fe^{3+}/[Fe^{2+} + Fe^{3+}]$) of some low Mg# ferropericlase inclusions suggestive of an oxidized subducted material reacting with reduced meta-peridotites to produce magnesiowustite and diamond [3, 68, 238–240].

Ideal end-member majoritic garnet (Fig. 20e) is characterized by four Si^{4+} atoms per formula unit (*apfu*) rather than three Si^{4+} *apfu* as observed in lithospheric garnets. However, as natural majoritic garnet never contains $Si^{4+} = 4$ *apfu*, one can more simply describe this mineral as having $Si^{4+} > 3$ *apfu*. Majoritic garnet inclusions have compositions between end-member majorite, $Mg_3(MgSi)(SiO_4)_3$ [241, 242] and Na-majorite, $(Na_2Mg)Si_2(SiO_4)_3$ [243, 244] which are commonly associated with meta-peridotitic and meta-basaltic parageneses, respectively [245]. Majoritic garnets often fall into two compositional groups: (1) *low-Cr majoritic garnet* with Cr_2O_3 < 1 wt% and relatively low Mg# (< ~ 0.70) and (2) high-Cr majoritic garnet with Cr_2O_3 = 1–20 wt%, low CaO (< 6 wt%) and relatively high Mg# (> 0.70–0.80). The composition of majoritic garnet synthesized from meta-basaltic and meta-harzburgitic assemblages is in accord with the compositions of low-Cr and high-Cr majoritic garnet [3, 6].

Inclusions of stoichiometry, ABO_3 are most often observed as breyite ($CaSiO_3$) (Fig. 20b) and enstatite ($MgSiO_3$) (Fig. 20a) but may also be observed as perovskite ($CaTiO_3$) and wollastonite ($CaSiO_3$) [246]. In general, $CaSiO_3$ inclusions fall into two distinct groups, with high and low-Ti contents [6] but show significant differences in terms of MgO, Al_2O_3, and FeO contents compared to $CaSiO_3$ inclusions from experiments [3, 6, 234–236, 247, 248]. $MgSiO_3$ inclusions are often grouped based on their Al_2O_3 content where low-Al $MgSiO_3$ inclusions have low CaO contents and high Mg# consistent with depleted lithologies such as harzburgite. The major-element chemistry of high-Al $MgSiO_3$ is not as well constrained but low Mg# in some inclusions is consistent with bridgmanites synthesized from meta-basaltic assemblages [67, 151, 249].

Several high P/T experiments in meta-peridotitic and meta-basaltic substrates have produced the perovskite-structured phases, $MgSiO_3$ (bridgmanite), and those along the $CaTiO_3$-$CaSiO_3$ join [242, 250–253]. Such experiments and observations of composite inclusions of partially exsolved $Ca(Si,Ti)O_3$ polymorphs, such as breyite ($CaSiO_3$) and $CaTiO_3$-perovskite, have led to the general acceptance that breyite [254] (and potentially other $CaSiO_3$ polymorphs, *i.e.,* wollastonite [113, 246]) may form from

retrogression of perovskite [67, 70, 88, 151, 246, 254–261]. However, such assumptions do not preclude a lower pressure origin of breyite inclusions in environments shallower than the transition zone, this is supported by evidence for primary breyite inclusions [254, 257, 262] or low-pressure crystallization of $CaSiO_3$-perovskite [66, 254, 258, 262, 263].

Although no $MgSiO_3$-enstatite have been observed (yet) in association with $MgSiO_3$-perovskite (bridgmanite), some authors have proposed that enstatite inclusions in SDDs may also form by retrogression of bridgmanite [67, 151, 261, 264]. Such assumptions generally rely on high-pressure synthesis of bridgmanite and ferropericlase from meta-peridotitic assemblages [265] and the predicted modal mineralogy of the lower mantle, which is estimated to comprise ~ 75–80% bridgmanite and ~ 15–20% ferropericlase [266]. However, at equilibrium, NiO is preferentially partitioned into ferropericlase rather than bridgmanite and, consequently, enstatite inclusions in SDDs show relatively low NiO contents (< 300 at.ppm) compared to lithospheric enstatite (> 1000 at.ppm) [88, 255, 267]. It follows that many high-NiO enstatite inclusions are likely primary and form in the upper mantle rather than from retrogression of bridgmanite formed in the lower mantle. However, experimental synthesis of bridgmanite in equilibrium with ferropericlase yields NiO contents higher than bridgmanite observed in SDDs [232–236, 268, 269] which suggests processes that result in low-Ni enstatite may be more complicated [6].

Clinopyroxene inclusions in SDDs (Fig. 20c) are relatively rare as their solubility in majoritic garnet increases significantly at depths of 400–500 km. Two distinct groups, high-Na (augitic, $Ca(Mg,Fe)Si_2O_6$ to omphacitic, $(Na,Ca,Fe,Mg)(Al,Fe,Mg)Si_2O_6$ and low-Na (augitic to diopsidic, $CaMgSi_2O_6$) clinopyroxenes are observed in SDDs. Although protoliths conducive to crystallization of low-Na clinopyroxene remain poorly understood, high-Na pyroxene inclusions are consistent with those produced by experiment in meta-basaltic and meta-pyroxenitic substrates [3, 270–272].

Like clinopyroxene, olivine is common in lithospheric diamonds but relatively rare in SDDs. The most common $(Mg, Fe)_2SiO_4$ polymorph observed in SDDs is olivine which may have retrogressed from its higher pressure polymorphs wadsleyite and ringwoodite [6, 273, 274]. Only three ringwoodite inclusions has been observed in SDDs (see [92, 274–276]) indicating pressures of > 20 GPa and depths of 525–660 km in the mantle-transition zone [266]. One ringwoodite inclusion was shown to be relatively hydrous (1.5% H_2O) [275] supporting models for H_2O cycling into the deep convecting mantle. The modal mineralogy of the upper mantle and transition zone is hypothesized to comprise 60% olivine, wadsleyite, and ringwoodite [266], in obvious contrast to the abundance of olivine (~ 4% of inclusions) in SDDs.

3.3.3 Fluid and melt inclusions

The study of microinclusions of fluid in diamonds, particularly fibrous diamonds, has tremendously improved our understanding of how diamonds form by metasomatic reactions ([52] and references therein). Metasomatism of mantle rock by carbon- and H_2O-bearing (C–O–H) fluids reduces (or in some cases oxidizes) carbon species in solution to form diamond [45, 277]. These diamonds may encapsulate fluids as

inclusions and provide the only direct means to sample diamond-forming mediums from the deep Earth.

Caution must be used when differentiating *fluids* and *melts* related to (1) inclusions in diamond, which are analyzed at surface temperatures and (2) diamond formation, where fluids and melts are modeled at P/T and f_{O2} conditions in the diamond stability field. With respect to (1), fluids inclusions, most often observed in fibrous diamonds, retain fluid-like properties from the moment of diamond formation to eruption at the surface. In contrast, melt inclusions are described based on their properties during diamond formation, and are not stable under decreased P/T conditions where they solidify to form glassy inclusions (e.g., [278]). With respect to (2), differentiating fluids and melts is much more complex and is dependent on P, T, f_{O2} and the composition of the fluid or melt. Here, only a brief description of fluid inclusions in diamond is provided and a more detailed description of how diamonds form from C–O–H fluids is given in Chapter 4.

Fluid inclusions are typically $\leq$ 1 μm (on average 0.2–0.5 μm) in size and fully fibrous cuboid diamonds or fibrous coats on monocrystalline cores may contain millions of inclusions resulting in a translucent or *cloudy* appearance [52]. In some cases, fluid inclusions result in strain, evidenced from highly birefringent fibrous zones [52]. At the time of diamond formation, fluid inclusions consist of supersolidus melts or high-density supercritical fluids (HDFs) [279, 280] until the temperature decreases during ascent of the diamond to the surface where HDFs separate into low-density fluids (LDFs) and mineral solutes [48, 206, 281]. C–O–H-HDFs and melts of similar composition (e.g., high-Mg carbonatitic HDFs and carbonate melts, see below) likely form in similar environments where HDFs represent (1) relatively low volume, low-degree partial melts or (2) residual fluids produced through fractional crystallization of parental melts [52]. At pressures conducive to SDD formation, H_2O-rich HDFs will likely exceed their second critical endpoint (the solidus termination in P/T space, [279, 280]) and have a high dissolved silicate content and thus are best described as melts rather than fluids [6, 280, 282–286]. In simplistic terms, LDFs are supercritical aqueous fluids with a lower dissolved solute (silicate) load than HDFs which include supersolidus melts and dense supercritical aqueous fluids above the second critical endpoint [52] where such fluids have a higher H_2O to dissolved solute ratio than melts.

In general, C–O–H fluids may contain H_2O, CO_2, CO_3, HCO_3, CH_4, and/or H_2 and the dense supercritical fluid-HDFs inferred from analysis of fluid inclusions in fibrous diamond are divided into four groups based on their major-element compositions [52, 287]:

(1) *Silicic*: HDFs rich in SiO_2, K_2O, Al_2O_3, and H_2O.
(2) *Low-Mg carbonatitic*: HDFs rich in CaO, FeO, MgO, and CO_2.
(3) *High-Mg carbonatitic*: HDFs rich in K_2O, CaO, FeO, MgO, and CO_2 and MgO contents > 15 wt%.
(4) *Saline*: HDFs rich in K, Na and Cl with varying amounts of FeO, BaO, CO_2, and H_2O.

Melt-HDFs are similarly classified based on similar compositional groups (see Sect. 4.2.2) as associated fluid and melt-HDFs with similar compositions likely form in the same geologic setting and/or from the same parental melt as described above.

A compositional join is observed between silicic and low-Mg carbonatitic HDFs (Fig. 21) which have been interpreted to form from hydrous, carbonated eclogites based on HDF inclusions in eclogitic mineral inclusions and experimental H_2O–CO_2–eclogitic melts [288, 289]. Elezar et al. [289] and Dvir et al. [290] showed that the position of such melts along the silicic to low-Mg carbonatitic array is likely a function of the H_2O/CO_2 ratio of the eclogitic source rock. Other interpretations involve dissolution of carbonates in H_2O- and K_2O-rich silicic melts [287], or the dissolution of silicates into carbonatitic melts [291], both with increasing temperature. High-Mg carbonatitic HDFs are associated with melting of carbonated peridotitic sources [287, 292]. Weiss et al. [52, 292] suggest both high-Mg carbonatitic HDFs and kimberlitic melts form from low- and high-degree partial melting of carbonated peridotites, respectively. Saline HDFs are interpreted to form from seawater-altered subducted slabs based on Sr isotopes signatures, high Cl-contents, low K/Cl ratios, positive Sr and Eu anomalies, and low $^3He/^4He$ ratios [48, 51, 293–296]. Weiss et al. [287] suggest that percolation of carbonated peridotite by saline HDFs may produce high-Mg HDFs in which the required trace-element load is supplied by the saline HDFs.

Major and trace elements in HDFs may de-couple as (1–4) show two distinct trace-element patterns: (1) a highly fractionated trace-element pattern enriched in LILE and LREE and depleted in HFSE and alkali elements consistent continental crust and

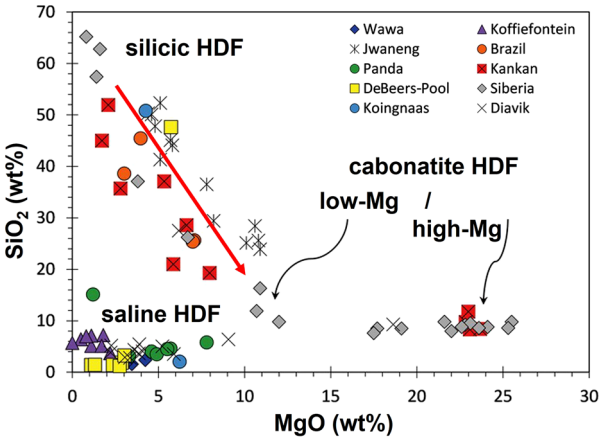

Fig. 21 A plot of SiO_2 (wt%) as a function of MgO (wt%) showing the four major groups of HDF compositions for fluid microinclusions in 89 fibrous diamonds from different localities. The high-Mg and saline groups are consistent with near-solidus melts from carbonate-peridotite and fluids from subducted slabs involving seawater [51], respectively. The low-Mg and silicic compositions form a continuous array (red arrow) in accord with fluids and melts produced by experiment in hydrous eclogite + carbonate systems [287, 288, 292]. Modified from Shirey et al. [48], data from diamonds from DeBeers-Pool, Koingnaas, Kankan, Koffiefontein, Brazil, Diavik and Siberia, Jwaneng, Panda, Wawa and can be retrieved from Shirey et al. [48]

(2) a relatively smooth trace-element pattern slightly depleted in LILE and LREE consistent oceanic basalt [297, 298]. Such trace-element patterns are also observed in kimberlites, and oceanic and continental volcanic rocks. These observations in addition to the enrichment in incompatible trace elements and volatiles observed in HDFs and their connection with subduction processes suggest that they play important roles in cycling and transport of H, C, and other volatiles into the deep Earth [52].

HDFs provide a distinct mechanism for the formation of both fibrous and non-fibrous (monocrystalline) diamonds compared to other C–O–H fluids such as low-density H_2O-rich fluids. For example, the alteration of depleted peridotitic and eclogitic garnets by HDFs produces sinusoidal REE patterns like those observed in harzburgitic garnet inclusions in monocrystalline diamonds (see Sect. 5.2) [42, 51]. Some compositional correlations have been made between core-to-rim HDF profiles in fibrous diamonds and saline and carbonatitic HDF inclusions in octahedral, monocrystalline diamond, and macles (twins) [299–301]. Further evidence for involvement of fluids during diamond growth is hydrous silicic fluid rims (1–5 μm-thick films of $Si(OH)_4$ and $Si_2O(OH)_6$ fluids) around inclusions (Fig. 22) observed in > 90 lithospheric diamonds from the Siberian and Kaapvaal cratons [302] and from the Voorspoed mine [246] and in several sub-lithospheric diamonds from Juina (Brazil) and Kankan (Guinea) [274]. Several other studies on fluid inclusions in monocrystalline diamonds have been conducted [303–305]; however, the results of such studies are mostly speculative due to difficulties constraining the timing of fluid entrapment (e.g., due to fractures permitting post-entrapment re-equilibration) and analytical limitations related to the extremely small size of most fluid inclusions. The above observations suggest that HDFs play a crucial role in the formation of both fibrous and monocrystalline lithospheric and sub-lithospheric diamonds.

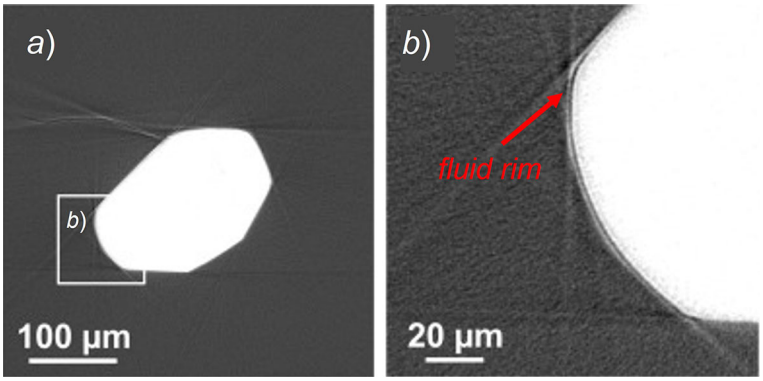

Fig. 22 A Synchrotron Radiation X-ray Tomographic Microscopy (SRXTM) image of an (**a**) eclogitic garnet inclusion in diamond surrounded by what has been interpreted as a hydrous fluid rim, indicated with a red arrow in (**b**). Modified from Nimis et al. [302]

4 Diamond formation and growth

In this chapter, we describe the fundamental physical and chemical mechanisms for diamond formation and growth. As covering all aspects of natural diamond formation would require an entire book, we focus on the diamond-forming fluids and the associated metasomatic (redox) reactions related to diamond nucleation and growth. Moreover, we evaluate how changing P, T, and redox (f_{O2}) conditions influence the composition and carbon speciation of C–O–H fluids for different redox reactions responsible for diamond nucleation and growth.

As the validity of all experimental (and to some extent, theoretical) models for diamond growth are completely reliant on accurately replicating the P/T conditions of natural diamond formation, a brief description of chemical and elastic thermobarometric practices for diamond are given in the following section followed by a synopsis of the major results produced by applying these methods to mineral inclusions in diamond.

4.1 Geothermobarometry of diamond

Geothermobarometry of diamond involves the determination of temperatures and pressures at which diamonds form, geothermometry and geobarometry refer to determinations of temperature and pressure, respectively. To determine the depth of diamond formation, one must rely on its mineral inclusions as, at present, there are no associated methods that are applicable to pure inclusion-free diamond. For an inclusion-free diamond, only residence temperature, T_{res}, in the mantle can be determined based on N-aggregation state (Sect. 3.1.1). We emphasize that *residence temperature* is different than *formation temperature*, where determination of the latter is the principal goal of diamond thermobarometry. For specific mineral inclusions, different chemical and/or elastic geothermobarometric methods can be applied to the diamond-inclusion system, a synopsis of these methods is given in the following sections.

4.1.1 Chemical geothermobarometry

Chemical geothermobarometry involves calculation of pressures and/or temperatures at which a single-mineral inclusion or a pair of mineral inclusions is/are in chemical equilibrium based on their measured chemical composition. However, to apply this approach to mineral inclusions within a diamond, we must assume that the inclusions formed simultaneously and from the same reaction (a *syngenetic* inclusion, see Sect. 3.3) that formed the diamond host in the mantle. Otherwise, in the case of a non-synchronous formation between diamond and its mineral inclusions, we must assume that when the host entraps its pre-existing mineral inclusions (a *protogenetic* inclusion, see Sect. 3.3), the chemical equilibrium is reset and the inclusion and diamond reflect the same crystallization conditions.

Following Nimis [4], we report the most commonly used thermometers and barometers used to derive temperature and pressures based on:

(1) The exchange of a chemical component between two inclusion minerals in equilibrium–*mineral-pair thermobarometry*.
(2) The measured contents of a given element in a single mineral–*monomineral thermobarometry*.

Pressure and temperature determination assumes that both (1) and (2) behave according to a specified (experimentally derived) calibration curve [4]. Examples of mineral-pair thermometers include the *clinopyroxene-orthopyroxene thermometer* based on exchange of an enstatite component ($MgSiO_3$) between both pyroxenes, the *Ni-in-garnet thermometer* based on the Ni content in garnet and olivine in equilibrium and the *Fe^{2+}–Mg thermometers* based on the distribution of Fe^{2+} and Mg between two associated mineral inclusions, such as olivine–garnet, clinopyroxene–garnet, and orthopyroxene–garnet. Monomineral thermometers are particularly useful when the number or size of diamond inclusions is limited and include the *Ca-in-orthopyroxene thermometer* [306], the *single-clinopyroxene thermometer* [4], and the *Al-in-olivine thermometer* [307, 308]. Examples of mineral-pair barometers include the *orthopyroxene–garnet barometer* based on the Al content of orthopyroxene in equilibrium with garnet and the clinopyroxene–garnet barometer based on the equilibrium reaction grossular + pyrope <–> diopside + Ca-Tschermak [309–311]. Examples of monomineral barometers include the *Cr-in-clinopyroxene barometer* based on the Cr content in diopside in equilibrium with garnet [5, 312], and the *Cr-in-garnet barometer* based on the Cr content of garnet in equilibrium with orthopyroxene and spinel [313, 314].

4.1.2 Elastic geobarometry

The elastic geobarometric method is an alternative approach to chemical geobarometry as described above and has been reviewed in detail by Angel et al. [219]. This method relies on differences in the thermoelastic properties (mainly thermal expansivity and compressibility, [315]) of the diamond host and its mineral inclusions [316]. Thus, this approach is not reliant on the chemical composition on mineral inclusions or aspects of their chemical equilibrium. The pressure at which the diamond entraps a mineral inclusion is defined as the *entrapment pressure* (P_{trap}) and corresponds to the depth of diamond formation [219, 220]. When the diamond is erupted to the Earth's surface, its volume expands but, at the same time, the inclusion within it tends to expand more (i.e., diamond has an extremely low compressibility and coefficient of thermal expansion, Sect. 2.1.3). It follows that that inclusion minerals remain under pressure after the diamond has reached the surface; this is called the *residual pressure* or *internal pressure* (P_{inc}). Once P_{inc} is determined, one can use the thermoelastic properties of the diamond and the inclusion mineral to back calculate the pressure at which the diamond entrapped the inclusion (P_{trap}) [219, 220]. In principle, the elastic geobarometric method can be applied to all possible inclusion minerals found in diamond, regardless of their chemical composition which strongly constrains the applicability of chemical barometric methods. It follows that use of elastic barometric methods may drastically increase the number of inclusion-bearing diamonds that are suitable targets for geobarometric analysis.

As mentioned above, elastic geobarometry requires that P_{inc} be derived; this can be done using three different methods: (1) measurement of the unit-cell volume of

the inclusion mineral at room temperature and pressure before and after it is extracted from the diamond host (this can be done by X-ray diffraction techniques); using the bulk modulus, K_{0T}, of the inclusion mineral (if known), the difference in unit-cell volume can be used to calculate P_{inc} [220]; (2) measurement of the Raman band shift of the inclusion (using Raman spectroscopy) before and after it is extracted from the diamond host; this approach requires that the Raman band shift as a function of pressure is known (e.g., [317].); and (3) evaluation of the strain-induced birefringence in natural diamonds, although not commonly used, this technique is also very reliable (e.g., [318]).

Once P_{inc} is determined using one of the above three methods and if the thermoelastic parameters of the inclusion and diamond are known, one can calculate P_{trap} for a given temperature, this is most easily done using the free downloadable software *EosFit-Pinc* (see [319]). By plotting P_{trap} at different temperatures, one can construct what is called an *isomeke* [219], a curved line in P–T space that provides the depth of formation of the diamond-inclusion pair at any reference temperature.

The elastic geobarometric approach is based on a few assumptions and involves several complexities that should be considered. For example, if the diamond-host system did not behave elastically, and instead plastically (or elasto-plastically), P_{inc} and the resulting P_{trap} will be strongly affected. In addition, the elasticity of minerals is often anisotropic (elasticity changes as a function of the direction of the applied stress), the effect of these features on the elastic geobarometric method is not fully understood but may produce erroneously low P_{trap} values. As a result, calculated P_{trap} is often reported as a minimum pressure at which the studied inclusion was entrapped (e.g., [87]).

4.1.3 Results from geobarometric analysis of mineral inclusions in diamond

In general, lithospheric diamonds form in mantle keel environments at depths of 120–200 km (average depth of 175 ± 15 km) and at an average temperature of 1160 ± 100 °C and pressure of 5–6 GPa [5, 43, 85]. Stachel and Luth [45] report an average temperature of 1140 °C and pressures of 5 GPa for diamond formation based on garnet-olivine thermometry. Nimis [4] compiled thermobarometric data for inclusions (using a single-clinopyroxene barometer and Ni-in-garnet thermometer) in lithospheric diamond and showed an average depth of formation of 190 km at pressures of ~ 6 GPa and temperatures of ~ 1200 °C.

Sub-lithospheric diamonds form below the sub-continental lithospheric mantle (SCLM) in the convecting mantle at depths of ~ 300–800 km and at average temperatures and pressures of 1200–1500 °C and 9–11 GPa [6, 7, 86, 87]. However, the majority of SDDs form around the transition zone at 410–660 km [88]. Based on analysis of high-pressure mineral inclusions, such as periclase, jeffbenite, breyite, corundum, and SiO_2, Harte [70] suggests that environments around the transition-zone-lower mantle boundary at depths of 600–800 km may also be conducive to SDD formation. Much of the recent thermobarometric work on diamonds has focused on SDDs, and thus, in the following section, several examples of how the phase relations of inclusions in SDDs can be used to constrain the pressures, temperatures, and depths

(and thus geologic settings) associated with formation of the inclusion (and in some cases the diamond) is given.

With respect to majoritic garnet, two different coupled substitution mechanisms produce compositions between end-member majorite, $Mg_3(MgSi)(SiO_4)_3$ [241, 242] and Na-majorite, $(Na_2Mg)Si_2(SiO_4)_3$ [243, 244]. Such substitution mechanisms are pressure dependent, and thus, the formula contents (*apfu*) of majoritic garnet can be used a barometer [245, 270, 320, 321]. Nimis [4] shows that many SDDs have depth estimates between 300 and 600 km which correspond to the depths at which subducted oceanic crust crosses its solidus (at 1100–1200 °C) [6] to produce carbonated melt required for diamond formation [3, 245, 248]. Pressure estimations using the barometer of Thomson et al. [245] show a bimodal distribution at 7–10 GPa and 12–15 GPa [6]. Thomson et al. [245] show that most low-Cr majoritic garnet of meta-basaltic paragenesis comprises the higher pressure distribution and may represent a unique (deeper) environment of SDD formation compared to high-Cr garnets of meta-peridotitic paragenesis that comprise the lower pressure paragenesis and likely form in a shallower environment.

With respect to $CaSiO_3$ inclusions, single-phase inclusions of breyite are common in SDDs and have been observed in association with perovskite, ($CaTiO_3$); $CaSi_2O_5$-titanite; larnite, (Ca_2SiO_4); merwinite, $Ca_3Mg(SiO_4)_2$; chromite, $(Fe,Mg)Cr_2O_4$; baddeleyite, ZrO_2; sulphides and Fe–Ni alloys [7, 53, 66, 254, 255, 257, 258, 261, 322]. As the phase relations in the $CaSiO_3$ system as a function of P, T, and Ti^{4+} content are well understood, it is possible to model the P/T history of a diamond based on the position of the $Ca(Si,Ti)O_3$ inclusions along the $CaSiO_3$–$CaTiO_3$ join. For example, end-member $CaSiO_3$-perovskite is stable at pressures > 13–14 GPa and decomposes to larnite and $CaSi_2O_5$-titanite between 10 and 13 GPa, to breyite between 9 and 10 GPa (at 800–1700 °C) and to wollastonite below 4–3 GPa (at 900–1500 °C) [6]. When breyite is observed as composite inclusions with larnite and/or $CaSi_2O_5$-titanite, one can assume a formation pressure of ~ 10 GPa (~ 300 km depth) [323]. Elastic barometric analysis of a breyite inclusion by Genzel et al. [7] indicates a minimum entrapment pressure of 9–10 GPa, at such pressures at ambient mantle temperature (1400–1500 °C), breyite is not stable suggesting retrogression from $CaSiO_3$-perovskite [7]. The case is much different for $CaTiO_3$ where Ti^{4+} acts to reduce the stability of perovskite at high pressure, i.e., end-member $CaTiO_3$ is stable at pressures < 5 GPa [262]. In any case, phase transitions occurring over large pressure ranges, 3 to 22 GPa, and thus large depth ranges, have prompted work on mechanisms of transport in the mantle, such as convection, mantle plumes, and melt percolation [65, 66, 258, 324, 325]; this is discussed more in Sect. 5.3.1.

The stability of the $MgSiO_3$ polymorphs as a function of pressure and Al_2O_3 content (mol. fraction) is well understood; thus, Al_2O_3 content can be used as a barometer. Although the formation pressure of bridgmanite is strongly controlled by equilibration with intergrown phases (e.g., majoritic garnet, ferropericlase, and corundum), high-Al $MgSiO_3$ typically form at relatively higher pressures as opposed to low-Al $MgSiO_3$ [6]. As discussed in Sect. 3.3.2, breyite, and especially enstatite, may form as primary inclusion minerals at lower pressures compared to their perovskite-structured polymorphs. When such inclusion minerals are observed in SDDs with single-mineral barometers like majoritic garnet, one may make more precise estimations about the

primary or secondary nature of breyite or enstatite inclusions. However, when observed with inclusions like ferropericlase that serve only as indirect barometers, more detailed work is required to constrain pressures of formation.

Another inclusion mineral that has received recent attention is jeffbenite (formerly known at TAPP, [326]), which has the same chemical composition as pyrope, $Mg_3Al_2Si_3O_{12}$ [327, 328]. It has been shown by experiment that primary Ti–rich jeffbenite may form at relatively high pressures (12–13 GPa) and temperatures (1400 °C) at depths of 360–390 km [249]; however, of the 23 jeffbenite inclusions observed in diamond, none contain significant quantities of TiO_2 [328]. Inspection of the theoretical stability field of Ti-free, Mg end-member of jeffbenite, supports an origin for these inclusions related to regression of Al-rich bridgmanite [329] as this phase becomes unstable at pressures > 4 GPa at 500 °C or > 2 GPa at 800 °C [328].

4.2 Models for diamond formation and growth in the lithospheric mantle

Above, a brief description of the thermobarometric methods and associated results for the P/T and depth conditions of diamond and the inclusions they contain is given. Now, attention is turned to the physiochemical processes associated with the formation of diamonds in the mantle. In general, the solubility of carbon in mantle silicates and oxides is low and carbon is stored as mobile high-density fluids and melts until it is reduced to allow nucleation of diamond. We begin by discussing lithospheric diamonds as there is a wealth of data regarding the composition of reduced fluids in lithospheric diamonds and xenoliths [240, 330]. For now, we refrain from specifying fluid or melt type (Sect. 3.3.3) (e.g., saline HDFs or carbonatitic melts) and, instead, assume the diamond-forming medium is simply a C–O–H fluid.

As discussed in Sect. 2.1, the stability of carbon as a function of P and T (Fig. 5) can be simply expressed as a phase transition from graphite to diamond with increasing pressure. The stability of diamond in the C–O system as a function of P, T, and f_{O2} is constrained by the reactions (4) and (5)

$$C_{\text{diamond}} \leftrightarrow C_{\text{graphite}} \tag{4}$$

$$C_{\text{diamond}} + O_2 \leftrightarrow CO_2. \tag{5}$$

However, diamond-forming (C–O–H) fluids contain H and, thus, the stability of different diamond-forming reactions [e.g. (6)] is reliant on the oxidation state of the mantle substrates (e.g., meta-peridotites), through which they percolate and needs to be considered.

$$CH_4 + O_2 \rightarrow C_{\text{diamond}} + 2H_2O. \tag{6}$$

To do this, the redox speciation of C–O–H fluids and the reduction potential (i.e., f_{O2}) of lithospheric mantle peridotites and eclogites at different P/T conditions must be evaluated. Akin to chemical thermobarometric techniques, oxy-thermobarometery of xenoliths has provided information about the redox conditions in cratonic mantle

lithologies [44, 240, 331, 332] and can be used to estimate the equilibrium f_{O2} for mineral assemblages observed in mantle xenoliths (e.g., the *garnet–olivine–orthopyroxene* (GOO) oxy-thermobarometer, [333]). These f_{O2} values are typically calculated against the buffer reaction (7) and reported at Δf_{O2}-FMQ [47, 334]

$$\text{fayalite } (3Fe_2SiO_4) + O_2 = \text{magnetite } (2Fe_3O_4) + \text{quartz } (3SiO_2) \text{ (FMQ buffer)}. \quad (7)$$

The FMQ buffer reaction constrains the upper bound of f_{O2} in the lithospheric mantle at a given P and T which has Δf_{O2}-FMQ = − 1.5 to − 3.5 at P/T conditions across the diamond stability field [48], as indicated by the average Δf_{O2}-FMQ from mantle xenoliths from depths of 140–180 km [335]. The lower bound of f_{O2} is constrained by the IW buffer reaction (8)

$$\text{(Ni-Fe alloy) } 2Fe + O_2 = \text{wüstite } 2FeO \text{ (IW buffer)}. \quad (8)$$

The f_{O2} conditions above the IW buffer are not adequate to reduce sufficient FeO to allow for Fe alloys to precipitate from Fe-silicates, such that the f_{O2} falls below the IW buffer curve. As f_{O2} fluctuates between the FMQ and IW buffers as a function of P/T, the stability of C-species in C–O–H fluids changes. At Δf_{O2}-FMQ < − 2, CH_4 is stable and predicted to be the dominant C–H species at Δf_{O2}-FMQ = − 4.5 [48, 336, 337].

The f_{O2} of the cratonic mantle at P/T conditions in the diamond stability field is shown to be sufficiently reducing to form diamond by reduction of C–O–H fluids. However, metasomatic reactions involving CO_2-bearing fluids and olivine-bearing substrates (i.e., peridotites) add complexity to this picture.

The buffer reaction (9) defining the upper bounds for f_{O2} conducive to diamond formation in carbonated peridotitic substrates is referred to as EMOD [277, 338, 339]

$$\text{enstatite } MgSiO_3 + \text{magnesite } MgCO_3 = \text{olivine } Mg_2SiO_4 + \text{diamond C} + O_2. \quad (9)$$

The EMOD equilibrium plots at Δf_{O2}-FMQ = − 0.5 to − 2.0 [47] and data from garnet–peridotite xenoliths suggests the cratonic mantle plots on the reducing side of the EMOD buffer [21, 49] where magnesite ($MgCO_3$) and CO_2 (at higher temperatures) are unstable, and the formation of diamond is favored. This is simply shown in Fig. 23, where log-f_{O2} is plotted as a function of temperature. Above the EMOD buffer, diamond is unstable and magnesite reacts with enstatite to produce CO_2 with increasing temperature (Fig. 23) as shown in reaction (10)

$$\text{enstatite} Mg_2Si_2O_6 + \text{magnesite } 2MgCO_3 = \text{forsterite } 2Mg_2SiO_4 + CO_2. \quad (10)$$

At relatively higher temperatures (compared to the EMOD buffer reaction), the DCO buffer reaction (11) represents the upper bound of f_{O2} in the P/T stability of diamond (Fig. 23)

$$CO_2 = \text{diamond C} + O_2 \text{(DCO buffer)}. \quad (11)$$

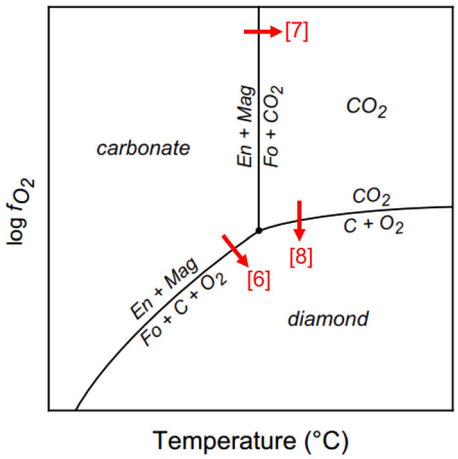

Fig. 23 A phase diagram for log f_{O2} as a function of temperature showing the stability fields of carbonate, CO_2, and diamond in relation to reactions [9, 10], and [11]. En = enstatite ($Mg_2Si_2O_6$), Mag = magnesite ($MgCO_3$), and Fo = forsterite (Mg_2SiO_4). Modified from Luth et al. [277]

The DCO is within 1 log-f_{O2} of the EMOD buffer, and at f_{O2} above the DCO buffer, reaction (10) proceeds and diamond is unstable. At f_{O2} below the DCO buffer, CO_2 in fluids is reduced to form diamond at appropriate pressures.

Determination of f_{O2} for eclogitic diamond substrates is relatively complex, and Luth [338, 340] suggests the buffer reaction DCDD (12) constrains f_{O2} in the diamond stability field

$$\text{dolomite } CaMg(CO_3)_2 + \text{ coesite } 2SiO_2 = \text{ diopside } CaMgSi_2O_6 + \text{ diamond } 2C + 2O_2. \quad (12)$$

The DCDD plots approximately one log-f_{O2} above the EMOD buffer curve suggesting that the f_{O2} stability field of diamond is wider in eclogitic substrates compared to peridotitic substrates over the same P/T conditions [47, 338, 340].

In peridotitic or eclogitic substrates, one may envision a hypothetical C–O–H fluid composition (L_{eq}) in equilibrium with a peridotitic mantle rock. Infiltration of this substrate by a compositionally different CO_2-rich fluid (L_{d1}) that is significantly more oxidizing than L_{eq} will result in diamond precipitation via CO_2 reduction (reaction (8)). Infiltration of this substrate by a CH_4-rich fluid that is significantly more reducing than L_{eq} will result in diamond precipitation via CH_4 oxidation [reaction (9)]. Such reactions are called *wall-rock-buffered redox reactions* as oxygen exchange is mediated by Fe^{2+}–Fe^{3+} in Fe-silicates and oxides of the peridotitic or eclogitic substrate (wall-rock) [19, 21, 48].

4.2.1 Isochemical precipitation of diamond from C–O–H fluids

In the previous section, wall-rock-buffered redox reactions, that constrain the f_{O2} stability field in which diamond form, are explained. Such reactions involve the oxidation or reduction of C-species in C–O–H fluids, as these reactions occur above the IW buffer, Ni–Fe alloys are unstable, and $Fe^{2+/3+}$ in silicates and oxides is free to mediate the

oxidation or reduction of C-species. However, the majority (~ 56%) of the cratonic mantle substrate is depleted harzburgite and dunite [48], which have relatively low Fe^{2+} contents significantly reducing the buffering capacity of such substrates and the degree to which C-species are reduces to form diamond. Luth and Stachel [21] showed that wall-rock-buffering by mantle peridotites is not sufficient to generate significant quantities of diamond by demonstrating that f_{O2} can be shifted from the EMOD to the IW buffer by removing < 50 ppm O_2 from the peridotitic substrate. Consequently, it is likely that the f_{O2} of some depleted cratonic substrates may be *fluid-buffered* (see below). This may explain the observed discrepancy between Δf_{O2}-FMQ of lithospheric mantle peridotites under diamond-stable P/T conditions in experiment and the Δf_{O2}-FMQ of mantle xenoliths which would be representative of the last fluid they were in contact with [47].

As f_{O2} crosses DCO buffer curve, CO_2 reduces to form diamond and O_2 and the H_2O content of the residual C–O–H fluids increases. At 2 log-f_{O2} below the DCO, (Δf_{O2}-FMQ close to that of peridotitic substrate at diamond-stable P/T), the fluid approaches the *H_2O-maximum*, and the residual fluid is nearly pure H_2O (90–99 mol%) with minimal CO_2 and CH_4 content [45]. In near H_2O-maximum fluids, diamond has a large solubility change with temperature, and as P/T conditions of such fluids decrease during ascent along a mantle geotherm, isochemical precipitation of diamond may occur (reaction (13)) at Δf_{O2}-FMQ slightly below the EMOD buffer (− 1.5 to − 2.4) [47]

$$CO_2 + CH_4 + \text{cooling} = 2C + 2H_2O. \tag{13}$$

If these near H_2O-maximum subsolidus fluids enter more reducing conditions where Δf_{O2}-FMQ ≤ -3, the following reaction (14) is more likely [134, 341]:

$$2C_2H_6 + \text{decompression} = 3CH_4 + C. \tag{14}$$

These reactions are redox-neutral and do not require oxygen exchange with Fe-silicates, Fe-oxides, and/or sulphides. Assuming an adequate (or frequent) fluid supply and low fluid–rock ratios, reaction (13) can produce significant quantities of diamond (> 5 carats/ton) [134], significantly more than peridotitic or eclogitic wall-rock-buffered reactions. This is supported by HPHT experiments where H_2O-rich fluids are shown to promote diamond growth [342, 343]. Diamond precipitation from near H_2O-maximum fluids can only occur in depleted harzburgites (or dunites) as dilution from partial melting in other substrates, with relatively lower solidus temperatures, may increase diamond solubility and prevent nucleation. Such processes have been attributed to the common association of lithospheric diamond and harzburgitic garnet [45].

Reactions (13) and (14) may also result from simple mixing of mantle-derived, reducing CH_4–C_2H_6-rich fluids and subduction-derived, oxidizing CO_2–CO_3-rich fluids. However, such mixing processes would result in extreme C isotope fluctuations across internal growth zones, a feature not observed in most lithospheric diamonds which show consistent (or gradational) C isotope compositions across growth zones [48].

4.2.2 C-speciation and composition of C–O–H high-density fluids and melts

In the previous section, we have treated C–O–H fluids generically and not specified how particular fluid states (e.g., melts vs high-density fluids) or compositions (e.g., saline vs. silicic HDFs) influence metasomatic processes and diamond formation at conditions with variable P, T, and f_{O2}. The speciation of C in C–O–H fluids can be predicted as a function of log-f_{O2}-FMQ as shown in Fig. 24 where it is shown that fluids dominated by C–H (e.g., CH_4, C_2H_6, H_2) and C–O (e.g., CO_2) are in equilibrium with diamond at relatively low and high f_{O2}, respectively. In Fig. 24, note the relatively wide range of log-f_{O2}-FMQ where fluids near the H_2O-maximum (indicated by *m* in Fig. 24) are in equilibrium with diamond. This range (− 3 to − 2 log-f_{O2}-FMQ) overlaps with the Δf_{O2}-FMQ of cratonic mantle peridotites on the reducing side of the EMOD buffer.

As discussed in Sect. 3.3.3, LDFs may be defined as supercritical fluids and HDFs include both supersolidus melts and supercritical fluids with a higher dissolved solute (silicate) load compared to LDFs and a composition that is H_2O-rich compared to melts. In the following section, we follow the description of LDFs and HDFs given in Sect. 3.3.3 but for the purposes of simplicity refer to both low-density and high-density fluids as simply *fluids* unless specification is warranted.

In most cases, the inclusions in diamond, particularly garnet, have a much more depleted character than cratonic peridotitic xenoliths and xenocrysts suggesting fluid or melt metasomatism is involved in diamond formation. Differentiating fluid and melt metasomatism is typically done using the incompatible trace-element composition of garnets [313, 344, 345]. The relatively high Zr/Y contents of most harzburgitic garnet suggest fluid metasomatism, and low Zr/Y values for most lherzolitic garnet suggest melt metasomatism and subsequent re-enrichment of the substrate. This has been attributed to harzburgite and lherzolite substrates forming at conditions below and above their hydrous solidus, respectively [45, 229]. It follows that only harzburgitic

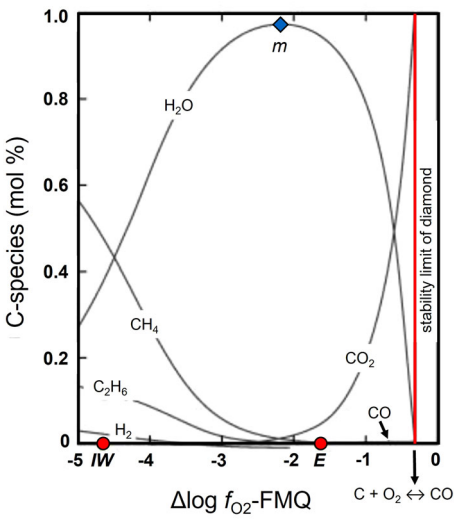

Fig. 24 A plot of the mol% of different carbon species in a C–O–H fluid that are in equilibrium with diamond as a function Δf_{O2}-FMQ. The *m* symbol (blue diamond) represents the Δf_{O2}-FMQ at the H_2O-maximum and the red line represents the stability limit of diamond where oxidation of diamond occurs to produce CO. The *IW* (iron-wustite) and EMOD (plotted as *E*) are shown using red circles. Modified from Wood, [180] after Stachel and Luth, [45]

substrates are permeable to fluid, as melt percolation will lead to equilibration and crystallization at depths < 180 km, and that suprasolidus lherzolitic substrates are permeable to melts [134].

One can now further constrain the type of fluid associated with metasomatism of peridotitic (e.g., harzburgitic) substrates. Such fluids are unlikely to have significant CO_2 contents (unless at f_{O2} above the EMOD buffer where diamond is unstable) due to the buffering reaction (10) [134, 346]. For efficient fluid interconnectivity and subsequent fluid percolation through olivine cumulates, the fluid–rock dihedral wetting angle, θ, must be below a threshold value, i.e.,$\theta \leq 60°$ in an ideal, isotropic system [347–349]. The dihedral wetting angle describes the angle between two different but adjacent solid (mineral)–fluid interfaces; at a triple grain boundary, there is complete fluid interconnectivity and the rock is completely wetted (has a high *wetness*) where $\theta = 0°$ [350]. The relatively high CO_2–olivine and CH_4–olivine dihedral wetting angles (θ = 80–90° for a CO_2–H_2O where $X_{CO2} = 0.9$), [349]) may prevent fluid interconnectivity and flow of CO_2- and CH_4-rich fluids through peridotitic substrates at P/T conditions in the lithospheric mantle. In contrast, the H_2O-olivine dihedral wetting angle decreases with increasing pressure to $\theta = 48°$ and 42° at pressures of 3 and 5 GPa, respectively, at 1000 °C [351]. Capizzi [352] shows that the dihedral wetting angle of carbonatitic liquids in mantle peridotites increases with H_2O content up to $\theta = 50°$. The above description is representative of an ideal isotropic, completely crystalline substrate. However, it is likely that some degree of partial melting occurs upon infiltration of diamond-forming fluids into peridotitic substrates. Here, even extremely low degrees of melt can significantly affect θ and thus the degree to which such fluids can percolate through the substrate [353]. Mu and Faul [354] show that for partially molten dunites (melt contents of 0.3–6.8%), additional variables, such as grain size, pore morphology, and melt content, control the distribution of melt and grain boundary wetness. As discussed in Sect. 4.2.1, fluids in peridotitic and eclogitic substrates are likely near the H_2O-maximum (90–99 mol%) at f_{O2} conditions in the diamond stability field. The addition of dissolved alkali species in H_2O–fluids does not significantly affect the dihedral wetting angle [349, 355]. The solubility of incompatible trace element in aqueous fluids is significantly larger than in CO_2- and CH_4-rich fluids [134, 356], and percolation of aqueous fluids with high concentrations of incompatible elements may explain the commonly observed re-enrichment (LREE enrichment) of melt-depleted peridotitic substrates, i.e., sinusoidal REE trends in harzburgitic garnets (see Sect. 5.2). Rather counterintuitively, the above discussion suggests fluids associated with metasomatism of peridotitic, specifically harzburgitic, substrates are H_2O-rich and have low contents of CO_2 and CH_4 (~ 2% at the H_2O-maximum). Such aqueous fluids at P/T conditions in the diamond stability field probably have a large concentration of incompatible elements and are thus best described as high-density fluids (HDFs) [51, 52].

Evidence from xenoliths and diamond inclusions for melt metasomatism of peridotitic, specifically lherzolitic, substrates points to four primary melt compositions; *carbonate*, *silico-carbonate*, *silicic*, and *hydrous* melts [134]; however, other types of melts, such as *metallic*, *sulfide,* and *saline* melts, have been identified [52]. In general, carbonated melts form in localized regions at high f_{O2}; it follows that temporary perturbations in the redox conditions of the reducing lithospheric mantle are

required. Carbonated melts may form from upwelling of metasomatized mantle rock into conditions of higher f_{O2} and subsequent redox melting [68, 134]. Carbonated melts may also form from melting of oceanic crust, although significant melt cannot be generated at depths < 400 km, below the anhydrous solidus of carbonated eclogite, incorporation of slab-derived fluids may permit melting at shallower levels. Moreover, in the hotter Archean and Paleoproterozoic lithospheric mantle, partial melting of carbonated subducted crust and subsequent metasomatism of the lithospheric mantle likely occurred in shallower levels [357]. Mantle metasomatism by silicic and silico-carbonate melts has been inferred from orthopyroxene-rich peridotitic xenoliths that form from Si enrichment of peridotitic substrates via hydrous melts [358, 359] or mafic melts [360]. Other studies attribute silicic melt metasomatism to the formation of large-igneous provinces and associated plume magmatism [361].

The fluid/melt compositions associated with metasomatism of eclogitic (or pyroxenitic) substrates are more difficult to constrain as most mantle eclogites are LREE-depleted and show no evidence of re-enrichment via metasomatism by diamond-forming fluids or melts (as described for peridotitic substrates above). However, Na-rich garnet and K-rich clinopyroxene inclusions have been attributed to diamond formation from saline HDFs (see Sect. 3.3.3) [134]. This is supported by the observation of saline HDF inclusions in eclogite [293, 362] and Na- and K-rich omphacite and saline HDF inclusions in associated eclogitic diamonds [295]. Based on the f_{O2} of eclogitic xenoliths, it is likely these HDFs are near the H_2O-maximum and form in subduction-related environments where they can dissolve and incorporate different C-species [338, 363]. In such environments, diamond formation may be fluid-buffered and oxidizing (e.g., CO_2-bearing fluid) and reducing (e.g., CH_4-bearing fluid) HDFs may precipitate diamond upon mixing via isochemical (oxygen-conserving) redox reactions (Sect. 4.2.1) [21, 341]. Of course, this does not preclude wall-rock-buffered reactions, such as diamond precipitation via oxidation of CH_4 and reduction of Fe^{3+} in the eclogitic substrate [364].

Some high-Mg eclogites show evidence (LREE enrichment) of metasomatism by silico-carbonate or kimberlitic melts [365]. Such melts are in equilibrium with eclogite and diamond over wider ranges of f_{O2} compared to peridotite. Moreover, diamond in eclogite is stable at higher f_{O2} compared to peridotite [338], and thus, transport of C and precipitation of diamond associated with metasomatism of eclogites may occur over large distances and a wide range of conditions [366]. This may explain the overrepresentation of diamonds with eclogitic paragenesis compared to the estimated eclogite content of the lithosphere [134, 367]. In general, clear evidence for metasomatism of eclogites is rare, and when observed, it is unique from that in peridotite. This may be due to the limited trace-element data for inclusions in eclogitic diamond or from overprinting of trace-element metasomatic signatures of eclogitic xenoliths by interaction with kimberlitic HDFs or melts [134].

4.3 Models for formation and growth of super-deep diamonds

At around the depth at the base of the upper mantle (~ 410 km), f_{O2} is likely close to, or at the IW buffer [reaction (8)] where Ni–Fe alloys begin to precipitate out of

high-pressure Fe-silicates [47]. Based on estimated upper mantle Fe/O contents, Frost and McCammon [240] predict that this process may begin at shallower depths of ~ 250 km. However, contradictory evidence is shown with high $Fe^{3+}/\sum Fe$ ratios in majoritic garnet (20% Fe^{3+} at 10 GPa, [368]) and wadsleyite (2% Fe^{3+}, [369]) from the transition zone and in $CaSiO_3$-perovskite (> 50% Fe^{3+}, [370]) from the lower mantle, all of which in equilibrium with Ni–Fe alloy at f_{O2} around the IW buffer. If one assumes that the estimated bulk Fe/O content ($Fe^{3+}/\sum Fe$ ratio of the upper mantle is < 2%, [369, 371]) is consistent across the entire mantle due to convection, how could the relatively small Fe^{3+} budget of the transition zone and lower mantle support assemblages of Fe^{3+}-rich silicates and Ni–Fe-rich alloys in equilibrium? The additional Fe^{3+} required is produced through the disproportionation reaction producing Ni–Fe alloy (Fe^0 metal); $3Fe^{2+}O = Fe^{3+}{}_2O_3 + Fe^0$ [47, 240, 330, 370]. This reaction is driven by the increasing solubility of Fe^{3+} in silicates with increasing pressure and is responsible for the nearly 1 wt% Fe^0 metal comprising the lower mantle [68, 368, 372]. This reaction also constrains f_{O2} in the base of the upper mantle, the transition zone and the lower mantle to values close to or at the IW buffer and thus to conditions sufficiently reducing to allow diamond formation from C-bearing fluids or melts [48, 68].

The stability of diamond in the transition zone and lower mantle is assessed by Rohrbach and Schmidt, [68] and Stagno et al. [373] who propose reaction (15) as a high-pressure version of the EMOD buffer

$$\text{ferropericlase MgO} + \text{diamond C} + O_2 = \text{magnesite } MgCO_3. \quad (15)$$

Although this buffer reaction plots 2–3 log-f_{O2} above the IW buffer, it assumes homogenous Fe/O contents throughout the transition zone and lower mantle and does not take into account the counteractive effect of FeO disproportionation on f_{O2}. In fact, carbon at P/T conditions in the transition zone and lower mantle is extremely soluble in Ni–Fe alloys (~ 2 wt% C), metallic Fe-rich liquids (~ 6 wt% C) and/or Fe-carbides (e.g., Fe_3C and Fe_7C_3) [374]. Thus, at f_{O2} conditions at or below the IW buffer, the majority of C in the deep mantle, which occurs in relatively low concentrations (50–200 ppm) compared to the lithospheric mantle, may be stored as Fe-metal or liquid in disequilibrium with diamond [48]. This is evidenced from Fe–metal and sulphide melt inclusions in many sub-lithospheric diamonds [53, 113, 375]. For example, Kaminsky and Wirth [376] observed Fe-carbides (Fe_3C, Fe_2C, and $Fe_{23}C_6$) in association with Fe-metal in diamonds from the Juina area.

Models for SDD formation are in some ways analogous to the *redox-* and *fluid-buffered* models for lithospheric diamond formation, albeit the SDD-forming media and substrates are significantly different. The *Redox-Freezing* model [68] for SDD formation involves the production of carbonated melts from subducted material, and their migration into the reducing, Fe-metal-saturated peridotites where C-species are reduced (via oxidation of FeO) to form diamond [248, 377]. Metasomatism of Fe-metal-rich peridotites by carbonated melts in HPHT experiments have produced periclase with variable composition (along the Mg–Fe join) and Ca-majoritic garnet and $Ca(Si,Ti)O_3$-perovskite with compositions in accord with inclusions in SDDs

[248, 377]. Moreover, the wide range of light carbon isotope values, the heavy oxygen isotopic composition and high Fe^{3+} content of majoritic garnet inclusions suggest involvement of subducted crustal rocks [66, 151, 378–380]. However, major- and trace-element data of SDDs suggest several different melting processes and subsequent melt compositions from which diamonds may precipitate.

Barometry of majoritic garnet in SDDs shows that the majority of SDDs form between depths of 300–600 km in the transition zone where slab subduction stagnates [381, 382] and undergoes partial melting [6]. Such SDDs often contain Cr-poor majoritic garnet and Ti–rich CaSiO3 inclusions in accord with low-degree partial melts of oceanic crust and a meta-basaltic assemblage [3, 66, 248, 258]. Here, melting likely occurs at 1100–1200 °C and at pressure of 13–18 GPa [6, 245]. Subduction systems may also transport diamonds from shallower environments in the upper mantle to higher pressure environments in the base of the upper mantle and transition zone. Lorenzon et al. [274] argue that zirconia + coesite and ringwoodite inclusions in a diamond formed as products of prograde phase transitions of zircon or reidite ($ZrSiO_4$) and olivine or wadsleyite, respectively, during transport of the host diamond from the upper mantle potentially hundreds of km to depths possibly > 610 km.

The observation of exsolved brucite and magnesioferrite in ferropericlase inclusions, hydrous inclusion minerals such as ice VII [61], a hydrous Al–silicate called *phase EGG* [$AlSiO_3(OH)$] [383], hydrous ringwoodite inclusions (e.g., 1.5 wt% H_2O, [276]), and hydrous fluid films around inclusions [92, 274, 302] point to the involvement of H_2O-rich fluids and melts across the transition zone and shallow lower mantle where SDDs form (e.g., [92]). Fluid phases rich in H_2O and CH_4 are theoretically stable in the deep reducing peridotitic mantle but unlikely to exist in any significant quantity due to the H-storage capacity of the deep upper mantle and transition zone (e.g., [384]). Instead, H_2O may be transported to the deep mantle in cold subducting slabs where H_2O is stored in dense-magnesium-silicate (DHMS) phases, which can contain 5–10 wt% H_2O (e.g., [385]). Upon stagnation and heating on the slab in the transition zone, DHMS phases may breakdown to form wadsleyite or ringwoodite and residual H_2O-rich fluid [6, 133]. Such fluids may be carbonated from melting of the slab (or percolation within the slab) and would thus precipitate diamond upon migration through the surrounding peridotitic substrate. Here, melting of the cold slab, at transition zone pressures, would occur at 1200–1300 °C where the predicted mineral assemblage is ringwoodite, akimotoite, bridgmanite, ferropericlase, and Ca-perovskite [133, 386], the latter may be observed (as retrogressed breyite) in association with ringwoodite inclusions in diamond [276].

Based on several high-pressure mineral inclusions, Harte [70] suggests environments at depths of 600–800 km at the transition zone-lower mantle boundary may also be conducive to SDD formation. The CLIPPIR diamonds and diamonds from the Collier-4 kimberlites [378] have been shown to form in this region and have extremely variable carbon isotope compositions; $\delta^{13}C = -26.9$ to -3.8‰ and $\delta^{13}C = -26$ to -8‰, respectively [6]. This suggests formation from carbonated melts from subducted oceanic crust. The CLIPPIR diamonds contain composite Fe–Ni–S–C-rich inclusions of the carbide mineral, cohenite ($(Fe, Ni)_3C$), Ni–Fe alloys, Fe-sulphides, Fe–Cr-oxides, and Fe-phosphates [54] some of which are also observed in Type IIb diamonds [53, 113]. Fe–Ni–Cr–S-rich metallic inclusions are interpreted as melt inclusions [53]

perhaps produced through metasomatism and partial melting of Fe-metal-saturated peridotites associated with deep-seated subducted slabs. Moreover, CH_4–H_2 fluid films observed in SDDs may have exsolved from metallic Fe-rich melt inclusions during decompression.

In general, our understanding of the redox reactions responsible for SDD formation is lacking compared lithospheric diamonds. This is largely due to a paucity of representative materials, SDDs are relatively rare and those with mineral and melt inclusions suitable for study, even more so. However, recent experimental work has provided several interesting results regarding the stability of different oxidized and reduced forms or carbon at P/T conditions of the deep lower mantle (see [387, 388]).

4.4 Models for the aqueous speciation of metasomatic, diamond-forming fluids

Until now, and in much of the current literature, models for the speciation of C-bearing molecules and other dissolved solutes (e.g., K_2O and Na_2O in diamond-forming fluids (see Sect. 3.3.3) are rather simplistic. Although extremely useful and informative (as shown above), such models assume C-bearing species are for the most part, neutral dissolved gases (e.g., CO_2 and CH_4) and that diamond-forming reactions behave according to simple redox reactions. In recent years, detailed thermodynamic modeling (e.g., the DEW model, [389, 390]) based on the aqueous solubilities of upper mantle lithologies and the mineralogical components therein (e.g., peridotite and eclogite), has shown that diamond-forming fluids may contain a much wider variety of mineral solutes, ionic species, and metal complexes [391] than previously known. Moreover, such works have shown that diamond-forming reactions may be more complicated than the standard redox controlled reactions as described above. Sverjensky and Huang [392] use models of mantle fluids containing ions to show that diamonds may form during water–rock interactions due to fluctuations in pH at relatively constant redox conditions (f_{O2}). For example, these authors show that metasomatism and dissolution of the clinopyroxene ($NaAlSi_2O_6$) and garnet ($Mg_3Al_2Si_3O_{12}$) components of an eclogitic substrate may produce Mg-rich carbonates ($MgCO_3$) and H^+, (reactions 16 and 17) thus lowering the pH of the system into the diamond stability field, such that diamond can precipitate via dissolution of $MgCO_3$ (reaction 18) at relatively constant $\log f_{O2}$

$$NaAlSi_2O_6 + Mg^{2+} + CO_2^0 + H_2O = MgCO_3 + Na^+ + AlO_2^- + 2SiO_2^0 + 2H^+ \quad (16)$$

$$Mg_3Al_2Si_3O_{12} + 3CO_2^0 + H_2O = 3MgCO_3 + 2(AlO_2)SiO_2^- + SiO_2^0 + 2H^+ \quad (17)$$

$$MgCO_3 + 2H^+ = C_{diamond} + Mg^{2+} + O_{2g} + H_2O. \quad (18)$$

In general, experimental fluid compositions after metasomatic reactions with silicate mantle lithologies (e.g., eclogite and peridotite) are in good agreement with siliceous fluid inclusions observed in diamond (e.g., [392]). Several C-bearing species

have been proposed based on the results of the DEW model that are not typically considered in most redox reactions, such as HCO_3^- and CO_3^{2-} and other organic carbon species such as $HCOO^-$, $HCOOH^0$, CH_3COO^-, CH_3COOH^0, and $CH_3CH_2COO^-$ [391] which have been proposed to react with H^+ in acidic solutions during metasomatism to produce diamond and water [392] (e.g., reactions 19 and 20)

$$HCOO^- + H^+ + H_{2aq} = C_{diamond} + 2H_2O \tag{19}$$

$$CH_3CH_2COO^- + H^+ = 3C_{diamond} + H_{2aq} + 2H_2O. \tag{20}$$

Similar studies modeling reactions between eclogitic fluids and peridotitic substrates (e.g., [393]) have shown that discrete reactions can form a wide variety of silicate minerals typically attributed to eclogitic, websteric, and peridotitic parageneses. It follows that a suite of different mineral inclusions in a single diamond may form syngenetically from the same metasomatic event that resulted in the precipitation of the host diamond. Above we have provided only a simplified synopsis of the work that has been done modeling the aqueous chemistry of diamond-forming fluids at mantle conditions and readers are referred to the work of D.A. Sverjensky and F. Huang (e.g., [389–393]) for more detailed explanations.

5 Mantle geodynamics of carbon through geologic time

Thus far, we have focused primarily on imperfections in diamonds and how they can be used to elucidate aspects of diamond formation from different mediums (e.g., fluids and melts) in different substrates (e.g., mantle peridotite and eclogite). Now, attention is turned to larger scale aspects of mantle geodynamics through geologic time as inferred from the study of imperfections in natural diamond. Here, recent, and more notable works, focused on (1) the extent to which C is recycled between crustal and mantle reservoirs, (2) the mechanisms and speciation associated with C transport in the mantle, and (3) the relation between the C and N isotopic composition of diamond (and diamond inclusions) and potential source reservoirs (e.g., [129]). We begin by evaluating the structural and compositional evolution of the mantle though geologic time based on the geochronology of diamond and associated temporal trends in the chemical (major and trace elements) and isotopic composition of mineral inclusions.

5.1 Geochronological methods and the age of diamonds

Accurate determination of the formation age of diamond is crucial to understand how the mechanisms and geologic settings of diamond formation have evolved through time. Diamonds are uniquely capable of capturing *samples* of the deep Earth through time, as far back as 3.5 Gya and thus may be used to reconstruct the geologic history of the mantle and Earth processes associated with diamond formation.

In general, geochronology (i.e., radiometric dating) is used to determine the age (or date) of inclusions by measuring the degree to which a *parent* nuclide, with a

known decay constant (λ) (or *half-life* ($t_{1/2}$)), has radioactively decayed to its *daughter* nuclide(s). For example, ^{187}Re decays to ^{187}Os according to $\lambda = 1.6689 \pm 0.0031 \times 10^{-11}$ a^{-1} [394] and $t_{1/2} = 0.693/\lambda$ [71]. Parent and daughter nuclides fractionate by differential partitioning into different mineral and fluid phases via diffusion and one must assume that a calculated crystallization (formation) age reflects the time that elapsed during fractionation until diffusion stopped and the isotopic system was *closed*. In the case of diamond, which does not contain sufficient concentrations of radiogenic elements, such as Sm, Nd, U, Pb, Re, and Os suitable for age dating (e.g., half-life of C is only 5730 years), one must rely on inclusions. In ideal cases, mineral inclusions crystallize at temperatures (at or above their *closure temperature*) high enough to isotopically homogenize the system (e.g., crystals ± residual melt). After diamond crystallization and encapsulation of a mineral inclusion, a rapid temperature decrease quenches the isotopic distribution among phases, such that the *geochronometer is set*. The surrounding diamond prevents further isotopic fractionation, and the mineral inclusion can be dated to determine the crystallization age of the diamond. The above description represents the simplest case, dating of diamonds is often much more complex and involves calculation of different types of ages using different geochronological methods (e.g., *model* vs. *isochron ages*, see [71, 221]) that may reflect the age of different geologic events distinct from diamond crystallization such as the crystallization of protogenetic mineral inclusions. However, ambiguous diamond formation ages are often supported by supplementary geochronological data from other diamonds or xenoliths associated with the same deposit (kimberlite pipe). For example, Bulanova et al. [66] dated a SDD from the Collier-4 kimberlite at 107 ± 7 Ma, although this date is only 14 Mya older than the host kimberlite, which may seem unrealistic, the N-aggregation state of associated diamonds suggests relatively short mantle residence times (< 10 Mya at 1500 °C) supporting this diamond formation age [66, 71]. For a detailed review of the geochronological methods and associated analytical techniques used for dating diamonds, readers are referred to [71].

Lithospheric diamonds have formed throughout much of Earth's history recording ages as old as 3.3–3.5 Ga (Diavik Mine, Slave Craton) and 3.5 Ga (Panda kimberlite, Ekati mine, Slave Craton) [23–25] and are usually significantly older than their host kimberlites which have average ages of 45 Ma to 1.2 Ga [26], suggesting prolonged mantle residence times. In contrast, SDDs appear to be Mesoproterozoic or younger and, in some cases, may be transported to the surface soon after formation as shown by Bulanova et al. [66] above. However, conclusions based on the ages of SDDs lack statistical meaning compared to those based on lithospheric diamonds as SDDs with inclusions of appropriate size and composition for dating are exceedingly rare; currently, there are only four Re-Os and Sm–Nd model ages and two U–Pb ages for SDDs [71]. Nevertheless, such diamonds have provided crucial information about the sources and recycling of C in the transition zone and lower mantle which is discussed briefly below.

5.2 Evolution of the Archean and Proterozoic lithospheric mantle

Age dating of lithospheric diamonds that formed in Archean and Proterozoic peridotitic (specifically harzburgitic) and eclogitic substrates have provided much information about how cratonic nuclei and the underlying *diamond factories* (mantle keels) have formed and evolved over this geologic period. By linking diamonds with known ages and paragenesis to geologic settings, one can make inferences about the recycling of C-bearing volatiles and fluids in the mantle. Following [71], the ages for peridotitic and eclogitic diamonds and associated tectonic events are shown in Fig. 25.

Garnet has been particularly useful as it shows evidence of metasomatism in the form of REE patterns [344, 395, 396] that are often consistent between garnets inside and outside of the diamond. Most harzburgitic and lherzolitic garnet inclusions in diamond, and those from cratonic peridotitic xenoliths, show sinusoidal chondrite-normalized (CN) REE patterns (Fig. 26) but may also show several types of non-sinusoidal patterns, such as *V-shaped*, *normal,* and *abnormal* patterns (see [134, 229, 344, 395]). This sinusoidal, REE pattern is perhaps the most widely recognized feature of subcalcic garnets associated with diamond formation [137, 144, 345]. To

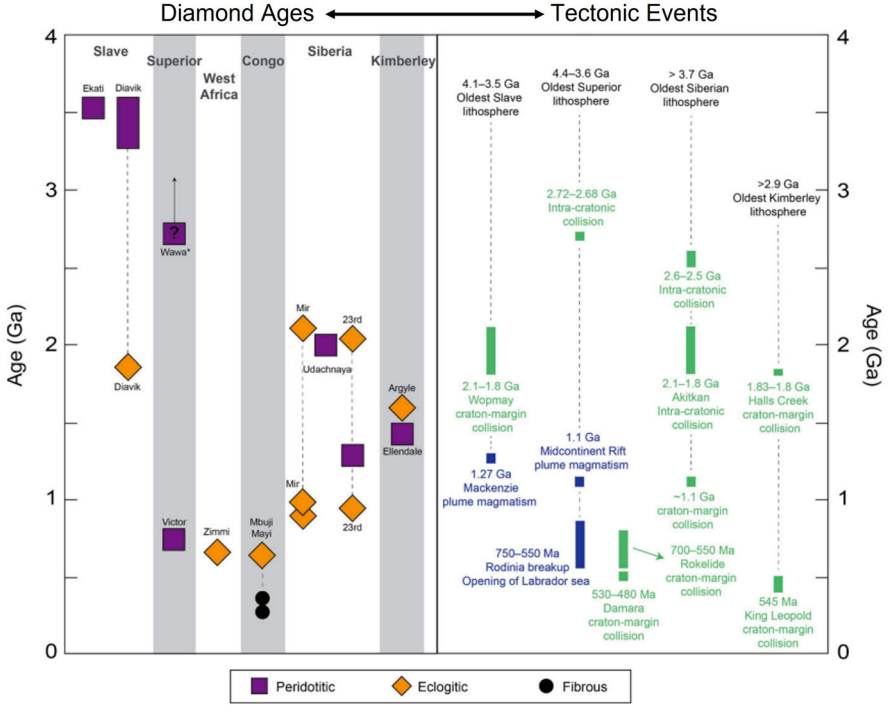

Fig. 25 A plot of all isochron ages of eclogitic and peridotitic diamonds and associated tectonic events. Diamonds from the Wawa locality were plotted based on the age of their sedimentary host rocks. Modified from Smit et al. [71] and Howell et al. [37]

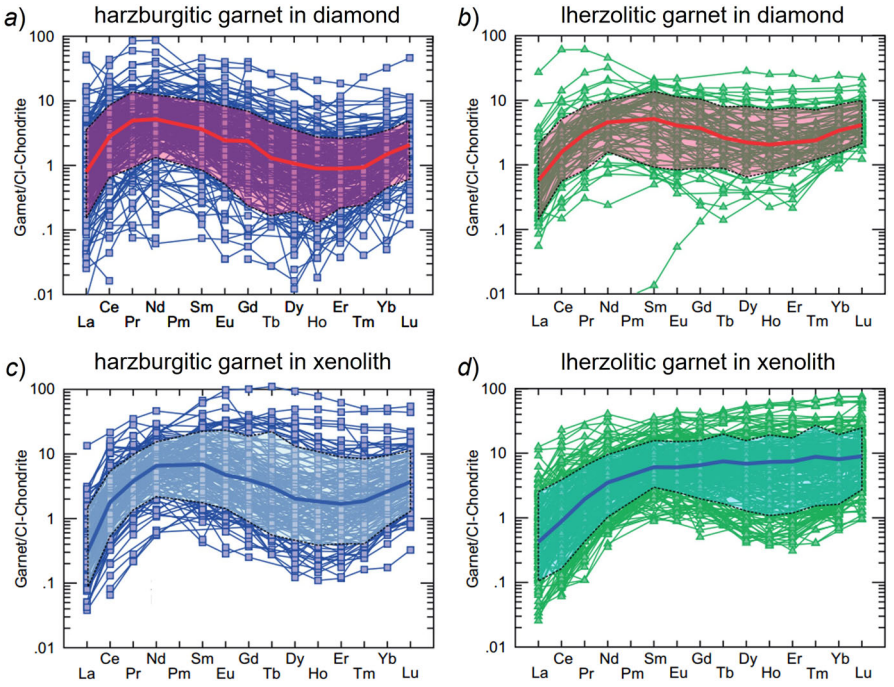

Fig. 26 Chondrite (CN) normalized rare-earth element (REE) patterns for **a** harzburgitic and **b** lherzolitic garnet inclusions in diamond and **c** harzburgitic and **d** lherzolitic garnets from xenoliths. For (**a**) and (**b**), 223 and 72 garnets are included, and for (**c**) and (**d**), 152 and 280 garnets are included. Thick blue and red lines show the median values and transparent blue and green fields represent the data ranges from the 10th to 90th percentile, respectively. Modified from Stachel et al. [134]

explain these patterns, the early evolution of lithospheric mantle peridotites is characterized by two major events, (1) extensive primary chemical depletion via partial melting by upwelling mantle plumes and (2) re-fertilization and re-oxidation via interaction with enriched melts and fluids [42, 397–400]. Other hypotheses suggest that the sinusoidal REE trend in garnet is primary and formed upon recrystallization of a pre-metasomatism Archean lithospheric mantle composed of chromite-rich harzburgite [401].

The origin of eclogitic substrates is linked to the onset of Wilson cycles of plate tectonics at ~ 3 Ga [29] after the formation of Paleo-Archean mantle keels and diamonds therein. The oldest eclogitic diamonds are ~ 3 Ga, before which only peridotitic, specifically harzburgitic, diamonds are observed with formation ages of ~ 3.5 to 3.0 Ga [29, 47]. Eclogitic diamonds and associated xenoliths with ages of ~ 3 Ga often show isotopic evidence for interaction with fluids produced in a subduction environment from crustal material. For example, the 2.9 Ga eclogitic diamonds from the Kimberley, Bobbejaan, Jwaneng, and Orapa localities [22, 27, 402] have been linked to collision and subduction processes associated with amalgamation of the Kaapvaal craton as they show isotopic evidence (e.g., S isotopes with atmospheric signatures) for the involvement of subducted oceanic lithosphere [71, 149, 150, 403]. Shirey and Richardson

[29] proposed that these 3 Ga eclogitic diamonds form due to continent collision and the subsequent incorporation of oceanic lithosphere and fluids into the cratonic mantle keel [24] and thus mark the onset of Earth's Wilson cycles. If one assumes that this is the case, processes by which Paleo- and early Meso-Archean mantle keels form must be distinct from that given by modern plate tectonics, although they likely involve localized subduction-like processes [36]. The most likely hypothesis for the formation of Paleo- and early Meso-Archean mantle keels involves the rise of mantle plumes and associated melt production resulting in melt-depleted peridotitic substrates characteristic of Archean mantle keels [24, 79, 140, 142]. Here, primary melt depletion was likely facilitated by elevated Archean mantle temperatures (100–300 °C higher than today) [404] and low FeO contents of cratonic peridotites have been used to support melting via mantle-plume upwelling [30, 140, 141]. This model is consistent with models for the formation of the Slave craton where the initial continental lithosphere was thickened by underplate melting due to mantle-plume upwelling [141], in accord with detrital chromite ages associated with komatiite magmatism in the Slave craton [405]. Komatiitic magmatism and other magmatic processes associated with the formation of large igneous provinces have been used to explain the observed Si (i.e., orthopyroxene) enrichment observed in cratonic peridotites, i.e., Si enrichment in the Kaapvaal craton has been attributed to the Ventersdorp large igneous province [406]. In general, the appearance of eclogitic diamonds at ~ 3 Ga may represent a transition from dominantly *vertical* modes to *horizontal* modes of plate tectonics [71]. Vertical modes involve mantle-plume upwelling, underplating, and subsequent thickening of the lithospheric mantle, vertical tectonism, and internal igneous crustal differentiation [407–410]. Horizontal modes involve lateral accretion of oceanic lithosphere, horizontal tectonism, advective thickening of the lithospheric mantle, and external igneous crustal differentiation [29, 79, 411]. There is an enormous amount of work on the evolution of plate tectonics and associated processes, and there is evidence for subduction (or subduction-like processes), accretionary tectonics and continental margin magmatism in the Paleo- and Eoarchean and even Hadean (e.g., [412–415]).

Several modes of lherzolitic diamonds are observed at 2.1–1.8 Ga [47], 1.4 Ga [416], 1.1–1.0 Ga [417, 418], and 0.72 Ga [419], and are associated with enrichment of depleted lithospheric mantle peridotites by diamond-forming melts and fluids [45]. As discussed in Sect. 4.2.1, initially melt-depleted peridotitic substrates have a relatively low wall-rock-buffering capacity for carbonate reduction (and thus diamond production) via Fe^{2+} oxidation. However, lherzolization may have introduced FeO to peridotitic lithologies [30] and thus increased the buffering capacity of such substrates. Evidence from enriched mantle xenoliths suggests that these melts had sufficiently high f_{O2} to re-oxidize regions of the depleted lithospheric mantle [19, 44, 46, 398, 420] which may have acted locally to decrease the depth at which lherzolitic diamonds would form via wall-rock-buffered redox precipitation. These melts likely produced pathways of re-oxidized and re-fertilized mantle peridotite which in turn would promote kimberlite eruption [46, 419], and therefore, such melts may be described as *proto-kimberlitic* [48]. However, magmatic (and metasomatic) processes associated with proto-kimberlitic melts and lherzolitic diamond formation are usually distinct from those associated with kimberlite magmatism and eruption as evidenced

by the large age differences between most lithospheric diamonds and their host kimberlites. It should be noted that although most lherzolitic diamonds formed in the Paleoproterozoic–Neoproterozoic, younger ages have been observed (e.g., Mesozoic lherzolitic diamond, [403]) and are associated with regions reworked by later tectonic events [146, 361, 421, 422] or with post-Archean lithospheric mantle settings [423–425].

5.2.1 Recycling of carbon and associated geologic processes

Since the inception of *The Deep Carbon Observatory* (DCO) and *The Diamonds and Mantle Geodynamics of Carbon* (DMGC) consortium, much effort has been made to understand the geological processes that drive carbon recycling between the crust and mantle. Processes related to the formation of Archean mantle keels and the oldest ~ 3.3–3.5 Ga diamonds represent the earliest traceable examples of carbon recycling in the mantle. The degree to which *vertical* and *horizontal* tectonics were operative in the Paleo-Archean and Eo-Archean is still debated (e.g., [426, 427]), and thus, the specific mechanisms by which C was transported between the lithospheric mantle and crust during this period is not fully understood. Nevertheless, diamond research has advanced our understanding of how different aspects of the carbon cycle have changed over the last ~ 3.5 Ga, specifically in Earth's early history when important geologic processes occurred, e.g., crustal growth and continent assembly, the onset of Wilson cycles, and major changes in atmospheric chemistry.

As outlined in Chapter 4, lithospheric diamonds form during periods of fluid infiltration into reducing substrates of lithospheric mantle keels; however, little attention has been given here to processes that control the migration and recycling of such fluids from subduction-related environments or the deep mantle to the mantle keel. The earliest traceable recycling of C (e.g., 3.3–3.5 Ga, [23–25]) related to peridotitic diamond formation is associated with the formation and subsequent metasomatism of the first cratonic blocks and associated mantle keels [27]. The onset of later subduction-related events, associated with the appearance of eclogitic diamonds (at ~ 3 Ga, [29]) involved stabilization of cratons via subduction (of a dominantly horizontal mode), and incorporation of oceanic crust and subsequent underplating [27, 402, 428–431] and likely involved more efficient recycling of C from crustal (surficial) sources.

In contrast, Proterozoic, lherzolitic diamonds are associated with metasomatic modification of the lithospheric mantle rather than formation (i.e., peridotitic diamonds) or stabilization (i.e., eclogitic diamonds) of mantle keels [432]. Lherzolitic metasomatism is inherently linked to recycling and migration of carbon-bearing fluids and melts and is not typically associated with subduction along cratonic margins. For example, the 719 ± 49 Ma lherzolitic diamonds [419] from the Victor Mine have been linked to rifting of the Rodinia supercontinent and subsequent migration of C-bearing fluids and/or melts into the lithospheric mantle of the Superior craton [71, 304]. Although non-subduction-related metasomatic re-fertilization is characteristic of lherzolitic diamonds, in many cases, recycling of C-bearing fluids in the lithospheric mantle is driven by orogenic- and subduction-related processes around cratonic margins [71]. Continental collision and consequent orogenesis (and subduction) at the margins of cratonic

nuclei have been linked to diamond formation through the production and introduction of diamond-forming fluids to the cratonic mantle [27, 403] and thus represent a key process by which carbon is recycled. Notable examples include Proterozoic subduction processes along Kimberley craton associated with the 1580 ± 30 Ma [433] *Argyle* diamonds (Halls Creek orogen, [434]) and the 1426 ± 120 Ma [416] Ellendale diamonds (King Leopold orogen) where diamonds in both localities form in >2.9 Archean mantle substrates [71, 416]. Similar processes are indicated by the 1.86 ± 0.19 Ga Diavik diamonds and associated eclogitic xenoliths [24, 435] which have been linked to the Wopmay orogen along the Slave craton [436].

5.2.2 Speciation of carbon in the lithospheric mantle: C and N isotopes

The stable isotopic composition of C is expressed in delta notation ($\delta^{13}C$) and given as

$$\delta^{13}C = \left(\left[{}^{13}C/{}^{12}C \right]_{sample} / \left[{}^{13}C/{}^{12}C \right]_{VPDB} - 1 \right) \times 1000‰.$$

Here, $\delta^{13}C$ is the deviation of the measured C isotope ratio ($[{}^{13}C/{}^{12}C]_{sample}$) compared to the C isotope ratio of an internal standard, typically the Vienna-Pee Dee Belemnite (VPDB) ($[{}^{13}C/{}^{12}C]_{VPDB}$, where $\delta^{13}C_{VPDB} = 0‰$). The isotopic composition of common impurities and mineral/fluid inclusions in diamond is calculated similarly, although many isotopic systems have been used to differentiate sources (or reservoirs) for diamond-forming fluids (e.g., [134] and references therein), we restrict our discussion here to C and N.

Accurate differentiation of potential carbon sources is often difficult as it requires that C and N isotope heterogeneity associated with different C and N sources is preserved and recorded during diamond formation. In many cases, the C and N source rocks undergo processes, such as high-T fractionation (e.g., [437]), metasomatism (i.e., partial melting or recrystallization), or mixing between different C/N reservoirs (e.g., recycled vs. primordial mantle reservoirs), these processes result in re-equilibration of C and N isotopes [47, 129]. If this occurs before diamond formation, the recorded isotopic composition reflects a homogenized (*mixed*) source and the original isotopic composition is lost along with information about the original source of C and/or N. It has also been shown that diamond precipitation in both fluid-buffered systems and wall-rock-buffered systems (sects. 4.2 and 4.2.1) may induce C isotope Rayleigh fractionation (see [48, 335, 438]). Fortunately, diffusion of C (and to a lesser extent N) has been shown to occur at negligible rates at lithospheric mantle temperatures [439–441] and thus the distribution of C and N in diamond is representative of formation (and subsequent growth) rather than post-crystallization residence [45, 129].

Stachel et al. [129] report a main mode of $\delta^{13}C = -5.1‰$ for a Kernel density estimation using 4308 inclusion-bearing diamonds from around the world where the modes for most lithospheric diamonds and SDD groups are within $\delta^{13}C = -5.1 \pm 0.2‰$ (Fig. 27). Howell et al. [37] report a similar value of $-5 \pm 2‰$ for 908 $\delta^{13}C$ measurements made on 144 fragments of peridotitic and eclogitic diamonds with formation ages of 3.5–1.4 Ga and 3.0–1.0 Ga, respectively. These $\delta^{13}C$ values are in accord

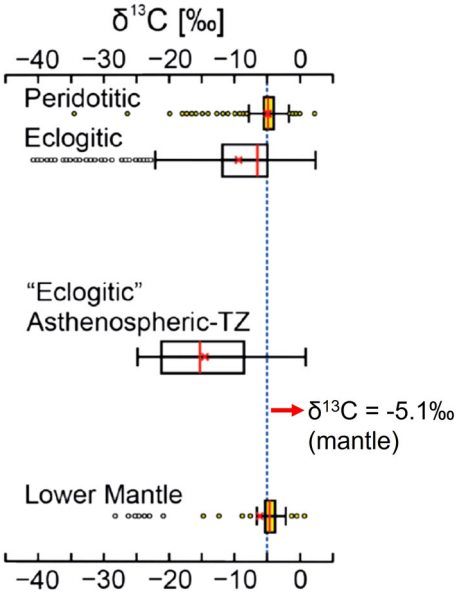

Fig. 27 The $\delta^{13}C$ values for peridotitic and eclogitic diamonds from the upper mantle, eclogitic diamonds from the transition zone, and diamonds from the lower mantle. Median values are shown with red lines, average values with red crosses, and the 25th to 75th percentile ranges for each diamond suite are shown with boxes where ranges are indicated with whiskers. Outliers are shown with small white and yellow circles for meta-basaltic and meta-peridotitic parageneses. The blue dashed lines indicate the isotopic composition of mantle C ($\delta^{13}C = -5.1‰$) and similarities between the $\delta^{13}C$ values of lithospheric peridotitic diamond and those from the lower mantle. From Stachel et al. [129]

with the average C isotopic composition of the Earth's mantle based on carbonatites, kimberlite carbonates, and mantle xenoliths [437, 442]. In general, these observations suggest that diamond-forming fluids generated in the mantle have remained constant with respect to C-speciation and f_{O2} since ~ 3.5 Ga and that diamonds must grow in fluids with excess carbon [37] or in an environment that is continually resupplied with C-rich fluid. Moreover, in the case of eclogitic diamonds, significant isotopic homogenization must occur between C-bearing fluids derived from oceanic crust (with sedimentary and/or organic carbon of more negative $\delta^{13}C$) and mantle-derived fluids and/or melts. However, additional modes of $\delta^{13}C$ at values significantly lower than − 5‰ are observed, particularly in eclogitic and websteritic diamonds (Fig. 27) [43, 129], and may represent different fluid sources (with mantle and slab $\delta^{13}C$ signatures) and/or varying degrees of isotopic fractionation as discussed below. The $\delta^{15}N$ values of diamond from the same dataset of Stachel et al. [129] show much greater variation in comparison to $\delta^{13}C$, ~ 2/3 of diamonds plot over the range $\delta^{15}N = -8.5$ to + 1.5‰ with a mode at 3.5 ± 5‰ which is skewed to positive values with respect to the $\delta^{15}N$ value of the mantle, − 5 ± 2‰ [443].

Overall, $\delta^{13}C$ and $\delta^{15}N$ range from − 41.4 to + 2.5‰ and − 39.4 to + 16.9‰, respectively, and several trends (covariations between $\delta^{13}C$ and $\delta^{15}N$) have been recognized (see [129]) and interpreted based on processes involving *kinetic* and *equilibrium*

isotopic fractionation models and *fluid mixing models* [129]. These models explain how preferential partitioning (given by isotope fractionation factors) of C and N isotopes changes as diamond growth proceeds and the isotopic composition of the diamond and residual fluid evolves. Such models may help one predict the C-speciation of diamond-forming fluids, and when coupled with geochronological and geochemical (paragenetic) information, allow one to infer evolutionary trends in C-speciation associated with different types of diamonds (e.g., peridotitic vs. eclogitic) through geologic time. As an example, consider the isochemical precipitation of diamond in fluid-buffered systems as described in Sect. 4.2.1, where diamond forms from fluids dominated by two C-species. Progressive growth of diamond from a CH_4–CO_2 fluid will result in a core-to-rim $\delta^{13}C$ enrichment of < 1‰ [48]. Precipitation of diamond from a fluid dominated by a single C-species in wall-rock-buffered systems (Sect. 4.2) may result in rimward $\delta^{13}C$ enrichment or depletion when associated with CO_2- or CH_4-dominated fluids, respectively [48]. In general, Rayleigh fractionation will result in higher $\delta^{13}C$ values of diamond precipitated from reducing (CH_4-rich) fluids compared to a more oxidizing (CO_2-rich) fluids if one assumes that the initial fluids are mantle-derived with mantle-like $\delta^{13}C$ of ~ − 5‰. Such relations have been used to suggest that the $\delta^{13}C$ of peridotitic diamonds (mode at − 5.2‰, [129]) must correspond to precipitation from fluids where CH_4 comprises ≥ 50% of the carbon species [48]. Stachel and Harris [43] attribute the relatively heavier $\delta^{13}C$ values of lherzolitic diamonds, compared to other peridotitic diamonds, to involvement of carbonate fluids ($\delta^{13}C$ − 5.5 to − 1.5‰) derived from subducted material. This observation may correspond to major changes in the Earths geodynamics during the Meso- and Neo-Archean where the transition of C recycling via partial melting and devolatilization of the mantle to C recycling via subduction occurred. It follows that diamond-forming fluids in the Eo- to Meso-Archean were likely more reducing and CH_4-rich. Progressive introduction of subducted crustal material in the MesoArchean to Proterozoic likely resulted in more oxidizing (CO_2-rich) fluids and diamond precipitation that occurred by reduction rather than oxidation [43, 47].

In general, perturbations in the C and N isotopic composition, due to fractionation and post-crystallization metasomatism, often result in interpretations about the diamond-forming medium and/or substrate that have some degree of uncertainty. However, isotopic analysis of mineral inclusions, which are protected from processes that may overprint isotopic signatures of source materials, can provide less ambiguous information about the generation and recycling of C-bearing fluids and melts in the mantle.

5.3 Geodynamics of carbon in the sub-lithospheric mantle

Sub-lithospheric diamonds comprise ~ 2% of studied diamonds [6, 42, 134] and the lack of geochronological work on SDDs (e.g., [71]) often results in ambiguous interpretations about the recycling of C in deep mantle. However, as no diamondiferous xenoliths with definitive origins in the transition zone or lower mantle have been discovered [6], SDDs are the only way to directly study the behavior and speciation of

C-, N-, B-, and H-bearing fluids in the deep mantle and the extent to which associated geochemical cycles (e.g., deep C and H_2O cycles) tap different recycled and primordial C reservoirs [58, 59] in transition zone and lower mantle. Consequently, attention has recently turned to the study of SDDs and the inclusions they contain; in this section, we focus on the major hypotheses regarding the geodynamic processes associated with C recycling in base of the upper mantle, transition zone, and lower mantle.

5.3.1 Subduction-related recycling of carbon and SDD formation

Using different seismic methods, namely seismic tomography, the depth and extent of subduction zones, i.e., Wadati–Benioff zones, can be directly imaged. Consequently, it is well understood that downward motion of slabs may stagnate as deep as the transition zone (410–660 km) due to high P phase transitions and subsequent changes in buoyancy forces [381, 382]. Here, slabs are displaced horizontally in the transition zone or at the boundary between the transition zone and lower mantle (~ 660 km) [48, 444] where thermalization via conduction may allow slabs to descend slightly deeper into the shallow lower mantle. The depths at which slabs stagnate is complex and largely dependent on the slab geotherm and composition; in many cases, slabs may stagnate and/or undergo partial melting at much shallower depths [445] and have been associated with formation of some lithospheric diamonds. At depths between 410 and 660 km, slabs can undergo carbonated melting starting generally at temperatures of 1100–1200 °C [6], although this is strongly dependent on slab geotherms and the H_2O content during melting. The pooling of slab materials at ~ 660 km likely forms major reservoirs for recycled C, N, S, and H_2O [56]. As briefly discussed in Sect. 4.3, slab subduction and stagnation are the principal means by which H_2O is recycled in the deep mantle [230, 322, 446].

There is a growing body of evidence that suggests some SDDs form from subducted material (e.g., [3, 6, 47, 48, 55, 67, 70, 71, 88, 133, 248, 258, 378, 379, 447]). In general, these formation models (described in the works cited above) involve the stagnation of subducting slabs in the transition zone and shallow lower mantle and subsequent melting of slab material (e.g., sediment, basalt, and peridotite) to produce small-volume, potentially hydrous, and carbonate melts. Although the properties (density and f_{O2}) of such melts vary as a function of P/T and composition, upon infiltration into the surrounding, highly reducing mantle rock, diamond may crystallize via *Redox-Freezing* (Sect. 4.2) [47, 48, 68]. It is important to note there is strong evidence for non-subduction-related formation of SDDs. For example, Gu et al. [92] provided evidence that polyphase inclusions of ringwoodite, ferropericlase, and low-Ni enstatite in diamond form at ~ 660 km at pressures and temperatures of 23.5 GPa and 1650 °C, respectively. These inclusions are accompanied by other hydrous phases and the source of H_2O is attributed to the dehydration of ringwoodite upon disproportionation into bridgmanite and ferropericlase. These findings are associated with a potentially H_2O-rich environment at the transition zone-lower mantle boundary and thus preclude the requirement for introducing slab-derived materials to produce a diamond-forming medium.

Slab-derived, hydrous, carbonated melts or fluids are highly mobile and several processes by which C-bearing species are transported in the mantle, where diamond may eventually precipitate, have been hypothesized (e.g., [23, 51, 63, 66].). Such fluids are likely aqueous, carbonated HDFs rich in dissolved Si and may infiltrate and metasomatize peridotite substrates within and outside of the slab to reduce C-species and produce diamond. However, many SDDs have several growth centers, complex internal zoning and irregular external morphologies (e.g., the CLIPPIR diamonds) [108] suggestive of multiple periods of diamond dissolution and re-growth. This observation in addition with composite phases interpreted as products of unmixing of high-P phases (e.g., [65, 66, 258]) suggests that some SDDs are transported hundreds of kilometers before incorporation in kimberlitic magma. One explanation involves cyclic *Redox Freezing-Melting*. Here, oxidized and C-rich regions of the mantle, metasomatized by diamond-forming fluids, undergo upwelling. Upon reaching a depth with the appropriate f_{O2} and C-content, diamond will oxidize (dissolve to some degree) to carbonate and lower the local solidus and redox melting will occur to produce another generation of carbonate melt [68, 448]. Such melts may infiltrate reducing mantle peridotitic substrates and, once again, precipitate diamonds via redox freezing [47, 48].

The relatively recent formation ages of SDDs may suggest that deep subduction and carbonated melt generation are required for not only SDD formation, but for the initiation of magmatic processes required to transport them toward the surface (e.g., kimberlite magmatism or mantle-plume upwelling). The absence of Archean SSDs (observed thus far) has helped elucidate the onset of modern-style deep subduction to at least the Mesoproterozoic [71] and provided a basis upon which one can begin to reconcile evidence for the onset of horizontal tectonics in the Meso-Archean (e.g., [29]) and its evolution toward modern-style tectonics in the Mesoproterozoic (e.g., [55]).

5.3.2 Carbon sources and mantle reservoirs: isotopic composition of SDDs

In general, meta-peridotitic and meta-basaltic SDDs show significant variability in $\delta^{13}C$ values compared to lithospheric diamonds. As shown in Fig. 27, SDDs from the asthenosphere-transition zone show significantly lighter $\delta^{13}C$ values; however, those with lower mantle origins show $\delta^{13}C$ values close to that of peridotitic diamonds and mantle C.

Relatively light $\delta^{13}C$ values for low-Cr majoritic garnet ($\delta^{13}C = -3$ to -25 ‰) compared to mantle carbon ($\delta^{13}C = -5 \pm 2$ ‰) in meta-basaltic SDDs have been attributed to diamond-forming fluids sourced from subducted, basaltic oceanic crust [66, 69, 151, 437, 449–452] where the $\delta^{13}C$ in the slab may vary from 0 ‰ for seawater C, to -25 ‰ for organic sedimentary C [66, 151, 450]. An oceanic crustal source for meta-basaltic SDDs is supported by heavy $\delta^{15}N$ values [69] relative to the primitive mantle, -5 ± 2‰ [443] and heavy $\delta^{18}O$ values in majoritic garnet and SiO_2 which points to incorporation of seawater in the subducted oceanic crust [378, 379]. Meta-peridotitic SDDs show generally heavier $\delta^{13}C$ values compared to meta-basaltic SDDs that often overlap with primitive mantle $\delta^{13}C$ values; however, in many cases, major- and trace-element analyses of inclusions in meta-peridotitic SDDs also indicate

a subduction-related origin (e.g., Na-rich clinopyroxene inclusions and anomalously light $\delta^{13}C$ values, [6]). This may suggest a higher degree of mixing of fluids derived from subducted oceanic crustal and mantle sources prior to diamond precipitation in meta-peridotitic SDDs compared to meta-basaltic SDDs. This is evidenced from highly variable core-to-rim $\delta^{13}C$ trends in meta-basaltic SDDs (e.g., $\delta^{13}C$ core-to-rim $= -20$ ‰ to -5%, [151]) attributed to mixing of carbonated melts derived from crustal and primitive mantle sources [6, 378]. SDDs characterized by Fe alloys and sulfide inclusions also show light $\delta^{13}C$ values (e.g., the CLIPPIR diamonds, $\delta^{13}C = -26.9$ to -3.8 ‰ and the Collier-4 diamonds, $\delta^{13}C = -26.0$ to -8.0 ‰, see Sect. 4.3) and Smith et al. [55] suggested that the extremely heavy $\delta^{56}Fe$ (0.79 to 0.90 ‰) compositions of metallic inclusions in CLIPPIR diamonds represent Fe–Ni alloys that crystallized during the serpentinization of peridotite in oceanic crust. Associated age dating of a CLIPPIR diamond [53–55] would place the minimum age of deep, modern-style subduction in the Mesoproterozoic. As is the case with the geochronological database of SDDs, more isotopic data are needed to constrain the source of C-bearing fluids and melts in the deep mantle.

6 Coda

The study of diamond, natural and synthetic, has seen considerable growth over the last 20 years. This is coincident with major developments in analytical methods and improvements to associated instrumental technologies that have allowed measurement (and in some cases, imaging) of impurities (e.g., defects) in diamonds at extremely low concentrations or of inclusions that are increasingly small and in the past, not identifiable. Moreover, recent technological advances have allowed extraction of data from inclusions and/or diamond that was previously overlooked. For example, it was not until the early 2000s that the first systematic X-ray crystallographic studies (e.g., [210].) of mineral inclusions in diamonds were published where important data regarding variations in unit-cell parameters (as a function of entrapment pressure) and relations between the crystallographic orientation of inclusions and their diamond hosts were rigorously treated. As a consequence of such works, several subdisciplines of diamond research have emerged, such as elastic geobarometry (e.g., [214, 220, 246]) and crystallographic orientation relations (CORs) (e.g., [216, 237, 453–455]) and have improved our understanding of the P/T conditions of diamond formation and the protogenetic (or syngenetic) nature of mineral inclusions in diamond (see [219] and references therein).

In general, the goal of geologic diamond research is to understand in what geologic settings, under what thermodynamic conditions, and by what chemical reactions do different types of natural diamonds form. As the analysis of diamond and its inclusions is the only means by which to directly sample the deep Earth, it is often used to support models or hypotheses regarding large-scale Earth processes (e.g., geodynamics of mantle C and the evolution of tectonic processes, see Sect. 5 and references therein) or general planetary processes (e.g., planetary differentiation, compositional evolution of the mantle, crust and atmosphere and sources of volatiles required for life, C (e.g., CO_2, CO_3), O (e.g., O_2, O_3), N (e.g., N_2, NO_2), and H (e.g., H_2O) (e.g.,

[456–459]). Fortunately, time and continued exploration has afforded diamond geologists with increasingly statistically robust datasets that, for lithospheric diamonds, contain thousands of different mineral and fluid inclusions (e.g., [42, 52, 134]). Careful examination of such data has (and will continue to) improve our understanding of how and where diamonds form in the Earth's Mantle.

Lithospheric diamonds precipitate from supercritical fluids and/or supersolidus melts with varying concentrations of C, O, and H and dissolved solutes such as silicates. The speciation of C in solution (e.g., CH_4 or CO_2) and the chemical reaction by which C-species are reduced or oxidized to form diamond, is controlled by the redox conditions (i.e., f_{O2}) of the fluids and diamond substrate into which such fluids may percolate. Lithospheric, peridotitic diamond is typically associated with melt-depleted substrates that comprise the cratonic mantle keel where the majority of lithospheric peridotitic diamonds are assumed to reside. The formation of eclogitic diamonds is likely more complex; it involves infiltration of carbonated melts and/or fluids derived from subducted oceanic lithosphere into the surrounding, relatively reducing, mantle lithologies or within the subducting slab. However, eclogitic diamonds are overrepresented with respect to the predicted abundance of eclogite in the lithospheric mantle and thus must form from processes that are relatively more efficient (condusive to higher growth rates) than those responsible for peridotitic diamond. Stachel et al. [134] suggest that diamond is stable in eclogite at higher f_{O2} than in peridotite and that precipitation of diamond from reduction of CO_2-bearing fluids or isochemical precipitation in a setting with sharp redox variations and large volumes of fluids supplied by dehydration of the subducting slab, could result in nucleation and growth of eclogitic diamond that is relatively more efficient than peridotitic diamond.

The dataset for sub-lithospheric diamonds is relatively small, and thus, models for the formation, growth, and transport of SDDs to the surface are still strongly debated. However, it is likely that SDDs also form from similar C–O–H fluids and melts, although the compositional range and redox properties of such mediums are not completely known [6]. SDDs are broadly grouped into meta-peridotitic and meta-basaltic paragenesis where the former shows heavier C isotopic compositions, similar to mantle C, and the latter shows relatively lighter C isotopic compositions more akin to subducted oceanic crust. It follows that meta-peridotitic SDDs may source C-bearing fluids from the mantle segment of the subducting slab and meta-basaltic SDDs may source fluids via melting and dehydration of the hydrous and carbonated oceanic crust segment of the subducting slab [129]. The study of inclusions in SDDs has provided strong evidence for deep subduction and stagnation of lithospheric material in the transition zone and shallow lower mantle and thus has major implications for the extent of Earths deep carbon and H_2O cycles (e.g., [61, 92, 274, 276, 302, 383]). Inclusions in SDDs are often composite in nature and show evidence of complex unmixing (phase retrogressions) histories that indicate transport from lower mantle to upper mantle conditions. This may be associated with mantle-plume upwelling and transport via melts during redox–freezing–melting cycles, but more work is required to constrain these processes.

In general, most of the work on natural diamond focuses on the mineral and fluid inclusions they contain, but it is likely that additional methods to interpret data related

to impurities (e.g., substitutional and interstitial defects, aggregation states, growth patterns, and structural dislocations) need be developed if the more complex questions regarding the formation of diamond in Mantle are to be addressed. Thus far, impurities (as defined in Chapter 3) have been used to determine the residence time and temperature of diamonds from both a qualitative (e.g., dislocation networks indicative of elasto-plastic deformation attributed to long, high-P residence times) and quantitative (e.g., calculation of mantle residence time/temperature based on N-aggregation state or the degree of platelet degradation) perspective. However, they have not been related, in any rigorous way, to the conditions of diamond formation in the mantle, a potential future direction for the geological research of diamond.

Acknowledgements The authors would like to thank P. Antignani and P. Cornale (Labigem, Vicenza, Italy) for their assistance acquiring FTIR spectra and Anetta Banas and Thomas Stachel (University of Alberta, Canada) for photos of mineral inclusions in diamond. The authors would also like to thank the anonymous reviewer for the helpful comments and suggestions which improved this paper considerably.

Author contributions All four authors contributed to planning, conception, and writing of the review. All four authors read and approved the manuscript.

Funding Open access funding provided by Università degli Studi di Padova within the CRUI-CARE Agreement. This work was funded by the European Union (ERC, INHERIT, starting Grant No. 101041620). Views and opinions expressed are, however, those of the author(s) only and do not necessarily reflect those of the European Union or the European Research Council Executive Agency. Neither the European Union nor the granting authority can be held responsible for them. This review paper is part of a project that has received funding from the European Research Council (ERC) under the European Union's [Seventh Framework Programme (FP7-2007-2013)] (starting Grant No. 307322). DN acknowledges funding from the *Rita Levi Montalcini* program of the Italian Ministry of University and Research

Data availability All data used in the manuscript are sourced from peer-reviewed journals and can be accessed from the corresponding references.

Declarations

Conflict of interest The authors confirm that this work is original and has not been published elsewhere, nor is it currently under consideration for publication elsewhere. The authors declare that they have no financial interests and have no other conflicts of interest to disclose.

References

1. L. Evgeniy, G. Dmitrii, Introductory Chapter, in: Some Aspects of Diamonds in Scientific Research and High Technology, (2020)
2. U.F.S. D'Haenens-Johansson, J.E. Butler, A.N. Katrusha, Synthesis of diamonds and their identification. Rev. Mineral. Geochem. (2022). https://doi.org/10.1515/9781501517044-013

3. A.R. Thomson, S.C. Kohn, G.P. Bulanova, C.B. Smith, D. Araujo, M.J. Walter, Trace element composition of silicate inclusions in sub-lithospheric diamonds from the Juina-5 kimberlite: evidence for diamond growth from slab melts. Lithos (2016). https://doi.org/10.1016/j.lithos.2016.08.035
4. P. Nimis, Pressure and temperature data for diamonds. Rev. Mineral. Geochem. (2022). https://doi.org/10.1515/9781501517044-010
5. P. Nimis, R. Preston, S.H. Perritt, I.L. Chinn, Diamond's depth distribution systematics. Lithos (2020). https://doi.org/10.1016/j.lithos.2020.105729
6. M.J. Walter, A.R. Thomson, E.M. Smith, Geochemistry of Silicate and Oxide Inclusions in Sublithospheric Diamonds, in: Diamond: Genesis, Mineralogy and Geochemistry, 2023. https://doi.org/10.2138/rmg.2022.88.07
7. P.-T. Genzel, M.G. Pamato, D. Novella, L. Santello, S. Lorenzon, S.B. Shirey, D.G. Pearson, F. Nestola, F.E. Brenker, Geobarometric evidence for a LM/TZ origin of CaSiO3 in a sub-lithospheric diamond. Geochem. Perspect. Lett. **25**, 41–45 (2023). https://doi.org/10.7185/geochemlet.2313
8. K. Smit, S. Shirey, G. Pearson, T. Stachel, F. Nestola, T. Moses, Preface. Rev. Mineral. Geochem. **88**, iv–v (2022). https://doi.org/10.2138/rmg.2022.88.00
9. R.D. Oldham, The constitution of the interior of the earth, as revealed by earthquakes. Q. J. Geol. Soc. Lon. (1906). https://doi.org/10.1144/GSL.JGS.1906.062.01-04.21
10. A. Mohorovicic, Earthquake of 8 October 1909, Geofizika. **9**, (1992)
11. P.H. Nixon, A review of mantle xenoliths and their role in diamond exploration. J. Geodyn. (1995). https://doi.org/10.1016/0264-3707(95)00025-5
12. D.G. Pearson, D. Canil, S.B. Shirey, Mantle samples included in volcanic rocks: xenoliths and diamonds, in *Treatise on geochemistry*. (Elsevier, 2003), pp.171–275. https://doi.org/10.1016/B0-08-043751-6/02005-3
13. D.E. Jacob, Nature and origin of eclogite xenoliths from kimberlites. Lithos (2004). https://doi.org/10.1016/j.lithos.2004.03.038
14. A.P. Martin, A review of the composition and chemistry of peridotite mantle xenoliths in volcanic rocks from Antarctica and their relevance to petrological and geophysical models for the lithospheric mantle. Geol. Soc. Memoir. (2023). https://doi.org/10.1144/M56-2021-26
15. S.E. Haggerty, V. Sautter, Ultradeep (greater than 300 kilometers), ultramafic upper mantle xenoliths. Science (1979). (1990). https://doi.org/10.1126/science.248.4958.993
16. V. Sautter, S.E. Haggerty, S. Field, Ultradeep (>300 kilometers) ultramafic xenoliths: petrological evidence from the transition zone. Science (1979). (1991). https://doi.org/10.1126/science.252.5007.827
17. S.E. Haggerty, Majorite-indicative ultradeep (>300 km) xenoliths with spinel associations from the Jagersfontein kimberlite South Africa. South Afr. J. Geol. **120**, 1–20 (2017). https://doi.org/10.25131/gssajg.120.1.1
18. P.J. Wyllie, Metasomatism and fluid generation in mantle xenoliths., Mantle Xenoliths. (1987)
19. C.A. McCammon, W.L. Griffin, S.R. Shee, H.S.C. O'Neill, Oxidation during metasomatism in ultramafic xenoliths from the Wesselton kimberlite, South Africa: implications for the survival of diamond. Contrib. Mineral. Petrol. (2001). https://doi.org/10.1007/s004100100244
20. V. Shatsky, A. Ragozin, D. Zedgenizov, S. Mityukhin, Evidence for multistage evolution in a xenolith of diamond-bearing eclogite from the Udachnaya kimberlite pipe. Lithos (2008). https://doi.org/10.1016/j.lithos.2008.04.008
21. R.W. Luth, T. Stachel, The buffering capacity of lithospheric mantle: implications for diamond formation. Contrib. Mineral. Petrol. (2014). https://doi.org/10.1007/s00410-014-1083-6
22. D.G. Pearson, S.B. Shirey, J.W. Harris, R.W. Carlson, Sulphide inclusions in diamonds from the Koffiefontein kimberlite, S Africa: constraints on diamond ages and mantle Re-Os systematics. Earth Planet. Sci. Lett. (1998). https://doi.org/10.1016/S0012-821X(98)00092-2
23. K.J. Westerlund, S.B. Shirey, S.H. Richardson, R.W. Carlson, J.J. Gurney, J.W. Harris, A subduction wedge origin for Paleoarchean peridotitic diamonds and harzburgites from the Panda kimberlite, Slave craton: evidence from Re-Os isotope systematics. Contrib. Mineral. Petrol. (2006). https://doi.org/10.1007/s00410-006-0101-8
24. S. Aulbach, T. Stachel, R.A. Creaser, L.M. Heaman, S.B. Shirey, K. Muehlenbachs, D. Eichenberg, J.W. Harris, Sulphide survival and diamond genesis during formation and evolution of Archaean subcontinental lithosphere: a comparison between the Slave and Kaapvaal cratons. Lithos (2009). https://doi.org/10.1016/j.lithos.2009.03.048
25. S. Aulbach, T. Stachel, L.M. Heaman, J.A. Carlson, Microxenoliths from the Slave craton: archives of diamond formation along fluid conduits. Lithos (2011). https://doi.org/10.1016/j.lithos.2011.07.012

26. B.A. Kjarsgaard, M. de Wit, L.M. Heaman, D.G. Pearson, J. Stiefenhofer, N. Januszczak, S.B. Shirey, A Review of the Geology of Global Diamond Mines and Deposits, in: Diamond: Genesis, Mineralogy and Geochemistry, 2023. https://doi.org/10.2138/rmg.2022.88.01
27. S.H. Richardson, S.B. Shirey, J.W. Harris, Episodic diamond genesis at Jwaneng, Botswana, and implications for Kaapvaal craton evolution. Lithos (2004). https://doi.org/10.1016/j.lithos.2004.04.027
28. D.G. Pearson, N. Wittig, Formation of Archaean continental lithosphere and its diamonds: the root of the problem. J. Geol. Soc. Lon. (2008). https://doi.org/10.1144/0016-76492008-003
29. S.B. Shirey, S.H. Richardson, Start of the wilson cycle at 3 Ga shown by diamonds from subcontinental mantle. Science (1979). (2011). https://doi.org/10.1126/science.1206275
30. S. Aulbach, Craton nucleation and formation of thick lithospheric roots. Lithos (2012). https://doi.org/10.1016/j.lithos.2012.02.011
31. J.R. Reimink, T. Chacko, R.A. Stern, L.M. Heaman, Earth's earliest evolved crust generated in an Iceland-like setting. Nat. Geosci. (2014). https://doi.org/10.1038/ngeo2170
32. S.F. Foley, T.P. Fischer, An essential role for continental rifts and lithosphere in the deep carbon cycle. Nat. Geosci. (2017). https://doi.org/10.1038/s41561-017-0002-7
33. H. Wang, J. van Hunen, D.G. Pearson, Making Archean cratonic roots by lateral compression: a two-stage thickening and stabilization model. Tectonophysics (2018). https://doi.org/10.1016/j.tecto.2016.12.001
34. M.E. Regier, A. Mišković, R.B. Ickert, D.G. Pearson, T. Stachel, R.A. Stern, M. Kopylova, An oxygen isotope test for the origin of Archean mantle roots. Geochem. Perspect. Lett. (2018). https://doi.org/10.7185/geochemlet.1830
35. K.V. Smit, S.B. Shirey, E.H. Hauri, R.A. Stern, Sulfur isotopes in diamonds reveal differences in continent construction. Science (1979). (2019). https://doi.org/10.1126/science.aaw9548
36. D.G. Pearson, J.M. Scott, J. Liu, A. Schaeffer, L.H. Wang, J. van Hunen, K. Szilas, T. Chacko, P.B. Kelemen, Deep continental roots and cratons. Nature (2021). https://doi.org/10.1038/s41586-021-03600-5
37. D. Howell, T. Stachel, R.A. Stern, D.G. Pearson, F. Nestola, M.F. Hardman, J.W. Harris, A.L. Jaques, S.B. Shirey, P. Cartigny, K.V. Smit, S. Aulbach, F.E. Brenker, D.E. Jacob, E. Thomassot, M.J. Walter, O. Navon, Deep carbon through time: Earth's diamond record and its implications for carbon cycling and fluid speciation in the mantle. Geochim. Cosmochim. Acta. **275**, 99–122 (2020). https://doi.org/10.1016/j.gca.2020.02.011
38. D.G. Pearson, N. Wittig, The formation and evolution of cratonic mantle lithosphere-evidence from mantle xenoliths, in *Treatise on geochemistry*. (Elsevier, 2014), pp.255–292
39. S.B. Shirey, S.H. Richardson, J.W. Harris, Integrated models of diamond formation and craton evolution. Lithos (2004). https://doi.org/10.1016/j.lithos.2004.04.018
40. O. Klein-BenDavid, E.S. Izraeli, E. Hauri, O. Navon, Mantle fluid evolution—a tale of one diamond. Lithos (2004). https://doi.org/10.1016/j.lithos.2004.04.003
41. O. Klein-BenDavid, E.S. Izraeli, E. Hauri, O. Navon, Fluid inclusions in diamonds from the Diavik mine, Canada and the evolution of diamond-forming fluids. Geochim. Cosmochim. Acta. (2007). https://doi.org/10.1016/j.gca.2006.10.008
42. T. Stachel, J.W. Harris, The origin of cratonic diamonds—constraints from mineral inclusions. Ore Geol. Rev. (2008). https://doi.org/10.1016/j.oregeorev.2007.05.002
43. T. Stachel, J.W. Harris, Formation of diamond in the Earth's mantle. J. Phys. Condens. Matter. (2009). https://doi.org/10.1088/0953-8984/21/36/364206
44. S. Creighton, T. Stachel, S. Matveev, H. Höfer, C. McCammon, R.W. Luth, Oxidation of the Kaapvaal lithospheric mantle driven by metasomatism. Contrib. Mineral. Petrol. (2009). https://doi.org/10.1007/s00410-008-0348-3
45. T. Stachel, R.W. Luth, Diamond formation—where, when and how? Lithos (2015). https://doi.org/10.1016/j.lithos.2015.01.028
46. G.M. Yaxley, A.J. Berry, A. Rosenthal, A.B. Woodland, D. Paterson, Redox preconditioning deep cratonic lithosphere for kimberlite genesis—evidence from the central Slave Craton. Sci. Rep. (2017). https://doi.org/10.1038/s41598-017-00049-3
47. S.B. Shirey, P. Cartigny, D.J. Frost, S. Keshav, F. Nestola, P. Nimis, D.G. Pearson, N.V. Sobolev, M.J. Walter, Diamonds and the geology of mantle carbon. Rev. Mineral. Geochem. (2013). https://doi.org/10.2138/rmg.2013.75.12
48. S.B. Shirey, K. V. Smit, D.G. Pearson, M.J. Walter, S. Aulbach, F.E. Brenker, H. Bureau, A.D. Burnham, P. Cartigny, T. Chacko, D.J. Frost, E.H. Hauri, D.E. Jacob, S.D. Jacobsen, S.C. Kohn, R.W.

Luth, S. Mikhail, O. Navon, F. Nestola, P. Nimis, M. Palot, E.M. Smith, T. Stachel, V. Stagno, A. Steele, R.A. Stern, E. Thomassot, A.R. Thomson, Y. Weiss, Diamonds and the Mantle Geodynamics of Carbon: Deep Mantle Carbon Evolution from the Diamond Record, in: Deep Carbon: Past to Present, 2019.
49. V. Stagno, D.O. Ojwang, C.A. McCammon, D.J. Frost, The oxidation state of the mantle and the extraction of carbon from Earth's interior. Nature (2013). https://doi.org/10.1038/nature11679
50. V. Matjuschkin, A.B. Woodland, D.J. Frost, G.M. Yaxley, Reduced methane-bearing fluids as a source for diamond. Sci. Rep. (2020). https://doi.org/10.1038/s41598-020-63518-2
51. Y. Weiss, J. McNeill, D.G. Pearson, G.M. Nowell, C.J. Ottley, Highly saline fluids from a subducting slab as the source for fluid-rich diamonds. Nature (2015). https://doi.org/10.1038/nature14857
52. Y. Weiss, J. Czas, O. Navon, Fluid Inclusions in Fibrous Diamonds, in: Diamond: Genesis, Mineralogy and Geochemistry, 2023. https://doi.org/10.2138/rmg.2022.88.09
53. E.M. Smith, S.B. Shirey, F. Nestola, E.S. Bullock, J. Wang, S.H. Richardson, W. Wang, Large gem diamonds from metallic liquid in Earth's deep mantle. Science (1979). (2016). https://doi.org/10.1126/science.aal1303
54. E.M. Smith, S.B. Shirey, W. Wang, The very deep origin of the world's biggest diamonds. Gems Gemol. (2017). https://doi.org/10.5741/GEMS.53.4.388
55. E.M. Smith, P. Ni, S.B. Shirey, S.H. Richardson, W. Wang, A. Shahar, Heavy iron in large gem diamonds traces deep subduction of serpentinized ocean floor. Sci. Adv. (2021). https://doi.org/10.1126/sciadv.abe9773
56. R.D. Van Der Hilst, S. Widiyantoro, E.R. Engdahl, Evidence for deep mantle circulation from global tomography. Nature (1997). https://doi.org/10.1038/386578a0
57. S.E. Haggerty, A diamond trilogy: superplumes, supercontinents, and supernovae. Science (1979). (1999). https://doi.org/10.1126/science.285.5429.851
58. M.G. Jackson, R.W. Carlson, M.D. Kurz, P.D. Kempton, D. Francis, J. Blusztajn, Evidence for the survival of the oldest terrestrial mantle reservoir. Nature (2010). https://doi.org/10.1038/nature09287
59. M. Touboul, I.S. Puchtel, R.J. Walker, 182W evidence for long-term preservation of early mantle differentiation products. Science (1979). (2012). https://doi.org/10.1126/science.1216351
60. F. Nestola, J.R. Smyth, Diamonds and water in the deep Earth: a new scenario. Int. Geol. Rev. (2016). https://doi.org/10.1080/00206814.2015.1056758
61. O. Tschauner, S. Huang, E. Greenberg, V.B. Prakapenka, C. Ma, G.R. Rossman, A.H. Shen, D. Zhang, M. Newville, A. Lanzirotti, K. Tait, Ice-VII inclusions in diamonds: evidence for aqueous fluid in Earth's deep mantle. Science (1979). (2018). https://doi.org/10.1126/science.aao3030
62. K. Li, L. Li, D.G. Pearson, T. Stachel, Diamond isotope compositions indicate altered igneous oceanic crust dominates deep carbon recycling. Earth Planet. Sci. Lett. (2019). https://doi.org/10.1016/j.epsl.2019.03.041
63. R. Tappert, T. Stachel, J.W. Harris, K. Muehlenbachs, T. Ludwig, G.P. Brey, Subducting oceanic crust: the source of deep diamonds. Geology (2005). https://doi.org/10.1130/G21637.1
64. R. Tappert, T. Stachel, J.W. Harris, K. Muehlenbachs, T. Ludwig, G.P. Brey, Diamonds from Jagersfontein (South Africa): messengers from the sub-lithospheric mantle. Contrib. Miner. Petrol. **150**, 505–522 (2005). https://doi.org/10.1007/s00410-005-0035-6
65. B. Harte, N. Cayzer, Decompression and unmixing of crystals included in diamonds from the mantle transition zone. Phys. Chem. Miner. (2007). https://doi.org/10.1007/s00269-007-0178-2
66. G.P. Bulanova, M.J. Walter, C.B. Smith, S.C. Kohn, L.S. Armstrong, J. Blundy, L. Gobbo, Mineral inclusions in sub-lithospheric diamonds from Collier 4 kimberlite pipe, Juina, Brazil: subducted protoliths, carbonated melts and primary kimberlite magmatism. Contrib. Miner. Petrol. **160**, 489–510 (2010). https://doi.org/10.1007/s00410-010-0490-6
67. M.J. Walter, S.C. Kohn, D. Araujo, G.P. Bulanova, C.B. Smith, E. Gaillou, J. Wang, A. Steele, S.B. Shirey, Deep mantle cycling of oceanic crust: evidence from diamonds and their mineral inclusions. Science (1979). (2011). https://doi.org/10.1126/science.1209300
68. A. Rohrbach, M.W. Schmidt, Redox freezing and melting in the Earths deep mantle resulting from carbon-iron redox coupling. Nature (2011). https://doi.org/10.1038/nature09899
69. M. Palot, P. Cartigny, J.W. Harris, F.V. Kaminsky, T. Stachel, Evidence for deep mantle convection and primordial heterogeneity from nitrogen and carbon stable isotopes in diamond. Earth Planet. Sci. Lett. (2012). https://doi.org/10.1016/j.epsl.2012.09.015

70. B. Harte, Diamond formation in the deep mantle: the record of mineral inclusions and their distribution in relation to mantle dehydration zones. Mineral. Mag. (2010). https://doi.org/10.1180/minmag.2010.074.2.189
71. K. V. Smit, S. Timmerman, S. Aulbach, S.B. Shirey, Geochronology of Diamonds, in: Diamond: Genesis, Mineralogy and Geochemistry, 2023. https://doi.org/10.2138/rmg.2022.88.11.
72. L.F. Dobrzhinetskaya, E.F. O'Bannon, H. Sumino, Non-cratonic diamonds from UHP metamorphic terranes, ophiolites and volcanic sources. Rev. Mineral. Geochem. **88**, 191–255 (2022). https://doi.org/10.2138/rmg.2022.88.04
73. R.S. Lewis, T. Ming, J.F. Wacker, E. Anders, E. Steel, Interstellar diamonds in meteorites. Nature **326**, 160–162 (1987). https://doi.org/10.1038/326160a0
74. V.M. Kvasnytsya, R. Wirth, Impact diamonds from meteorite craters and Neogene placers in Ukraine. Mineral. Petrol. **116**, 169–187 (2022). https://doi.org/10.1007/s00710-022-00778-y
75. A. Giuliani, D.G. Pearson, Kimberlites: from deep earth to diamond mines. Elements (2019). https://doi.org/10.2138/GSELEMENTS.15.6.377
76. M. De Wit, Z. Bhebhe, J. Davidson, S.E. Haggerty, P. Hundt, J. Jacob, M. Lynn, T.R. Marshall, C. Skinner, K. Smithson, J. Stiefenhofer, M. Robert, A. Revitt, R. Spaggiari, J. Ward, Overview of diamond resources in Africa. Episodes (2016). https://doi.org/10.18814/epiiugs/2016/v39i2/95776
77. S.C. Bergman, Lamproites and other potassium-rich igneous rocks: a review of their occurrence, mineralogy and geochemistry. Geol. Soc. Spec. Publ. (1987). https://doi.org/10.1144/GSL.SP.1987.030.01.08
78. E.M.W. Skinner, Contrasting Group 1 and Group 2 kimberlite petrology: Towards a genetic model for kimberlites, in: International Kimberlite Conference Extended Abstracts: 1986, University of Alberta, 1986. https://doi.org/10.29173/ikc1118.
79. T.H. Jordan, Composition and development of the continental tectosphere. Nature (1978). https://doi.org/10.1038/274544a0
80. T.H. Jordan, The continental tectosphere. Rev. Geophys. **13**, 1 (1975). https://doi.org/10.1029/RG013i003p00001
81. F.R. Boyd, J.J. Gurney, Diamonds and the african lithosphere. Science (1986). (1986). https://doi.org/10.1126/science.232.4749.472
82. J. Ritsema, H.J. van Heijst, J.H. Woodhouse, Global transition zone tomography. J. Geophys. Res. Solid Earth. (2004). https://doi.org/10.1029/2003jb002610
83. A.L. Perchuk, T.V. Gerya, V.S. Zakharov, W.L. Griffin, Building cratonic keels in Precambrian plate tectonics. Nature (2020). https://doi.org/10.1038/s41586-020-2806-7
84. T.N. Clifford, Tectono-metallogenic units and metallogenic provinces of Africa. Earth Planet. Sci. Lett. (1966). https://doi.org/10.1016/0012-821X(66)90039-2
85. S. Thomas, Chapter 1: Diamonds, Mineralogical Association of Canada Short Course. **44**, 1–28 (2014).
86. C. Anzolini, R.J. Angel, M. Merlini, M. Derzsi, K. Tokár, S. Milani, M.Y. Krebs, F.E. Brenker, F. Nestola, J.W. Harris, Depth of formation of CaSiO3-walstromite included in super-deep diamonds. Lithos (2016). https://doi.org/10.1016/j.lithos.2016.09.025
87. C. Anzolini, F. Nestola, M.L. Mazzucchelli, M. Alvaro, P. Nimis, A. Gianese, S. Morganti, F. Marone, M. Campione, M.T. Hutchison, J.W. Harris, Depth of diamond formation obtained from single periclase inclusions. Geology (2019). https://doi.org/10.1130/G45605.1
88. T. Stachel, G.P. Brey, J.W. Harris, Inclusions in sub-lithospheric diamonds: glimpses of deep earth. Elements (2005). https://doi.org/10.2113/gselements.1.2.73
89. M.E. Straumanis, E.Z. Aka, Precision determination of lattice parameter, coefficient of thermal expansion and atomic weight of carbon in diamond. J. Am. Chem. Soc. (1951). https://doi.org/10.1021/ja01156a043
90. J.S. Stephen, *A first-principles study on bulk and transfer doping of diamond* (University of Exeter, 2007)
91. I. Silvera, Diamond: Molten under pressure. Nat. Phys. (2010). https://doi.org/10.1038/nphys1491
92. T. Gu, M.G. Pamato, D. Novella, M. Alvaro, J. Fournelle, F.E. Brenker, W. Wang, F. Nestola, Hydrous peridotitic fragments of Earth's mantle 660 km discontinuity sampled by a diamond. Nat. Geosci. (2022). https://doi.org/10.1038/s41561-022-01024-y
93. P. Nemeth, L.A.J. Garvie, T. Aoki, N. Dubrovinskaia, L. Dubrovinsky, P.R. Buseck, Lonsdaleite is faulted and twinned cubic diamond and does not exist as a discrete material. Nat. Commun. (2014). https://doi.org/10.1038/ncomms6447

94. P. Németh, H.J. Lancaster, C.G. Salzmann, K. McColl, Z. Fogarassy, L.A.J. Garvie, L. Illés, B. Pécz, M. Murri, F. Corá, R.L. Smith, M. Mezouar, C.A. Howard, P.F. McMillan, Shock-formed carbon materials with intergrown sp3- and sp2-bonded nanostructured units. Proc. Natl. Acad. Sci. USA. (2022). https://doi.org/10.1073/pnas.2203672119
95. R.J. Angel, M. Alvaro, F. Nestola, M.L. Mazzucchelli, Diamond thermoelastic properties and implications for determining the pressure of formation of diamond-inclusion systems. Russ. Geol. Geophys. (2015). https://doi.org/10.1016/j.rgg.2015.01.014
96. K.S. Scheidl, A. Kurnosov, D.M. Trots, T. Boffa Ballaran, R.J. Angel, R. Miletich, Extending the single-crystal quartz pressure gauge up to hydrostatic pressure of 19 GPa. J. Appl. Crystallogr. (2016). https://doi.org/10.1107/S1600576716015351
97. F. Nestola, D. Pasqual, J.R. Smyth, D. Novella, L. Secco, M.H. Manghnani, A.D. Negro, New accurate elastic parameters for the forsterite-fayalite solid solution. Am. Mineral. (2011). https://doi.org/10.2138/am.2011.3829
98. R.J. Angel, Equations of state of plagioclase feldspars. Contrib. Mineral. Petrol. (2004). https://doi.org/10.1007/s00410-003-0515-5
99. W.A. Deer, R.A. Howie, J. Zussman, An Introduction to the Rock-Forming Minerals. Mineralogical Society of Great Britain and Ireland (2013). https://doi.org/10.1180/DHZ
100. M.E. Thomas, W.J. Tropf, Optical properties of diamond, Johns Hopkins APL Technical Digest (Applied Physics Laboratory). **14**, (1993). https://doi.org/10.1201/9780429283260-7.
101. B.L. Green, A.T. Collins, C.M. Breeding, Diamond spectroscopy, defect centers, color, and treatments. Rev. Mineral. Geochem. (2022). https://doi.org/10.1515/9781501517044-012
102. T.W. Overton, J.E. Shigley, A history of diamond treatments. Gems Gemol. (2008). https://doi.org/10.5741/GEMS.44.1.32
103. T.W. Overton, J.E. Shigley, A History of Diamond Treatments. The Global Diamond Industry: Economics and Development (2015). https://doi.org/10.1057/9781137537614_8
104. R. Robert, J.F. John, A.E. Martin, Two types of diamond, Philosophical Transactions of the Royal Society of London. Series A, Containing Papers of a Mathematical or Physical Character. **232**, 463–535 (1933). https://doi.org/10.1098/rsta.1934.0013
105. J.E. Graebner, Thermal Conductivity of Diamond, in: Diamond: Electronic Properties and Applications, Springer US, Boston, MA, 1995: pp. 285–318. https://doi.org/10.1007/978-1-4615-2257-7_7.
106. E.A. Ekimov, V.A. Sidorov, E.D. Bauer, N.N. Mel'nik, N.J. Curro, J.D. Thompson, S.M. Stishov, Superconductivity in diamond. Nature (2004). https://doi.org/10.1038/nature02449
107. G. Wulff, On the question of speed of growth and dissolution of crystal surfaces. Zeitschrift Fur Kristallographie. **34**, 449–449 (1901)
108. J.W. Harris, K. V. Smit, Y. Fedortchouk, M. Moore, Morphology of Monocrystalline Diamond and its Inclusions, in: Diamond: Genesis, Mineralogy and Geochemistry, 2023. https://doi.org/10.2138/rmg.2022.88.02.
109. G. A. C., Yu. L. Orlov 1977. The Mineralogy of the Diamond. x + 235 pp., 84 figs, 26 tables. New York: John Wiley. Price £17.00; U.S. $32.00. ISBN 0 471 01869 4., Geol Mag. **115**, 474–474 (1978). https://doi.org/10.1017/S001675680004190X.
110. M. Moore, A.R. Lang, On the internal structure of natural diamonds of cubic habit. Phil. Mag. **26**, 1313–1325 (1972). https://doi.org/10.1080/14786437208220345
111. C.R. Clement, J.W. Harris, D.N. Robinson, J.B. Hawthorne, The de Beers kimberlite pipe : a historic South African diamond mine, Kimberley, South Africa, 1986.
112. S. Yamaoka, H. Komatsu, H. Kanda, N. Setaka, Growth of diamond with rhombic dodecahedral faces. J. Cryst. Growth. (1977). https://doi.org/10.1016/0022-0248(77)90131-2
113. E.M. Smith, S.B. Shirey, S.H. Richardson, F. Nestola, E.S. Bullock, J. Wang, W. Wang, Blue boron-bearing diamonds from Earth's lower mantle. Nature (2018). https://doi.org/10.1038/s41586-018-0334-5
114. M. Moore, A.R. Lang, On the origin of the rounded dodecahedral habit of natural diamond. J. Cryst. Growth. (1974). https://doi.org/10.1016/0022-0248(74)90213-9
115. Y. Fedortchouk, D. Canil, E. Semenets, Mechanisms of diamond oxidation and their bearing on the fluid composition in kimberlite magmas. Am. Miner. **92**, 1200–1212 (2007). https://doi.org/10.2138/am.2007.2416
116. Y. Fedortchouk, D. Canil, Diamond oxidation at atmospheric pressure: development of surface features and the effect of oxygen fugacity. Eur. J. Mineral. (2009). https://doi.org/10.1127/0935-1221/2009/0021-1929

117. F.C. Frank, K.E. Puttick, E.M. Wilks, Etch pits and trigons on diamond: I. Philos. Mag. (1958). https://doi.org/10.1080/14786435808233308
118. A. Lüttge, Crystal dissolution kinetics and Gibbs free energy. J. Electron. Spectros Relat. Phenomena. (2006). https://doi.org/10.1016/j.elspec.2005.06.007
119. A. Lang, X-ray topography of diamond, in *Physical properties of diamonds*. ed. by R. Berman (Glarendon Press, Oxford, 1965), pp.69–115
120. A. Lang, Dislocations in diamond and the origin of trigones. Proc. R. Soc. Lond. A Math. Phys. Sci. **278**, 234–242 (1964). https://doi.org/10.1098/rspa.1964.0057
121. Z. Li, Y. Fedortchouk, A. Fulop, I.L. Chinn, N. Forbes, Positively oriented trigons on diamonds from the Snap Lake kimberlite dike, Canada: implications for fluids and kimberlite cooling rates. Am. Mineral. (2018). https://doi.org/10.2138/am-2018-6496
122. J.R. Sutton, Diamond: a descriptive treatise, T. Murby. (1928)
123. A.R. Lang, Glimpses into the growth history of natural diamonds. J Cryst. Growth. (1974). https://doi.org/10.1016/0022-0248(74)90287-5
124. D.E. Jacob, S. Mikhail, Polycrystalline Diamonds from Kimberlites: Snapshots of Rapid and Episodic Diamond Formation in the Lithospheric Mantle, in: Diamond: Genesis, Mineralogy and Geochemistry, 2023. https://doi.org/10.2138/rmg.2022.88.03
125. G. Kurat, G. Dobosi, Garnet and diopside-bearing diamondites (framesites). Mineral Petrol. **69**, 143–159 (2000). https://doi.org/10.1007/s007100070018
126. R.I. Kostov, Crystals: Growth, Morphology and Perfection: by I. Sunagawa, Cambridge University Press, Cambridge, U.K., 2005, 295 + xii pages. CAN $127.95. Hardbound. ISBN 0 521 841 895., The Canadian Mineralogist. **43**, (2005). https://doi.org/10.2113/gscanmin.43.3.1127
127. S. Mikhail, F.M. McCubbin, F.E. Jenner, S.B. Shirey, D. Rumble, R. Bowden, Diamondites: evidence for a distinct tectono-thermal diamond-forming event beneath the Kaapvaal craton. Contrib. Miner. Petrol. **174**, 71 (2019). https://doi.org/10.1007/s00410-019-1608-0
128. R. Robertson, J.J. Fox, A.E. Martin, Two types of diamond, Nature. **134**, (1934). https://doi.org/10.1038/134485a0
129. T. Stachel, P. Cartigny, T. Chacko, D.G. Pearson, Carbon and Nitrogen in Mantle-Derived Diamonds, in: Diamond: Genesis, Mineralogy and Geochemistry, 2023. https://doi.org/10.2138/rmg.2022.88.15
130. A. Ishida, K. Kitajima, K. Hashizume, M.J. Spicuzza, A. Zaitsev, D.J. Schulze, J.W. Valley, Microscale simultaneous measurement of carbon and nitrogen isotopes on natural diamond. Geostand Geoanal. Res. (2023). https://doi.org/10.1111/ggr.12485
131. B. Dischler, Handbook of Spectral Lines in Diamond, 2012. https://doi.org/10.1007/978-3-642-22215-3
132. S. Salustro, F.S. Gentile, A. Erba, P. Carbonniére, K.E. El-Kelany, R. Dovesi, The characterization of the VNxHy defects in diamond through the infrared vibrational spectrum. A quantum mechanical investigation. Carbon N Y (2018). https://doi.org/10.1016/j.carbon.2018.02.045
133. S.B. Shirey, L.S. Wagner, M.J. Walter, D.G. Pearson, P.E. van Keken, Slab transport of fluids to deep focus earthquake depths—thermal modeling constraints and evidence from diamonds. AGU Adv. (2021). https://doi.org/10.1029/2020av000304
134. T. Stachel, S. Aulbach, J.W. Harris, Mineral Inclusions in Lithospheric Diamonds, in: Diamond: Genesis, Mineralogy and Geochemistry, 2023. https://doi.org/10.2138/rmg.2022.88.06
135. N. V Sobolev, yev Y.G. Lavrent, L.N. Pospelova, Y. V Sobolev, Chrome pyrope from Yakutian diamonds, Transactions (Doklady) of the U.S.S.R. Academy of Sciences: Earth Science Sections. **189**, (1970)
136. N.V. Sobolev, Y.G. Lavrent'ev, N.P. Pokhilenko, L.V. Usova, Chrome-rich garnets from the kimberlites of yakutia and their parageneses. Contrib. Mineral. Petrol. (1973). https://doi.org/10.1007/BF00371762
137. H.S. Grütter, J.J. Gurney, A.H. Menzies, F. Winter, An updated classification scheme for mantle-derived garnet, for use by diamond explorers. Lithos (2004). https://doi.org/10.1016/j.lithos.2004.04.012
138. J.R. Clark, J.J. Papike, Crystal-chemical characterization of omphacites. Am. Miner. **53**, 840–868 (1968)
139. J.J. Gurney, A correlation between garnets and diamonds in kimberlites., Kimberlite Occurrence and Origin. (1984)
140. F.R. Boyd, Compositional distinction between oceanic and cratonic lithosphere. Earth Planet. Sci. Lett. (1989). https://doi.org/10.1016/0012-821X(89)90120-9

141. W.L. Griffin, The composition and origin of sub-continental lithospheric mantle, Mantle Petrology: Field Observations and High Pressure Experimentation, A Tribute to Francis R.(Joe) Boyd . 13–45 (1999)
142. C. Herzberg, Geodynamic information in peridotite petrology. J. Petrol. (2004). https://doi.org/10.1093/petrology/egh039
143. B.L. Beard, K.N. Fraracci, L.A. Taylor, G.A. Snyder, R.A. Clayton, T.K. Mayeda, N.V. Sobolev, Petrography and geochemistry of eclogites from the Mir kimberlite, Yakutia, Russia. Contrib. Mineral. Petrol. (1996). https://doi.org/10.1007/s004100050223
144. T. Stachel, S. Aulbach, G.P. Brey, J.W. Harris, I. Leost, R. Tappert, K.S. Viljoen, The trace element composition of silicate inclusions in diamonds: a review. Lithos (2004). https://doi.org/10.1016/j.lithos.2004.03.027
145. D.J. Schulze, B. Harte, J.W. Valley, J.M. Brenan, D.M.D.R. Channer, Extreme crustal oxygen isotope signatures preserved in coesite in diamond. Nature (2003). https://doi.org/10.1038/nature01615
146. T. Stachel, J.W. Harris, L. Hunt, K. Muehlenbachs, A.F. Kobussen, Argyle Diamonds: How Subduction Along the Kimberley Craton Edge Generated the World's Biggest Diamond Deposit*, in: Geoscience and Exploration of the Argyle, Bunder, Diavik, and Murowa Diamond Deposits, Society of Economic Geologists, 2018: pp. 145–167. https://doi.org/10.5382/SP.20.06
147. M. Chaussidon, F. Albarède, S.M.F. Sheppard, Sulphur isotope heterogeneity in the mantle from ion microprobe measurements of sulphide inclusions in diamonds. Nature (1987). https://doi.org/10.1038/330242a0
148. C.S. Eldridge, W. Compston, I.S. Williams, J.W. Harris, J.W. Bristow, Isotope evidence for the involvement of recycled sediments in diamond formation. Nature (1991). https://doi.org/10.1038/353649a0
149. J. Farquhar, B.A. Wing, K.D. McKeegan, J.W. Harris, P. Cartigny, M.H. Thiemens, Mass-independent sulfur of inclusions in diamond and sulfur recycling on early Earth. Science (1979). (2002). https://doi.org/10.1126/science.1078617
150. E. Thomassot, P. Cartigny, J.W. Harris, J.P. Lorand, C. Rollion-Bard, M. Chaussidon, Metasomatic diamond growth: A multi-isotope study (13C, 15N, 33S, 34S) of sulphide inclusions and their host diamonds from Jwaneng (Botswana). Earth Planet. Sci. Lett. (2009). https://doi.org/10.1016/j.epsl.2009.03.001
151. A.R. Thomson, S.C. Kohn, G.P. Bulanova, C.B. Smith, D. Araujo, EIMF, M.J. Walter, Origin of sub-lithospheric diamonds from the Juina-5 kimberlite (Brazil): constraints from carbon isotopes and inclusion compositions. Contrib. Mineral. Petrol. (2014). https://doi.org/10.1007/s00410-014-1081-8
152. J.M. Garber, S. Maurya, J.A. Hernandez, M.S. Duncan, L. Zeng, H.L. Zhang, U. Faul, C. McCammon, J.P. Montagner, L. Moresi, B.A. Romanowicz, R.L. Rudnick, L. Stixrude, Multidisciplinary constraints on the abundance of diamond and eclogite in the cratonic lithosphere. Geochem. Geophys. Geosyst. (2018). https://doi.org/10.1029/2018GC007534
153. M.B. Kirkley, J.J. Gurney, A.A. Levinson, Age, Origin, and Emplacement of Diamonds: Scientific Advances in the Last Decade, Gems and Gemology. **27**, (1991).
154. R.A. Howie, G. E. Harlow (ed). The Nature of Diamonds, Cambridge (Cambridge University Press), 1997, x + 278 pp. Price £55.00 (hardback, ISBN 0–521–62083X); £19.95 (paperback, ISBN 0–521–62935–7)., Mineral Mag. **62**, 578–579 (1998). https://doi.org/10.1180/minmag.1998.62.4.06
155. D.G. Pearson, J. Woodhead, P.E. Janney, Kimberlites as geochemical probes of earth's mantle. Elements (2019). https://doi.org/10.2138/GSELEMENTS.15.6.387
156. C.B. Smith, Pb, Sr and Nd isotopic evidence for sources of southern African Cretaceous kimberlites. Nature (1983). https://doi.org/10.1038/304051a0
157. A.R. Woolley, S.C. Bergman, A.D. Edgar, M.J. Le Bas, R.H. Mitchell, N.M.S. Rock, B.H.S. Smith, Classification of lamprophyres, lamproites, kimberlites, and the kalsilitic, melilitic, and leucitic rocks. Can. Mineral. **34**, 175–186 (1996)
158. R.H. Mitchell, *Kimberlites, orangeites, and related rocks* (Springer US, 1995)
159. R.W. Le Maitre, P. Bateman, A. Dudek, J. Keller, J. Lameyre, M.J. Le Bas, P.A. Sabine, R. Schmit, H. Sorensen, A. Streckeisen, A.R. Woolley, B. Zanettin, *A classification of Igneous rocks and glossary of terms: recommendations of the International Union of Geological Sciences subcommission on the systematic of igneous rocks* (Blackwell Scientific, Oxford, 1989), p.193

160. R.J. Brown, S. Manya, I. Buisman, G. Fontana, M. Field, C. Mac Niocaill, R.S.J. Sparks, F.M. Stuart, Eruption of kimberlite magmas: Physical volcanology, geomorphology and age of the youngest kimberlitic volcanoes known on earth (the Upper Pleistocene/Holocene Igwisi Hills volcanoes, Tanzania). Bull. Volcanol. (2012). https://doi.org/10.1007/s00445-012-0619-8
161. C.L. Donnelly, T. Stachel, S. Creighton, K. Muehlenbachs, S. Whiteford, Diamonds and their mineral inclusions from the A154 South pipe, Diavik Diamond Mine, Northwest territories, Canada. Lithos (2007). https://doi.org/10.1016/j.lithos.2007.03.003
162. A.M. Ferrari, S. Salustro, F.S. Gentile, W.C. Mackrodt, R. Dovesi, Substitutional nitrogen atom in diamond. A quantum mechanical investigation of the electronic and spectroscopic properties. Carbon N Y. (2018). https://doi.org/10.1016/j.carbon.2018.03.091
163. E. Sideras-Haddad, S.H. Connell, J.P.F. Sellschop, I.Z. Machi, D. Rebuli, R.D. Maclear, B.P. Doyle, Hydrogen and oxygen chemistry and dynamics in diamond studied by nuclear microscopic techniques. Nucl. Instrum. Methods Phys. Res. B (2001). https://doi.org/10.1016/S0168-583X(01)00595-X
164. P.R.W. Hudson, I.S.T. Tsong, Hydrogen impurity in natural gem diamond. J. Mater. Sci. (1977). https://doi.org/10.1007/BF00553924
165. J.P. Goss, R. Jones, M.I. Heggie, C.P. Ewels, P.R. Briddon, S. Öberg, Theory of hydrogen in diamond. Phys. Rev. B. **65**, 115207 (2002). https://doi.org/10.1103/PhysRevB.65.115207
166. A. Upadhyay, A.K. Singh, A. Kumar, Electronic structure and stability of hydrogen defects in diamond and boron doped diamond: a density functional theory study. Comput. Mater. Sci. (2014). https://doi.org/10.1016/j.commatsci.2014.03.022
167. J.P. Goss, P.R. Briddon, Calculated strain response of vibrational modes for H-containing point defects in diamond. Phys. Chem. Chem. Phys. **13**, 11488 (2011). https://doi.org/10.1039/c1cp00038a
168. F.S. Gentile, S. Salustro, J.K. Desmarais, A.M. Ferrari, P. D'Arco, R. Dovesi, Vibrational spectroscopy of hydrogens in diamond: a quantum mechanical treatment. Phys. Chem. Chem. Phys. **20**, 11930–11940 (2018). https://doi.org/10.1039/C8CP00596F
169. E. Gaillou, J.E. Post, D. Rost, J.E. Butler, Boron in natural type IIb blue diamonds: chemical and spectroscopic measurements. Am. Mineral. (2012). https://doi.org/10.2138/am.2012.3925
170. C. Saguy, R. Kalish, C. Cytermann, Z. Teukam, J. Chevallier, F. Jomard, A. Tromson-Carli, J.E. Butler, C. Baron, A. Deneuville, n-type diamond with high room temperature electrical conductivity by deuteration of boron doped diamond layers. Diam. Relat. Mater. (2004). https://doi.org/10.1016/j.diamond.2003.11.066
171. J. Chevallier, B. Theys, A. Lusson, C. Grattepain, A. Deneuville, E. Gheeraert, Hydrogen-boron interactions in p-type diamond. Phys. Rev. B. **58**, 7966–7969 (1998). https://doi.org/10.1103/PhysRevB.58.7966
172. F.S. Gentile, S. Salustro, M. Causà, A. Erba, P. Carbonniére, R. Dovesi, The VN3H defect in diamond: a quantum-mechanical characterization. Phys. Chem. Chem. Phys. (2017). https://doi.org/10.1039/c7cp03957c
173. T. Gu, S. Ritterbex, T. Tsuchiya, W. Wang, Novel configurations of VN4 and VN4H defects in diamond platelets: structure, energetics and vibrational properties. Diam. Relat. Mater. **108**, 107957 (2020). https://doi.org/10.1016/j.diamond.2020.107957
174. C.V. Peaker, J.P. Goss, P.R. Briddon, A.B. Horsfall, M.J. Rayson, The vacancy-hydrogen defect in diamond: a computational study. Phys. Status Solidi (A). **212**, 2431–2436 (2015). https://doi.org/10.1002/pssa.201532215
175. C.V. Peaker, J.P. Goss, P.R. Briddon, A.B. Horsfall, M.J. Rayson, Di-nitrogen-vacancy-hydrogen defects in diamond: a computational study. Phys. Status Solidi (A). **212**, 2616–2620 (2015). https://doi.org/10.1002/pssa.201532216
176. F. Pascale, S. Salustro, A.M. Ferrari, M. Rérat, P. D'Arco, R. Dovesi, The Infrared spectrum of very large (periodic) systems: global versus fragment strategies—the case of three defects in diamond. Theor. Chem. Acc. **137**, 170 (2018). https://doi.org/10.1007/s00214-018-2380-3
177. S. Salustro, F.S. Gentile, P. D'Arco, B. Civalleri, M. Rérat, R. Dovesi, Hydrogen atoms in the diamond vacancy defect. A quantum mechanical vibrational analysis. Carbon N Y. **129**, 349–356 (2018). https://doi.org/10.1016/j.carbon.2017.12.011
178. E. Fritsch, T. Hainschwang, L. Massi, B. Rondeau, Hydrogen-related optical centers in natural diamond: an update. New Diam. Front. Carbon Technol. **17**, 63 (2007)
179. M.N.R. Ashfold, J.P. Goss, B.L. Green, P.W. May, M.E. Newton, C.V. Peaker, Nitrogen in diamond. Chem. Rev. **120**, 5745–5794 (2020). https://doi.org/10.1021/acs.chemrev.9b00518
180. J.O. Wood, *An elusive impurity: studying hydrogen in natural diamonds* (University of Bristol, 2020)

181. M.J. Mendelssohn, H.J. Milledge, Geologically significant information from routine analysis of the mid-infrared spectra of diamonds. Int. Geol. Rev. **37**, 95–110 (1995). https://doi.org/10.1080/00206819509465395
182. W.R. Taylor, D. Canil, H. Judith Milledge, Kinetics of Ib to IaA nitrogen aggregation in diamond. Geochim. Cosmochim. Acta. **60**, 4725–4733 (1996). https://doi.org/10.1016/S0016-7037(96)00302-X
183. L. Speich, S.C. Kohn, QUIDDIT—quantification of infrared active defects in diamond and inferred temperatures. Comput. Geosci. (2020). https://doi.org/10.1016/j.cageo.2020.104558
184. D. Howell, C.J. O'Neill, K.J. Grant, W.L. Griffin, N.J. Pearson, S.Y. O'Reilly, μ-FTIR mapping: distribution of impurities in different types of diamond growth. Diam. Relat. Mater. (2012). https://doi.org/10.1016/j.diamond.2012.06.003
185. W.R. Taylor, A.L. Jaques, M. Ridd, Nitrogen-defect aggregation characteristics of some Australasian diamonds: time-temperature constraints on the source regions of pipe and alluvial diamonds, Am. Mineral. **75**, (1990).
186. S.C. Kohn, L. Speich, C.B. Smith, G.P. Bulanova, FTIR thermochronometry of natural diamonds: a closer look. Lithos (2016). https://doi.org/10.1016/j.lithos.2016.09.021
187. J.P. Goss, P.R. Briddon, V. Hill, R. Jones, M.J. Rayson, Identification of the structure of the 3107 cm-1 H-related defect in diamond. J. Phys. **26**, 145801 (2014). https://doi.org/10.1088/0953-8984/26/14/145801
188. G.S. Woods, A.T. Collins, Infrared absorption spectra of hydrogen complexes in type I diamonds. J. Phys. Chem. Solids. (1983). https://doi.org/10.1016/0022-3697(83)90078-1
189. K. Czelej, P. Śpiewak, Hydrogen passivation of vacancies in diamond: electronic structure and stability from ab initio calculations. MRS Adv. **2**, 309–314 (2017). https://doi.org/10.1557/adv.2017.100
190. M.Y. Lai, C.M. Breeding, T. Stachel, R.A. Stern, Spectroscopic features of natural and HPHT-treated yellow diamonds. Diam. Relat. Mater. (2020). https://doi.org/10.1016/j.diamond.2019.107642
191. G.L. Melton, T. Stachel, R.A. Stern, J. Carlson, J.W. Harris, Infrared spectral and carbon isotopic characteristics of micro- and macro-diamonds from the Panda kimberlite (Central Slave Craton, Canada). Lithos (2013). https://doi.org/10.1016/j.lithos.2013.06.019
192. L. Speich, S.C. Kohn, R. Wirth, G.P. Bulanova, C.B. Smith, The relationship between platelet size and the B′ infrared peak of natural diamonds revisited. Lithos (2017). https://doi.org/10.1016/j.lithos.2017.02.010
193. M.I. Heggie, S. Jenkins, C.P. Ewels, P. Jemmer, R. Jones, P.R. Briddon, Theory of dislocations in diamond and silicon and their interaction with hydrogen. J. Phys. Condens. Matter. (2000). https://doi.org/10.1088/0953-8984/12/49/327
194. A.T. Blumenau, R. Jones, T. Frauenheim, B. Willems, O.I. Lebedev, G. Van Tendeloo, D. Fisher, P.M. Martineau, Dislocations in diamond: dissociation into partials and their glide motion. Phys. Rev. B. **68**, 014115–014117 (2003). https://doi.org/10.1103/PhysRevB.68.014115
195. J. Blanc, Thermodynamics of 'glide' and 'shuffle' dislocations in the diamond lattice. Phil. Mag. **32**, 1023–1032 (1975). https://doi.org/10.1080/14786437508221670
196. F. Louchet, J. Thibault-Desseaux, Dislocation cores in semiconductors. From the « shuffle or glide » dispute to the « glide and shuffle » partnership. Rev. Phys. Appl. (1987). https://doi.org/10.1051/rphysap:01987002204020700
197. J.P. Goss, B.J. Coomer, R. Jones, C.J. Fall, P.R. Briddon, S. Öberg, Extended defects in diamond: the interstitial platelet. Phys. Rev. B Condens. Matter. Mater. Phys. (2003). https://doi.org/10.1103/PhysRevB.67.165208
198. P. Humble, The structure and mechanism of formation of platelets in natural type Ia diamond, Proceedings of the Royal Society of London. A. Mathematical and Physical Sciences. **381**, 65–81 (1982). https://doi.org/10.1098/rspa.1982.0059
199. L. Speich, S.C. Kohn, G.P. Bulanova, C.B. Smith, The behaviour of platelets in natural diamonds and the development of a new mantle thermometer. Contrib. Mineral. Petrol. (2018). https://doi.org/10.1007/s00410-018-1463-4
200. N. Sumida, A.R. Lang, Cathodoluminescence evidence of dislocation interactions in diamond. Philos. Mag. A. (1981). https://doi.org/10.1080/01418618108236156
201. A. Mainwood, Nitrogen and nitrogen-vacancy complexes and their formation in diamond. Phys. Rev. B. (1994). https://doi.org/10.1103/PhysRevB.49.7934
202. I. Kiflawi, J. Bruley, The nitrogen aggregation sequence and the formation of voidites in diamond. Diam. Relat. Mater. **9**, 87–93 (2000). https://doi.org/10.1016/S0925-9635(99)00265-4

203. H.O.A. Meyer, Chrome pyrope: an inclusion in natural diamond. Science (1979). (1968). https://doi.org/10.1126/science.160.3835.1446
204. H.O.A. Meyer, F.R. Boyd, Composition and origin of crystalline inclusions in natural diamonds. Geochim. Cosmochim. Acta. (1972). https://doi.org/10.1016/0016-7037(72)90048-8
205. H.O.A. Meyer, *Inclusions in diamond mantle xenoliths* (Wiley, 1987)
206. O. Navon, I.D. Hutcheon, G.R. Rossman, G.J. Wasserburg, Mantle-derived fluids in diamond micro-inclusions. Nature (1988). https://doi.org/10.1038/335784a0
207. J.W. Harris, Recognition of diamond inclusions. 2. Epigenetic mineral inclusions. Ind. Diamond Rev. **28**, 458–458 (1968)
208. J.W. Harris, Recognition of diamond inclusions. 1. Syngenetic mineral inclusions. Ind. Diamond Rev. **28**, 402–402 (1968)
209. J.W. Harris, J.J. Gurney, Inclusions in diamond, in *The properties of diamonds*. ed. by J.E. Field (Academic Press, London, 1979), pp.555–591
210. F. Nestola, P. Nimis, R.J. Angel, S. Milani, M. Bruno, M. Prencipe, J.W. Harris, Olivine with diamond-imposed morphology included in diamonds. Syngenesis or protogenesis? Int Geol Rev. (2014). https://doi.org/10.1080/00206814.2014.956153
211. G. Agrosì, F. Nestola, G. Tempesta, M. Bruno, E. Scandale, J. Harris, X-ray topographic study of a diamond from Udachnaya: implications for the genetic nature of inclusions. Lithos (2016). https://doi.org/10.1016/j.lithos.2016.01.028
212. F. Nestola, H. Jung, L.A. Taylor, Mineral inclusions in diamonds may be synchronous but not syngenetic. Nat. Commun. (2017). https://doi.org/10.1038/ncomms14168
213. F. Nestola, D.E. Jacob, M.G. Pamato, L. Pasqualetto, B. Oliveira, S. Greene, S. Perritt, I. Chinn, S. Milani, N. Kueter, N. Sgreva, P. Nimis, L. Secco, J.W. Harris, Protogenetic garnet inclusions and the age of diamonds. Geology (2019). https://doi.org/10.1130/G45781.1
214. F. Nestola, G. Zaffiro, M.L. Mazzucchelli, P. Nimis, G.B. Andreozzi, B. Periotto, F. Princivalle, D. Lenaz, L. Secco, L. Pasqualetto, A.M. Logvinova, N.V. Sobolev, A. Lorenzetti, J.W. Harris, Diamond-inclusion system recording old deep lithosphere conditions at Udachnaya (Siberia). Sci. Rep. (2019). https://doi.org/10.1038/s41598-019-48778-x
215. P. Nimis, R.J. Angel, M. Alvaro, F. Nestola, J.W. Harris, N. Casati, F. Marone, Crystallographic orientations of magnesiochromite inclusions in diamonds: what do they tell us? Contrib. Mineral. Petrol. (2019). https://doi.org/10.1007/s00410-019-1559-5
216. S. Milani, F. Nestola, R.J. Angel, P. Nimis, J.W. Harris, Crystallographic orientations of olivine inclusions in diamonds. Lithos (2016). https://doi.org/10.1016/j.lithos.2016.06.010
217. T.A. Griffiths, G. Habler, R. Abart, Crystallographic orientation relationships in host-inclusion systems: new insights from large EBSD data sets. Am. Mineral. (2016). https://doi.org/10.2138/am-2016-5442
218. G. Habler, T. Griffiths, Crystallographic orientation relationships, European Mineralogical Union Notes in Mineralogy. **16**, (2017). https://doi.org/10.1180/EMU-notes.16.15
219. R.J. Angel, M. Alvaro, F. Nestola, Crystallographic methods for non-destructive characterization of mineral inclusions in diamonds. Rev. Mineral. Geochem. (2022). https://doi.org/10.2138/rmg.2022.88.05
220. F. Nestola, How to apply elastic geobarometry in geology. Am. Mineral. (2021). https://doi.org/10.2138/am-2021-7845
221. M.G. Pamato, D. Novella, D.E. Jacob, B. Oliveira, D.G. Pearson, S. Greene, J.C. Afonso, M. Favero, T. Stachel, M. Alvaro, F. Nestola, Protogenetic sulfide inclusions in diamonds date the diamond formation event using Re-Os isotopes. Geology (2021). https://doi.org/10.1130/G48651.1
222. L.A. Taylor, M. Anand, Diamonds: time capsules from the Siberian mantle. Chem. Erde. (2004). https://doi.org/10.1016/j.chemer.2003.11.006
223. M.G. Barth, S.F. Foley, I. Horn, Partial melting in Archean subduction zones: constraints from experimentally determined trace element partition coefficients between eclogitic minerals and tonalitic melts under upper mantle conditions. Precambrian Res. (2002). https://doi.org/10.1016/S0301-9268(01)00216-9
224. T.R. Ireland, R.L. Rudnick, Z. Spetsius, Trace elements in diamond inclusions from eclogites reveal link to Archean granites. Earth Planet. Sci. Lett. **128**, 199–213 (1994). https://doi.org/10.1016/0012-821X(94)90145-7
225. S. Foley, M. Tiepolo, R. Vannucci, Growth of early continental crust controlled by melting of amphibolite in subduction zones. Nature (2002). https://doi.org/10.1038/nature00799

226. N. Miyajima, T. Yagi, K. Hirose, T. Kondo, K. Fujino, H. Miura, Potential host phase of aluminum and potassium in the Earth's lower mantle. Am. Mineral. (2001). https://doi.org/10.2138/am-2001-5-614
227. L. Liu, An alternative interpretation of lower mantle mineral associations in diamonds. Contrib. Miner. Petrol. **144**, 16–21 (2002). https://doi.org/10.1007/s00410-002-0389-y
228. P. Nimis, F. Nestola, M. Schiazza, R. Reali, G. Agrosì, D. Mele, G. Tempesta, D. Howell, M.T. Hutchison, R. Spiess, Fe-rich ferropericlase and magnesiowüstite inclusions reflecting diamond formation rather than ambient mantle. Geology (2019). https://doi.org/10.1130/G45235.1
229. T. Stachel, J.W. Harris, Syngenetic inclusions in diamond from the Birim field (Ghana)—a deep peridotitic profile with a history of depletion and re-enrichment. Contrib. Miner. Petrol. **127**, 336–352 (1997). https://doi.org/10.1007/s004100050284
230. G.P. Brey, V. Bulatov, A. Girnis, J.W. Harris, T. Stachel, Ferropericlase—a lower mantle phase in the upper mantle. Lithos (2004). https://doi.org/10.1016/j.lithos.2004.03.013
231. H.M. Seitz, G.P. Brey, J.W. Harris, S. Durali-Müller, T. Ludwig, H.E. Höfer, Ferropericlase inclusions in ultradeep diamonds from Sao Luiz (Brazil): high Li abundances and diverse Li-isotope and trace element compositions suggest an origin from a subduction mélange. Mineral. Petrol. (2018). https://doi.org/10.1007/s00710-018-0572-0
232. M.J. Walter, E. Nakamura, R.G. Trønnes, D.J. Frost, Experimental constraints on crystallization differentiation in a deep magma ocean. Geochim. Cosmochim. Acta. (2004). https://doi.org/10.1016/j.gca.2004.03.014
233. T. Irifune, T. Shinmei, C.A. McCammon, N. Miyajima, D.C. Rubie, D.J. Frost, Iron partitioning and density changes of pyrolite in earth's lower mantle. Science **1979**(327), 193–195 (2010). https://doi.org/10.1126/science.1181443
234. T. Ishii, H. Kojitani, M. Akaogi, Post-spinel transitions in pyrolite and Mg2SiO4 and akimotoite-perovskite transition in MgSiO3: precise comparison by high-pressure high-temperature experiments with multi-sample cell technique. Earth Planet. Sci Lett. (2011). https://doi.org/10.1016/j.epsl.2011.06.023
235. T. Ishii, H. Kojitani, M. Akaogi, Phase relations and mineral chemistry in pyrolitic mantle at 1600–2200 °C under pressures up to the uppermost lower mantle: phase transitions around the 660-km discontinuity and dynamics of upwelling hot plumes. Phys. Earth Planet. Inter. (2018). https://doi.org/10.1016/j.pepi.2017.10.005
236. H. Kuwahara, R. Nomura, R. Nakada, T. Irifune, Simultaneous determination of melting phase relations of mantle peridotite and mid-ocean ridge basalt at the uppermost lower mantle conditions. Phys. Earth Planet. Inter. (2018). https://doi.org/10.1016/j.pepi.2018.08.012
237. S. Lorenzon, M. Wenz, P. Nimis, S.D. Jacobsen, L. Pasqualetto, M.G. Pamato, D. Novella, D. Zhang, C. Anzolini, M. Regier, T. Stachel, D.G. Pearson, J.W. Harris, F. Nestola, Dual origin of ferropericlase inclusions within super-deep diamonds. Earth Planet. Sci. Lett. **608**, 118081 (2023). https://doi.org/10.1016/j.epsl.2023.118081
238. C.A. McCammon, T. Stachel, J.W. Harris, Iron oxidation state in lower mantle mineral assemblages. Earth Planet. Sci. Lett. (2004). https://doi.org/10.1016/j.epsl.2004.03.019
239. C. McCammon, M. Hutchison, J. Harris, Ferric iron content of mineral inclusions in diamonds from Sao Luiz: a view into the lower mantle. Science (1979) (1997). https://doi.org/10.1126/science.278.5337.434
240. D.J. Frost, C.A. McCammon, The redox state of earth's mantle. Annu Rev Earth Planet Sci. **36**, 389–420 (2008). https://doi.org/10.1146/annurev.earth.36.031207.124322
241. M. Akaogi, S. Akimoto, Pyroxene-garnet solid-solution equilibria in the systems Mg4Si4O12Mg3Al2Si3O12 and Fe4Si4O12Fe3Al2Si3O12 at high pressures and temperatures. Phys. Earth Planet. Inter. (1977). https://doi.org/10.1016/0031-9201(77)90013-9
242. T. Irifune, An experimental investigation of the pyroxene-garnet transformation in a pyrolite composition and its bearing on the constitution of the mantle. Phys. Earth Planet. Inter. (1987). https://doi.org/10.1016/0031-9201(87)90040-9
243. A.M. Dymshits, A.V. Bobrov, L. Bindi, Y.A. Litvin, K.D. Litasov, A.F. Shatskiy, E. Ohtani, Na-bearing majoritic garnet in the Na2MgSi5O12-Mg3Al2Si3O12 join at 11–20GPa: phase relations, structural peculiarities and solid solutions. Geochim. Cosmochim. Acta. (2013). https://doi.org/10.1016/j.gca.2012.11.032

244. T. Irifune, W.O. Hibberson, A.E. Ringwood, J. Ross, Eclogite-garnetite transformation at high pressure and its bearing on the occurrence of garnet inclusions in diamond. Kimberlites Related Rocks. **2**, 877–882 (1989)
245. A.R. Thomson, S.C. Kohn, A. Prabhu, M.J. Walter, Evaluating the formation pressure of diamond-hosted majoritic garnets: a machine learning majorite barometer. J. Geophys. Res. Solid Earth. (2021). https://doi.org/10.1029/2020JB020604
246. F. Nestola, N. Korolev, M. Kopylova, N. Rotiroti, D.G. Pearson, M.G. Pamato, M. Alvaro, L. Peruzzo, J.J. Gurney, A.E. Moore, J. Davidson, CaSiO3 perovskite in diamond indicates the recycling of oceanic crust into the lower mantle. Nature **555**, 237–241 (2018). https://doi.org/10.1038/nature25972
247. E.S. Kiseeva, G.M. Yaxley, A.S. Stepanov, H. Tkalčić, K.D. Litasov, V.S. Kamenetsky, Metapyroxenite in the mantle transition zone revealed from majorite inclusions in diamonds. Geology (2013). https://doi.org/10.1130/G34311.1
248. A.R. Thomson, M.J. Walter, S.C. Kohn, R.A. Brooker, Slab melting as a barrier to deep carbon subduction. Nature (2016). https://doi.org/10.1038/nature16174
249. L.S. Armstrong, M.J. Walter, Tetragonal almandine pyrope phase (TAPP): retrograde Mg-perovskite from subducted oceanic crust? Eur. J. Mineral. (2012). https://doi.org/10.1127/0935-1221/2012/0024-2211
250. L.G. Liu, A.E. Ringwood, Synthesis of a perovskite-type polymorph of CaSiO3. Earth Planet. Sci. Lett. (1975). https://doi.org/10.1016/0012-821X(75)90229-0
251. E. Ito, E. Takahashi, Y. Matsui, The mineralogy and chemistry of the lower mantle: an implication of the ultrahigh-pressure phase relations in the system MgO FeO SiO2. Earth Planet. Sci. Lett. **67**, 238–248 (1984). https://doi.org/10.1016/0012-821X(84)90119-5
252. S.E. Kesson, J.D. Fitz Gerald, J.M.G. Shelley, R.L. Withers, Phase relations, structure and crystal chemistry of some aluminous silicate perovskites. Earth Planet. Sci. Lett. (1995). https://doi.org/10.1016/0012-821X(95)00112-P
253. S.E. Kesson, J.D. Fitz Gerald, J.M.G. Shelley, Mineral chemistry and density of subducted basaltic crust at lower-mantle pressures. Nature **372**, 767–769 (1994). https://doi.org/10.1038/372767a0
254. F.E. Brenker, F. Nestola, L. Brenker, L. Peruzzo, J.W. Harris, Origin, properties, and structure of breyite: the second most abundant mineral inclusion in super-deep diamonds. Am. Miner. **106**, 38–43 (2021). https://doi.org/10.2138/am-2020-7513
255. T. Stachel, J.W. Harris, G.P. Brey, W. Joswig, Kankan diamonds (Guinea) II: lower mantle inclusion parageneses. Contrib. Mineral. Petrol. (2000). https://doi.org/10.1007/s004100000174
256. F.E. Brenker, T. Stachel, J.W. Harris, Exhumation of lower mantle inclusions in diamond: ATEM investigation of retrograde phase transitions, reactions and exsolution. Earth Planet. Sci. Lett. (2002). https://doi.org/10.1016/S0012-821X(02)00514-9
257. F.E. Brenker, L. Vincze, B. Vekemans, L. Nasdala, T. Stachel, C. Vollmer, M. Kersten, A. Somogyi, F. Adams, W. Joswig, J.W. Harris, Detection of a Ca-rich lithology in the Earth's deep (> 300 km) convecting mantle. Earth Planet. Sci. Lett. (2005). https://doi.org/10.1016/j.epsl.2005.05.021
258. M.J. Walter, G.P. Bulanova, L.S. Armstrong, S. Keshav, J.D. Blundy, G. Gudfinnsson, O.T. Lord, A.R. Lennie, S.M. Clark, C.B. Smith, L. Gobbo, Primary carbonatite melt from deeply subducted oceanic crust. Nature (2008). https://doi.org/10.1038/nature07132
259. R. Tappert, J. Foden, T. Stachel, K. Muehlenbachs, M. Tappert, K. Wills, The diamonds of South Australia. Lithos (2009). https://doi.org/10.1016/j.lithos.2009.04.029
260. D. Zedgenizov, H. Kagi, E. Ohtani, T. Tsujimori, K. Komatsu, Retrograde phases of former bridgmanite inclusions in superdeep diamonds. Lithos (2020). https://doi.org/10.1016/j.lithos.2020.105659
261. A.D. Burnham, G.P. Bulanova, C.B. Smith, S.C. Whitehead, S.C. Kohn, L. Gobbo, M.J. Walter, Diamonds from the Machado River alluvial deposit, Rondônia, Brazil, derived from both lithospheric and sub-lithospheric mantle. Lithos (2016). https://doi.org/10.1016/j.lithos.2016.05.022
262. A.B. Woodland, A.V. Girnis, V.K. Bulatov, G.P. Brey, H.E. Höfer, Breyite inclusions in diamond: experimental evidence for possible dual origin. Eur. J. Mineral. (2020). https://doi.org/10.5194/ejm-32-171-2020
263. A. Kubo, T. Suzuki, M. Akaogi, High pressure phase equilibria in the system CaTiO3-CaSiO3: stability of perovskite solid solutions. Phys. Chem. Miner. (1997). https://doi.org/10.1007/s002690050063
264. M.T. Hutchison, M.B. Hursthouse, M.E. Light, Mineral inclusions in diamonds: associations and chemical distinctions around the 670-km discontinuity. Contrib. Mineral. Petrol. (2001). https://doi.org/10.1007/s004100100279

265. D.J. Frost, The upper mantle and transition zone. Elements **4**, 171–176 (2008). https://doi.org/10.2113/GSELEMENTS.4.3.171
266. A.E. Ringwood, Phase transformations and their bearing on the constitution and dynamics of the mantle. Geochim. Cosmochim. Acta. (1991). https://doi.org/10.1016/0016-7037(91)90090-R
267. B. Harte, J.W. Harris, M.T. Hutchison, G.R. Watt, M.C. Wilding, Lower mantle mineral associations in diamonds from Sao Luiz, Brazil., in: Y. Fei, B.O. Mysen, C.M. Bertka (Eds.), Mantle Petrology: Field Observations and High Pressure Experimentation, A Tribute to Francis R (Joe) Boyd., The Geochemical Society, Houston, 1999: pp. 125–153.
268. K. Hirose, Phase transitions in pyrolitic mantle around 670-km depth: implications for upwelling of plumes from the lower mantle. J. Geophys. Res. Solid Earth. (2002). https://doi.org/10.1029/2001jb000597
269. R.G. Tronnes, D.J. Frost, Peridotite melting and mineral-melt partitioning of major and minor elements at 22–24.5 GPa. Earth Planet. Sci. Lett. (2002). https://doi.org/10.1016/S0012-821X(02)00466-1
270. C. Beyer, D.J. Frost, The depth of sub-lithospheric diamond formation and the redistribution of carbon in the deep mantle. Earth Planet. Sci. Lett. (2017). https://doi.org/10.1016/j.epsl.2016.12.017
271. T. Ishii, H. Kojitani, M. Akaogi, Phase relations of harzburgite and MORB up to the uppermost lower mantle conditions: precise comparison with pyrolite by multisample cell high-pressure experiments with implication to dynamics of subducted slabs. J. Geophys. Res. Solid Earth. **124**, 3491–3507 (2019). https://doi.org/10.1029/2018JB016749
272. K. Okamoto, S. Maruyama, The eclogite-garnetite transformation in the MORB + H2O system. Phys. Earth Planet. Inter. (2004). https://doi.org/10.1016/j.pepi.2003.07.029
273. D.A. Zedgenizov, V.S. Shatsky, A.V. Panin, O.V. Evtushenko, A.L. Ragozin, H. Kagi, Evidence for phase transitions in mineral inclusions in superdeep diamonds of the São Luiz deposit (Brazil). Russ. Geol. Geophys. **56**, 296–305 (2015). https://doi.org/10.1016/j.rgg.2015.01.021
274. S. Lorenzon, D. Novella, P. Nimis, S.D. Jacobsen, E. Thomassot, M.G. Pamato, L. Prosperi, A. Lorenzetti, M. Alvaro, F. Brenker, F. Salvadego, F. Nestola, Ringwoodite and zirconia inclusions indicate downward travel of super-deep diamonds. Geology (2022). https://doi.org/10.1130/G50111.1
275. D.G. Pearson, F.E. Brenker, F. Nestola, J. McNeill, L. Nasdala, M.T. Hutchison, S. Matveev, K. Mather, G. Silversmit, S. Schmitz, B. Vekemans, L. Vincze, Hydrous mantle transition zone indicated by ringwoodite included within diamond. Nature **507**, 221–224 (2014). https://doi.org/10.1038/nature13080
276. D.G. Pearson, F.E. Brenker, F. Nestola, J. McNeil, L. Nasdala, M. Hutchison, S. Matveev, K. Mather, L. Vincze, S. Schmitz, B. Vekemens, Water and Slabs in the Transition Zone - Hydrous Ringwoodite in Diamond, in: American Geophysical Union, Fall Meeting 2014, Abstract Id. DI32A-01, AGU Fall Meeting Abstracts (2014)
277. R.W. Luth, Y.N. Palyanov, H. Bureau, Experimental petrology applied to natural diamond growth. Rev. Mineral. Geochem. (2022). https://doi.org/10.2138/rmg.2022.88.14
278. V. Shatsky, D. Zedgenizov, A. Ragozin, V. Kalinina, Silicate melt inclusions in diamonds of eclogite paragenesis from placers on the northeastern Siberian craton. Minerals. **9**, 412 (2019). https://doi.org/10.3390/min9070412
279. P.J. Wyllie, I.D. Ryabchikov, Volatile components, magmas, and critical fluids in upwelling mantle. J. Petrol. (2000). https://doi.org/10.1093/petrology/41.7.1195
280. R. Kessel, P. Ulmer, T. Pettke, M.W. Schmidt, A.B. Thompson, The water-basalt system at 4 to 6 GPa: phase relations and second critical endpoint in a K-free eclogite at 700 to 1400 °C. Earth Planet. Sci. Lett. (2005). https://doi.org/10.1016/j.epsl.2005.06.018
281. R.J. Bodnar, Introduction to fluid inclusions, in *Fluid inclusions: analysis and interpretation, short course 32*. ed. by I. Samson, A. Anderson, D. Marsh (Mineralogical Association of Canada, 2003), pp.1–8
282. K. Mibe, M. Kanzaki, T. Kawamoto, K.N. Matsukage, Y. Fei, S. Ono, Second critical endpoint in the peridotite-H $_2$ O system. J. Geophys. Res. **112**, B03201 (2007). https://doi.org/10.1029/2005JB004125
283. Y. Liu, L.A. Taylor, A.B. Sarbadhikari, J.W. Valley, T. Ushikubo, M.J. Spicuzza, N. Kita, R.A. Ketcham, W. Carlson, V. Shatsky, N.V. Sobolev, Metasomatic origin of diamonds in the world's largest diamondiferous eclogite. Lithos (2009). https://doi.org/10.1016/j.lithos.2009.06.036
284. K. Mibe, T. Kawamoto, K.N. Matsukage, Y. Fei, S. Ono, Slab melting versus slab dehydration in subduction-zone magmatism. Proc. Natl. Acad. Sci. USA. (2011). https://doi.org/10.1073/pnas.1010968108

285. J. Wang, E. Takahashi, X. Xiong, L. Chen, L. Li, T. Suzuki, M.J. Walter, The water-saturated solidus and second critical endpoint of peridotite: implications for magma genesis within the mantle wedge. J. Geophys. Res. Solid Earth. (2020). https://doi.org/10.1029/2020JB019452
286. T. Kawamoto, M. Kanzaki, K. Mibe, K.N. Matsukage, S. Ono, Separation of supercritical slab-fluids to form aqueous fluid and melt components in subduction zone magmatism. Proc. Natl. Acad. Sci. **109**, 18695–18700 (2012). https://doi.org/10.1073/pnas.1207687109
287. Y. Weiss, R. Kessel, W.L. Griffin, I. Kiflawi, O. Klein-BenDavid, D.R. Bell, J.W. Harris, O. Navon, A new model for the evolution of diamond-forming fluids: evidence from microinclusion-bearing diamonds from Kankan, Guinea. Lithos (2009). https://doi.org/10.1016/j.lithos.2009.05.038
288. O. Klein-BenDavid, D.G. Pearson, G.M. Nowell, C. Ottley, J.C.R. McNeill, A. Logvinova, N.V. Sobolev, The sources and time-integrated evolution of diamond-forming fluids—trace elements and isotopic evidence. Geochim. Cosmochim. Acta. (2014). https://doi.org/10.1016/j.gca.2013.09.022
289. O. Elazar, D. Frost, O. Navon, R. Kessel, Melting of H2O and CO2-bearing eclogite at 4–6 GPa and 900–1200 °C: implications for the generation of diamond-forming fluids. Geochim. Cosmochim. Acta. **255**, 69–87 (2019). https://doi.org/10.1016/j.gca.2019.03.025
290. O. Dvir, R. Kessel, The effect of CO2 on the water-saturated solidus of K-poor peridotite between 4 and 6 GPa. Geochim. Cosmochim. Acta. (2017). https://doi.org/10.1016/j.gca.2017.02.028
291. K.D. Litasov, O.G. Safonov, E. Ohtani, Origin of Cl-bearing silica-rich melt inclusions in diamonds: experimental evidence for an eclogite connection. Geology (2010). https://doi.org/10.1130/G31325.1
292. Y. Weiss, W.L. Griffin, D.R. Bell, O. Navon, High-Mg carbonatitic melts in diamonds, kimberlites and the sub-continental lithosphere. Earth Planet. Sci. Lett. **309**, 337–347 (2011). https://doi.org/10.1016/j.epsl.2011.07.012
293. E.S. Izraeli, J.W. Harris, O. Navon, Brine inclusions in diamonds: a new upper mantle fluid. Earth Planet. Sci. Lett. (2001). https://doi.org/10.1016/S0012-821X(01)00291-6
294. E.L. Tomlinson, A.P. Jones, J.W. Harris, Co-existing fluid and silicate inclusions in mantle diamond. Earth Planet. Sci. Lett. (2006). https://doi.org/10.1016/j.epsl.2006.08.005
295. Y. Weiss, S.L. Goldstein, The involvement of diamond-forming fluids in the metasomatic 'cocktail' of kimberlite sources. Mineral. Petrol. (2018). https://doi.org/10.1007/s00710-018-0613-8
296. S. Timmerman, I.L. Chinn, D. Fisher, G.R. Davies, Formation of unusual yellow Orapa diamonds. Mineral. Petrol. (2018). https://doi.org/10.1007/s00710-018-0592-9
297. Y. Weiss, W.L. Griffin, O. Navon, Diamond-forming fluids in fibrous diamonds: the trace-element perspective. Earth Planet. Sci. Lett. (2013). https://doi.org/10.1016/j.epsl.2013.06.021
298. E.L. Tomlinson, W. Müller, EIMF, a snapshot of mantle metasomatism: trace element analysis of coexisting fluid (LA-ICP-MS) and silicate (SIMS) inclusions in fibrous diamonds. Earth Planet. Sci. Lett. **279**, 362–372 (2009). https://doi.org/10.1016/j.epsl.2009.01.010
299. A.A. Shiryaev, E.S. Izraeli, E.H. Hauri, O.D. Zakharchenko, O. Navon, Chemical, optical, and isotopic investigations of fibrous diamonds from Brazil. Geol. Geofiz. **46**, 1207–1222 (2005)
300. Y. Weiss, I. Kiflawi, N. Davies, O. Navon, High-density fluids and the growth of monocrystalline diamonds. Geochim. Cosmochim. Acta. (2014). https://doi.org/10.1016/j.gca.2014.05.050
301. B.M. Jablon, O. Navon, Most diamonds were created equal. Earth Planet. Sci. Lett. (2016). https://doi.org/10.1016/j.epsl.2016.03.013
302. P. Nimis, M. Alvaro, F. Nestola, R.J. Angel, K. Marquardt, G. Rustioni, J.W. Harris, F. Marone, First evidence of hydrous silicic fluid films around solid inclusions in gem-quality diamonds. Lithos (2016). https://doi.org/10.1016/j.lithos.2016.05.019
303. E.M. Smith, M.G. Kopylova, M.L. Frezzotti, V.P. Afanasiev, N-rich fluid inclusions in octahedrally-grown diamond. Earth Planet. Sci. Lett. (2014). https://doi.org/10.1016/j.epsl.2014.02.033
304. M.Y. Krebs, D.G. Pearson, T. Stachel, F. Laiginhas, S. Woodland, I. Chinn, J. Kong, A common parentage-low abundance trace element data of gem diamonds reveals similar fluids to fibrous diamonds. Lithos (2019). https://doi.org/10.1016/j.lithos.2018.11.025
305. E.M. Smith, M.G. Kopylova, M.L. Frezzotti, V.P. Afanasiev, Fluid inclusions in Ebelyakh diamonds: evidence of CO2 liberation in eclogite and the effect of H2O on diamond habit. Lithos **216–217**, 106–117 (2015). https://doi.org/10.1016/j.lithos.2014.12.010
306. G.P. Brey, T. Köhler, Geothermobarometry in four-phase lherzolites II. new thermobarometers, and practical assessment of existing thermobarometers. J. Petrol. (1990). https://doi.org/10.1093/petrology/31.6.1353

307. J.C.M. De Hoog, L. Gall, D.H. Cornell, Trace-element geochemistry of mantle olivine and application to mantle petrogenesis and geothermobarometry. Chem. Geol. (2010). https://doi.org/10.1016/j.chemgeo.2009.11.017
308. Y. Bussweiler, G.P. Brey, D.G. Pearson, T. Stachel, R.A. Stern, M.F. Hardman, B.A. Kjarsgaard, S.E. Jackson, The aluminum-in-olivine thermometer for mantle peridotites—experimental versus empirical calibration and potential applications. Lithos (2017). https://doi.org/10.1016/j.lithos.2016.12.015
309. S.K. Simakov, Garnet-clinopyroxene and clinopyroxene geothermobarometry of deep mantle and crust eclogites and peridotites. Lithos (2008). https://doi.org/10.1016/j.lithos.2008.06.013
310. C. Beyer, D.J. Frost, N. Miyajima, Experimental calibration of a garnet–clinopyroxene geobarometer for mantle eclogites. Contrib. Mineral. Petrol. (2015). https://doi.org/10.1007/s00410-015-1113-z
311. C. Beyer, A. Rosenthal, R. Myhill, W.A. Crichton, T. Yu, Y. Wang, D.J. Frost, An internally consistent pressure calibration of geobarometers applicable to the Earth's upper mantle using in situ XRD. Geochim. Cosmochim. Acta. (2018). https://doi.org/10.1016/j.gca.2017.10.031
312. Z.J. Sudholz, G.M. Yaxley, A.L. Jaques, G.P. Brey, Experimental recalibration of the Cr-in-clinopyroxene geobarometer: improved precision and reliability above 4.5 GPa. Contrib. Mineral. Petrol. (2021). https://doi.org/10.1007/s00410-020-01768-z
313. W.L. Griffin, C.G. Ryan, Trace elements in indicator minerals: area selection and target evaluation in diamond exploration. J. Geochem. Explor. (1995). https://doi.org/10.1016/0375-6742(94)00015-4
314. H. Grütter, D. Latti, A. Menzies, Cr-saturation arrays in concentrate garnet compositions from kimberlite and their use in mantle barometry. J. Petrol. (2006). https://doi.org/10.1093/petrology/egi096
315. R.J. Angel, M. Alvaro, F. Nestola, 40 years of mineral elasticity: a critical review and a new parameterisation of equations of state for mantle olivines and diamond inclusions. Phys. Chem. Miner. (2018). https://doi.org/10.1007/s00269-017-0900-7
316. F. Nestola, The crucial role of crystallography in diamond research. Rend. Lincei. (2015). https://doi.org/10.1007/s12210-015-0398-1
317. C. Anzolini, M. Prencipe, M. Alvaro, C. Romano, A. Vona, S. Lorenzon, E.M. Smith, F.E. Brenker, F. Nestola, Depth of formation of super-deep diamonds: Raman barometry of CaSiO3-walstromite inclusions. Am. Miner. **103**, 69–74 (2018). https://doi.org/10.2138/am-2018-6184
318. D. Howell, Strain-induced birefringence in natural diamond: a review. Eur. J. Mineral. **24**, 575–585 (2012). https://doi.org/10.1127/0935-1221/2012/0024-2205
319. R.J. Angel, M.L. Mazzucchelli, M. Alvaro, F. Nestola, EosFit-Pinc: a simple GUI for host-inclusion elastic thermobarometry. Am. Mineral. (2017). https://doi.org/10.2138/am-2017-6190
320. K.D. Collerson, Q. Williams, B.S. Kamber, S. Omori, H. Arai, E. Ohtani, Majoritic garnet: a new approach to pressure estimation of shock events in meteorites and the encapsulation of sub-lithospheric inclusions in diamond. Geochim. Cosmochim. Acta. (2010). https://doi.org/10.1016/j.gca.2010.07.005
321. R. Tao, Y. Fei, E.S. Bullock, C. Xu, L. Zhang, Experimental investigation of Fe3+-rich majoritic garnet and its effect on majorite geobarometer. Geochim. Cosmochim. Acta. (2018). https://doi.org/10.1016/j.gca.2018.01.008
322. P.C. Hayman, M.G. Kopylova, F.V. Kaminsky, Lower mantle diamonds from Rio Soriso (Juina area, Mato Grosso, Brazil). Contrib. Mineral. Petrol. (2005). https://doi.org/10.1007/s00410-005-0657-8
323. T. Gasparik, K. Wolf, C.M. Smith, Experimental determination of phase relations in the CaSiO3 system from 8 to 15 GPa. Am. Mineral. **79**, 1219–1222 (1994)
324. R.M. Davies, W.L. Griffin, S.Y. O'Reilly, B.J. Doyle, Mineral inclusions and geochemical characteristics of microdiamonds from the DO27, A154, A21, A418, DO18, DD17 and Ranch Lake kimberlites at Lac de Gras, Slave Craton, Canada. Lithos (2004). https://doi.org/10.1016/j.lithos.2004.04.016
325. Y. Sun, S. Hier-Majumder, Y. Xu, M. Walter, Stability and migration of slab-derived carbonate-rich melts above the transition zone. Earth Planet. Sci. Lett. (2020). https://doi.org/10.1016/j.epsl.2019.116000
326. J. Harris, M.T. Hutchison, M. Hursthouse, M. Light, B. Harte, A new tetragonal silicate mineral occurring as inclusions in lower-mantle diamonds. Nature **387**, 486–488 (1997). https://doi.org/10.1038/387486a0
327. F. Nestola, A.D. Burnham, L. Peruzzo, L. Tauro, M. Alvaro, M.J. Walter, M. Gunter, C. Anzolini, S.C. Kohn, Tetragonal Almandine-Pyrope Phase, TAPP: finally a name for it, the new mineral jeffbenite. Mineral Mag. **80**, 1219–1232 (2016). https://doi.org/10.1180/minmag.2016.080.059

328. F. Nestola, M. Prencipe, D. Belmonte, Mg3Al2Si3O12 jeffbenite inclusion in super-deep diamonds is thermodynamically stable at very shallow Earth's depths. Sci Rep. **13**, 83 (2023). https://doi.org/10.1038/s41598-022-27290-9
329. L.S. Armstrong, M.J. Walter, J.R. Tuff, O.T. Lord, A.R. Lennie, A.K. Kleppe, S.M. Clark, Perovskite phase relations in the system CaO-MgO-TiO2-SiO2 and implications for deep mantle lithologies. J. Petrol. **53**, 611–635 (2012). https://doi.org/10.1093/petrology/egr073
330. K.V. Smit, S.B. Shirey, R.A. Stern, A. Steele, W. Wang, Diamond growth from C-H–N–O recycled fluids in the lithosphere: evidence from CH4 micro-inclusions and δ13C–δ15N–N content in Marange mixed-habit diamonds. Lithos (2016). https://doi.org/10.1016/j.lithos.2016.03.015
331. R.W. Luth, D. Virgo, F.R. Boyd, B.J. Wood, Ferric iron in mantle-derived garnets—implications for thermobarometry and for the oxidation state of the mantle. Contrib. Mineral. Petrol. (1990). https://doi.org/10.1007/BF00310646
332. M. Lazarov, A.B. Woodland, G.P. Brey, Thermal state and redox conditions of the Kaapvaal mantle: a study of xenoliths from the Finsch mine, South Africa. Lithos (2009). https://doi.org/10.1016/j.lithos.2009.03.035
333. G. Gudmundsson, B.J. Wood, Experimental tests of garnet peridotite oxygen barometry. Contrib. Mineral. Petrol. (1995). https://doi.org/10.1007/BF00310717
334. B.R. Frost, D.H. Lindsley, D.J. Anderson, Fe-Ti oxide-silicate equilibria; assemblages with fayalitic olivine. Am. Miner. **73**, 727–740 (1988)
335. T. Stachel, T. Chacko, R.W. Luth, Carbon isotope fractionation during diamond growth in depleted peridotite: counterintuitive insights from modelling water-maximum CHO fluids as multi-component systems. Earth Planet. Sci. Lett. (2017). https://doi.org/10.1016/j.epsl.2017.05.037
336. S. Matveev, C. Ballhaus, K. Fricke, J. Truckenbrodt, D. Ziegenbein, Volatiles in the Earth's mantle: I. Synthesis of CHO fluids at 1273 K and 2.4 GPa. Geochim. Cosmochim. Acta. (1997). https://doi.org/10.1016/S0016-7037(97)00142-7
337. C. Zhang, Z. Duan, A model for C-O-H fluid in the Earth's mantle. Geochim. Cosmochim. Acta. (2009). https://doi.org/10.1016/j.gca.2009.01.021
338. R.W. Luth, Diamonds, eclogites, and the oxidation state of the earth's mantle. Science (1979). (1993). https://doi.org/10.1126/science.261.5117.66
339. D.H. Eggler, D.R. Baker, Reduced volatiles in the system C–O–H; implications to mantle melting, fluid formation, and diamond genesis, in *High pressure research in geophysics*. ed. by S. Akimoto, M.H. Manghnani (Center for Academic Publications Japan, Tokyo, 1982), pp.237–250
340. R.W. Luth, Carbon and carbonates in the mantle, in: mantle petrology: field observations and high pressure experimentation: a tribute to Francis R. (Joe) Boyd (1999)
341. P. Deines, The carbon isotopic composition of diamonds: relationship to diamond shape, color, occurrence and vapor composition. Geochim. Cosmochim. Acta. (1980). https://doi.org/10.1016/0016-7037(80)90284-7
342. H. Bureau, F. Langenhorst, A.L. Auzende, D.J. Frost, I. Estève, J. Siebert, The growth of fibrous, cloudy and polycrystalline diamonds. Geochim. Cosmochim. Acta. (2012). https://doi.org/10.1016/j.gca.2011.11.016
343. H. Bureau, D.J. Frost, N. Bolfan-Casanova, C. Leroy, I. Esteve, P. Cordier, Diamond growth in mantle fluids. Lithos (2016). https://doi.org/10.1016/j.lithos.2016.10.004
344. N. Shimizu, S.H. Richardson, Trace element abundance patterns of garnet inclusions in peridotite-suite diamonds. Geochim. Cosmochim. Acta. (1987). https://doi.org/10.1016/0016-7037(87)90085-8
345. T. Stachel, K.S. Viljoen, G. Brey, J.W. Harris, Metasomatic processes in lherzolitic and harzburgitic domains of diamondiferous lithospheric mantle: REE in garnets from xenoliths and inclusions in diamonds. Earth Planet. Sci. Lett. (1998). https://doi.org/10.1016/S0012-821X(98)00064-8
346. G. Brey, W.R. Brice, D.J. Ellis, D.H. Green, K.L. Harris, I.D. Ryabchikov, Pyroxene-carbonate reactions in the upper mantle. Earth Planet. Sci. Lett. **62**, 63–74 (1983)
347. Y. Huang, T. Nakatani, M. Nakamura, C. McCammon, Saline aqueous fluid circulation in mantle wedge inferred from olivine wetting properties. Nat. Commun. (2019). https://doi.org/10.1038/s41467-019-13513-7
348. M.B. Holness, M.J. Cheadle, D. McKenzie, On the use of changes in dihedral angle to decode late-stage textural evolution in cumulates. J. Petrol. **46**, 1565–1583 (2005). https://doi.org/10.1093/petrology/egi026
349. E. Bruce Watson, J.M. Brenan, Fluids in the lithosphere, 1. Experimentally-determined wetting characteristics of CO2H2O fluids and their implications for fluid transport, host-rock physical properties,

and fluid inclusion formation. Earth Planet. Sci. Lett. **85**, 497–515 (1987). https://doi.org/10.1016/0012-821X(87)90144-0
350. T. Yoshino, D. Yamazaki, K. Mibe, Well-wetted olivine grain boundaries in partially molten peridotite in the asthenosphere. Earth Planet. Sci. Lett. **283**, 167–173 (2009). https://doi.org/10.1016/j.epsl.2009.04.007
351. K. Mibe, T. Fujii, A. Yasuda, Connectivity of aqueous fluid in the Earth's upper mantle. Geophys. Res. Lett. (1998). https://doi.org/10.1029/98GL00872
352. L.S. Capizzi, Experimental study of interconnectivity and grain boundary wetness of hydrous carbonatitic liquids in mantle peridotite. PLINUS, Italian Society of Mineralogy and Petrology. **44**, 33–40 (2018)
353. D. Laporte, C. Rapaille, A. Provost, *Wetting angles, equilibrium melt geometry, and the permeability threshold of partially molten crustal protoliths* (Springer Netherlands, 1997), pp.31–54. https://doi.org/10.1007/978-94-017-1717-5_3
354. S. Mu, U.H. Faul, Grain boundary wetness of partially molten dunite. Contrib. Miner. Petrol. **171**, 40 (2016). https://doi.org/10.1007/s00410-016-1250-z
355. E. Bruce Watson, A. Lupulescu, Aqueous fluid connectivity and chemical transport in clinopyroxene-rich rocks. Earth Planet. Sci. Lett. **117**, 279–294 (1993). https://doi.org/10.1016/0012-821X(93)90133-T
356. J.K. Meen, D.H. Eggler, J.C. Ayers, Experimental evidence for very low solubility of rare-earth elements in C02-rich fluids at mantle conditions. Nature (1989). https://doi.org/10.1038/340301a0
357. R. Dasgupta, M.M. Hirschmann, The deep carbon cycle and melting in Earth's interior. Earth Planet. Sci. Lett. (2010). https://doi.org/10.1016/j.epsl.2010.06.039
358. P.B. Kelemen, S.R. Hart, S. Bernstein, Silica enrichment in the continental upper mantle via melt/rock reaction. Earth Planet. Sci. Lett. (1998). https://doi.org/10.1016/S0012-821X(98)00233-7
359. A.L. Mitchell, T.L. Grove, Melting the hydrous, subarc mantle: the origin of primitive andesites. Contrib. Mineral. Petrol. (2015). https://doi.org/10.1007/s00410-015-1161-4
360. P.B. Kelemen, H.J.B. Dick, J.E. Quick, Formation of harzburgite by pervasive melt/rock reaction in the upper mantle. Nature (1992). https://doi.org/10.1038/358635a0
361. S.B. Shirey, J.W. Harris, S.H. Richardson, M.J. Fouch, D.E. James, P. Cartigny, P. Deines, F. Viljoen, Diamond genesis, seismic structure, and evolution of the Kaapvaal-Zimbabwe craton. Science (1979). (2002). https://doi.org/10.1126/science.1072384
362. E.S. Izraeli, J.W. Harris, O. Navon, Fluid and mineral inclusions in cloudy diamonds from Koffiefontein, South Africa. Geochim. Cosmochim. Acta. **68**, 2561–2575 (2004). https://doi.org/10.1016/j.gca.2003.09.005
363. F. Huang, I. Daniel, H. Cardon, G. Montagnac, D.A. Sverjensky, Immiscible hydrocarbon fluids in the deep carbon cycle. Nat. Commun. **8**, 15798 (2017). https://doi.org/10.1038/ncomms15798
364. K.V. Smit, T. Stachel, R.W. Luth, R.A. Stern, Evaluating mechanisms for eclogitic diamond growth: an example from Zimmi Neoproterozoic diamonds (West African craton). Chem. Geol. (2019). https://doi.org/10.1016/j.chemgeo.2019.04.014
365. S. Aulbach, K.S. Viljoen, A. Gerdes, Diamondiferous and barren eclogites and pyroxenites from the western Kaapvaal craton record subduction processes and mantle metasomatism, respectively. Lithos (2020). https://doi.org/10.1016/j.lithos.2020.105588
366. D.S. Mikhailenko, V. Stagno, A.V. Korsakov, G.B. Andreozzi, G. Marras, V. Cerantola, E.V. Malygina, Redox state determination of eclogite xenoliths from Udachnaya kimberlite pipe (Siberian craton), with some implications for the graphite/diamond formation. Contrib. Mineral. Petrol. (2020). https://doi.org/10.1007/s00410-020-01748-3
367. V. Stagno, D.J. Frost, C.A. McCammon, H. Mohseni, Y. Fei, The oxygen fugacity at which graphite or diamond forms from carbonate-bearing melts in eclogitic rocks. Contrib. Mineral. Petrol. (2015). https://doi.org/10.1007/s00410-015-1111-1
368. A. Rohrbach, C. Ballhaus, U. Golla-Schindler, P. Ulmer, V.S. Kamenetsky, D.V. Kuzmin, Metal saturation in the upper mantle. Nature (2007). https://doi.org/10.1038/nature06183
369. H.S.C. O'Neil, C.A. McCammon, D. Canil, D.C. Rubie, C.R. Ross, F. Seifert, Mössbauer spectroscopy of mantle transition zone phases and determination of minimum Fe3+ content. Am. Miner. **78**, 456–460 (1993)
370. D.J. Frost, B.T. Poe, R.G. Trønnes, C. Liebske, A. Duba, D.C. Rubie, A new large-volume multianvil system. Phys. Earth Planet. Inter. (2004). https://doi.org/10.1016/j.pepi.2004.03.003

371. D. Canil, H.S.C. O'Neill, Distribution of ferric iron in some upper-mantle assemblages. J. Petrol. (1996). https://doi.org/10.1093/petrology/37.3.609
372. P.M. Bell, H.K. Mao, R.A. Weeks, A.V. Valkenburg, High-pressure disproportionation study of iron in synthetic basalt glass. Carnegie Instit. Washington Yearbook. **75**, 515–520 (1976)
373. V. Stagno, Y. Tange, N. Miyajima, C.A. McCammon, T. Irifune, D.J. Frost, The stability of magnesite in the transition zone and the lower mantle as function of oxygen fugacity. Geophys. Res. Lett. (2011). https://doi.org/10.1029/2011GL049560
374. Y. Nakajima, E. Takahashi, T. Suzuki, K. Ichi Funakoshi, "Carbon in the core" revisited. Phys. Earth Planet. Inter. (2009). https://doi.org/10.1016/j.pepi.2008.05.014
375. E.M. Smith, M.G. Kopylova, Implications of metallic iron for diamonds and nitrogen in the sublithospheric mantle. Can. J. Earth Sci. (2014). https://doi.org/10.1139/cjes-2013-0218
376. F.V. Kaminsky, R. Wirth, Iron carbide inclusions in lower-mantle diamond from Juina, Brazil. Can. Mineral. **49**, 555–572 (2011). https://doi.org/10.3749/canmin.49.2.555
377. Y.N. Palyanov, Y.V. Bataleva, A.G. Sokol, Y.M. Borzdov, I.N. Kupriyanov, V.N. Reutsky, N.V. Sobolev, Mantle-slab interaction and redox mechanism of diamond formation. Proc. Natl. Acad. Sci. USA. (2013). https://doi.org/10.1073/pnas.1313340110
378. A.D. Burnham, A.R. Thomson, G.P. Bulanova, S.C. Kohn, C.B. Smith, M.J. Walter, Stable isotope evidence for crustal recycling as recorded by superdeep diamonds. Earth Planet. Sci. Lett. (2015). https://doi.org/10.1016/j.epsl.2015.10.023
379. R.B. Ickert, T. Stachel, R.A. Stern, J.W. Harris, Extreme 18O-enrichment in majorite constrains a crustal origin of transition zone diamonds. Geochem. Perspect. Lett. (2015). https://doi.org/10.7185/geochemlet.1507
380. E.S. Kiseeva, B.J. Wood, S. Ghosh, T. Stachel, The pyroxenite-diamond connection. Geochem. Perspect. Lett. (2016). https://doi.org/10.7185/geochemlet.1601
381. C.R. Bina, Patterns of deep seismicity reflect buoyancy stresses due to phase transitions. Geophys. Res. Lett. (1997). https://doi.org/10.1029/97GL53189
382. M.I. Billen, Modeling the dynamics of subducting slabs. Annu. Rev. Earth Planet. Sci. **36**, 325–356 (2008). https://doi.org/10.1146/annurev.earth.36.031207.124129
383. R. Wirth, C. Vollmer, F. Brenker, S. Matsyuk, F. Kaminsky, Inclusions of nanocrystalline hydrous aluminium silicate "Phase Egg" in superdeep diamonds from Juina (Mato Grosso State, Brazil). Earth Planet. Sci. Lett. (2007). https://doi.org/10.1016/j.epsl.2007.04.041
384. M.M. Hirschmann, T. Tenner, C. Aubaud, A.C. Withers, Dehydration melting of nominally anhydrous mantle: the primacy of partitioning. Phys. Earth Planet. Inter. (2009). https://doi.org/10.1016/j.pepi.2009.04.001
385. H. Iwamori, Phase relations of peridotites under H2O-saturated conditions and ability of subducting plates for transportation of H2O. Earth Planet. Sci. Lett. (2004). https://doi.org/10.1016/j.epsl.2004.08.013
386. L. Stixrude, C. Lithgow-Bertelloni, Thermodynamics of mantle minerals—II. Phase equilibria. Geophys. J. Int. (2011). https://doi.org/10.1111/j.1365-246X.2010.04890.x
387. S.M. Dorfman, J. Badro, F. Nabiei, V.B. Prakapenka, M. Cantoni, P. Gillet, Carbonate stability in the reduced lower mantle. Earth Planet. Sci. Lett. **489**, 84–91 (2018). https://doi.org/10.1016/j.epsl.2018.02.035
388. E. Boulard, A. Gloter, A. Corgne, D. Antonangeli, A.L. Auzende, J.P. Perrillat, F. Guyot, G. Fiquet, New host for carbon in the deep earth. Proc. Natl. Acad. Sci. USA. (2011). https://doi.org/10.1073/pnas.1016934108
389. D.A. Sverjensky, Thermodynamic modelling of fluids from surficial to mantle conditions. J. Geol. Soc. Lon. **176**, 348–374 (2019). https://doi.org/10.1144/jgs2018-105
390. D.A. Sverjensky, B. Harrison, D. Azzolini, Water in the deep Earth: the dielectric constant and the solubilities of quartz and corundum to 60kb and 1200°C. Geochim. Cosmochim. Acta. **129**, 125–145 (2014). https://doi.org/10.1016/j.gca.2013.12.019
391. F. Huang, D.A. Sverjensky, Extended deep earth water model for predicting major element mantle metasomatism. Geochim. Cosmochim. Acta. **254**, 192–230 (2019). https://doi.org/10.1016/j.gca.2019.03.027
392. D.A. Sverjensky, F. Huang, Diamond formation due to a pH drop during fluid–rock interactions. Nat. Commun. **6**, 8702 (2015). https://doi.org/10.1038/ncomms9702

393. S. Mikhail, M. Rinaldi, E.R. Mare, D.A. Sverjensky, A genetic metasomatic link between eclogitic and peridotitic diamond inclusions. Geochem. Perspect. Lett. **17**, 33–38 (2021). https://doi.org/10.7185/geochemlet.2111
394. D. Selby, R.A. Creaser, H.J. Stein, R.J. Markey, J.L. Hannah, Assessment of the 187Re decay constant by cross calibration of Re-Os molybdenite and U-Pb zircon chronometers in magmatic ore systems. Geochim. Cosmochim. Acta. (2007). https://doi.org/10.1016/j.gca.2007.01.008
395. N. Shimizu, Rare earth elements in garnets and clinopyroxenes from garnet lherzolite nodules in kimberlites. Earth Planet. Sci. Lett. (1975). https://doi.org/10.1016/0012-821X(75)90206-X
396. K.E.O. Hoal, B.G. Hoal, A.J. Erlank, N. Shimizu, Metasomatism of the mantle lithosphere recorded by rare earth elements in garnets. Earth Planet. Sci. Lett. (1994). https://doi.org/10.1016/0012-821X(94)90114-7
397. O. Klein-BenDavid, D. Graham Pearson, Origins of subcalcic garnets and their relation to diamond forming fluids-case studies from Ekati (NWT-Canada) and Murowa (Zimbabwe). Geochim. Cosmochim. Acta. (2009). https://doi.org/10.1016/j.gca.2008.04.044
398. S. Aulbach, W.L. Griffin, N.J. Pearson, S.Y. O'Reilly, Nature and timing of metasomatism in the stratified mantle lithosphere beneath the central Slave craton (Canada). Chem. Geol. (2013). https://doi.org/10.1016/j.chemgeo.2013.05.037
399. Q. Shu, G.P. Brey, Ancient mantle metasomatism recorded in subcalcic garnet xenocrysts: temporal links between mantle metasomatism, diamond growth and crustal tectonomagmatism. Earth Planet. Sci. Lett. (2015). https://doi.org/10.1016/j.epsl.2015.02.038
400. E.V. Shchukina, A.M. Agashev, V.S. Shchukin, Diamond-bearing root beneath the northern east european platform (Arkhangelsk region, russia): evidence from cr-pyrope trace-element geochemistry. Minerals. (2019). https://doi.org/10.3390/min9050261
401. V.G. Malkovets, W.L. Griffin, S.Y. O'Reilly, B.J. Wood, Diamond, subcalcic garnet, and mantle metasomatism: Kimberlite sampling patterns define the link. Geology **35**, 339 (2007). https://doi.org/10.1130/G23092A.1
402. S.H. Richardson, S.B. Shirey, J.W. Harris, R.W. Carlson, Archean subduction recorded by Re-Os isotopes in eclogitic sulfide inclusions in Kimberley diamonds. Earth Planet. Sci. Lett. (2001). https://doi.org/10.1016/S0012-821X(01)00419-8
403. S. Aulbach, S.B. Shirey, T. Stachel, S. Creighton, K. Muehlenbachs, J.W. Harris, Diamond formation episodes at the southern margin of the Kaapvaal Craton: Re-Os systematics of sulfide inclusions from the Jagersfontein Mine. Contrib. Mineral. Petrol. (2009). https://doi.org/10.1007/s00410-008-0350-9
404. S. Aulbach, N.T. Arndt, Origin of high-Mg bimineralic eclogite xenoliths in kimberlite–reply to comment from Claude Herzberg. Earth Planet. Sci. Lett. (2019). https://doi.org/10.1016/j.epsl.2019.01.009
405. R. Haugaard, P. Waterton, L. Ootes, D.G. Pearson, Y. Luo, K. Konhauser, Detrital chromites reveal Slave craton's missing komatiite. Geology (2021). https://doi.org/10.1130/G48840.1
406. M. Branchetti, J.C.O. Zepper, S.T.J. Peters, J.M. Koornneef, G.R. Davies, Multi-stage garnet formation and destruction in Kimberley harzburgitic xenoliths, South Africa. Lithos (2021). https://doi.org/10.1016/j.lithos.2021.106119
407. J.H. Bédard, From the LIPS of a serial killer: endogenic retardation of biological evolution on unstable stagnant-lid planets. Planet. Space Sci. **192**, 105068 (2020). https://doi.org/10.1016/j.pss.2020.105068
408. M.J. Van Kranendonk, Two types of Archean continental crust: plume and plate tectonics on early Earth. Am J Sci. **310**, 1187–1209 (2010). https://doi.org/10.2475/10.2010.01
409. R. Fischer, T. Gerya, Early Earth plume-lid tectonics: a high-resolution 3D numerical modelling approach. J. Geodyn. **100**, 198–214 (2016). https://doi.org/10.1016/j.jog.2016.03.004
410. E. Sizova, T. Gerya, K. Stüwe, M. Brown, Generation of felsic crust in the Archean: a geodynamic modeling perspective. Precambrian Res. (2015). https://doi.org/10.1016/j.precamres.2015.10.005
411. J.M. Scott, J. Liu, D.G. Pearson, G.A. Harris, T.A. Czertowicz, S.J. Woodland, A.J.V. Riches, R.W. Luth, Continent stabilisation by lateral accretion of subduction zone-processed depleted mantle residues; insights from Zealandia. Earth Planet. Sci. Lett. (2019). https://doi.org/10.1016/j.epsl.2018.11.039
412. S.M. Aarons, J.R. Reimink, N.D. Greber, A.W. Heard, Z. Zhang, N. Dauphas, Titanium isotopes constrain a magmatic transition at the Hadean-Archean boundary in the Acasta Gneiss Complex. Sci. Adv. (2020). https://doi.org/10.1126/sciadv.abc9959

413. B.F. Windley, T. Kusky, A. Polat, Onset of plate tectonics by the Eoarchean. Precambrian Res. **352**, 105980 (2021). https://doi.org/10.1016/j.precamres.2020.105980
414. C.J. Hawkesworth, P.A. Cawood, B. Dhuime, The evolution of the continental crust and the onset of plate tectonics. Front. Earth Sci. (Lausanne). (2020). https://doi.org/10.3389/feart.2020.00326
415. S. Turner, T. Rushmer, M. Reagan, J.-F. Moyen, Heading down early on? Start of subduction on Earth. Geology **42**, 139–142 (2014). https://doi.org/10.1130/G34886.1
416. K.V. Smit, S.B. Shirey, S.H. Richardson, A.P. le Roex, J.J. Gurney, Re-Os isotopic composition of peridotitic sulphide inclusions in diamonds from Ellendale, Australia: age constraints on Kimberley cratonic lithosphere. Geochim. Cosmochim. Acta. (2010). https://doi.org/10.1016/j.gca.2010.03.001
417. J.M. Koornneef, M.U. Gress, I.L. Chinn, H.A. Jelsma, J.W. Harris, G.R. Davies, Archaean and Proterozoic diamond growth from contrasting styles of large-scale magmatism. Nat. Commun. (2017). https://doi.org/10.1038/s41467-017-00564-x
418. D.F. Wiggers de Vries, D.G. Pearson, G.P. Bulanova, A.P. Smelov, A.D. Pavlushin, G.R. Davies, Re–Os dating of sulphide inclusions zonally distributed in single Yakutian diamonds: evidence for multiple episodes of Proterozoic formation and protracted timescales of diamond growth. Geochim. Cosmochim. Acta. **120**, 363–394 (2013). https://doi.org/10.1016/j.gca.2013.06.035
419. S. Aulbach, R.A. Creaser, T. Stachel, L.M. Heaman, I.L. Chinn, J. Kong, Diamond ages from Victor (Superior Craton): intra-mantle cycling of volatiles (C, N, S) during supercontinent reorganisation. Earth Planet. Sci. Lett. (2018). https://doi.org/10.1016/j.epsl.2018.03.016
420. N.S.C. Simon, G.J. Irvine, G.R. Davies, D.G. Pearson, R.W. Carlson, The origin of garnet and clinopyroxene in "depleted" Kaapvaal peridotites. Lithos (2003). https://doi.org/10.1016/S0024-4937(03)00118-X
421. S.H. Richardson, S.B. Shirey, Continental mantle signature of Bushveld magmas and coeval diamonds. Nature **453**, 910–913 (2008). https://doi.org/10.1038/nature07073
422. K.V. Smit, T. Stachel, R.A. Creaser, R.B. Ickert, S.A. DuFrane, R.A. Stern, M. Seller, Origin of eclogite and pyroxenite xenoliths from the Victor kimberlite, Canada, and implications for Superior craton formation. Geochim. Cosmochim. Acta. (2014). https://doi.org/10.1016/j.gca.2013.10.019
423. A. Banas, T. Stachel, K. Muehlenbachs, T.E. McCandless, Diamonds from the Buffalo Head Hills, Alberta: formation in a non-conventional setting. Lithos (2007). https://doi.org/10.1016/j.lithos.2006.07.001
424. L. Hunt, T. Stachel, R. Morton, H. Grütter, R.A. Creaser, The Carolina kimberlite, Brazil—insights into an unconventional diamond deposit. Lithos (2009). https://doi.org/10.1016/j.lithos.2009.04.018
425. J. Czas, D.G. Pearson, T. Stachel, B.A. Kjarsgaard, G.H. Read, A Palaeoproterozoic diamond-bearing lithospheric mantle root beneath the Archean Sask Craton, Canada. Lithos (2020). https://doi.org/10.1016/j.lithos.2019.105301
426. R.J. Stern, M.I. Leybourne, T. Tsujimori, Kimberlites and the start of plate tectonics. Geology (2016). https://doi.org/10.1130/G38024.1
427. M. Brown, T. Johnson, N.J. Gardiner, Plate tectonics and the archean Earth. Annu. Rev. Earth Planet. Sci. (2020). https://doi.org/10.1146/annurev-earth-081619-052705
428. M.D. Schmitz, S.A. Bowring, M.J. de Wit, V. Gartz, Subduction and terrane collision stabilize the western Kaapvaal craton tectosphere 2.9 billion years ago. Earth Planet. Sci. Lett. (2004). https://doi.org/10.1016/j.epsl.2004.03.036
429. R.W. Carlson, D.G. Pearson, F.R. Boyd, S.B. Shirey, G. Irvine, A.H. Menzies, J.J. Gurney, Re–Os systematics of lithospheric peridotites: implications for lithosphere formation and preservation, in: Proceedings of the 7th International Kimberlite Conference, Cape Town: Red Roof Design, 1999: pp. 99–108.
430. S.H. Richardson, J.W. Harris, J.J. Gurney, Three generations of diamonds from old continental mantle. Nature **366**, 256–258 (1993). https://doi.org/10.1038/366256a0
431. H.H. Helmstaedt, D.J. Schulze, Evidence for subduction and spreading in the Archean rock record: implications for Archean tectonic style and the evolution of the subcontinental lithosphere, Workshop on the Archean Mantle. 42–42. (1989)
432. N.S.C. Simon, R.W. Carlson, D.G. Pearson, G.R. Davies, The origin and evolution of the Kaapvaal Cratonic Lithospheric Mantle. J. Petrol. (2007). https://doi.org/10.1093/petrology/egl074
433. S.H. Richardson, Latter-day origin of diamonds of eclogitic paragenesis. Nature (1986). https://doi.org/10.1038/322623a0

434. S.L. Hancock, R.W.R. Rutland, Tectonics of an early Proterozoic geosuture: the Halls Creek orogenic sub-province, northern Australia. J. Geodyn. **1**, 387–432 (1984). https://doi.org/10.1016/0264-3707(84)90017-6
435. S.S. Schmidberger, A. Simonetti, L.M. Heaman, R.A. Creaser, S. Whiteford, Lu-Hf, in-situ Sr and Pb isotope and trace element systematics for mantle eclogites from the Diavik diamond mine: evidence for Paleoproterozoic subduction beneath the Slave craton, Canada. Earth Planet. Sci. Lett. (2007). https://doi.org/10.1016/j.epsl.2006.11.020
436. P.F. Hoffman, A.W. Bally, A.R. Palmer, Precambrian geology and tectonic history of North America, in *The geology of North America—an overview*. (Geological Society of America, 1989), pp.447–512
437. P. Cartigny, M. Palot, E. Thomassot, J.W. Harris, Diamond formation: a stable isotope perspective. Annu. Rev. Earth Planet. Sci. (2014). https://doi.org/10.1146/annurev-earth-042711-105259
438. J.S. Ray, R. Ramesh, Rayleigh fractionation of stable isotopes from a multicomponent source. Geochim. Cosmochim. Acta. (2000). https://doi.org/10.1016/S0016-7037(99)00181-7
439. K.T. Koga, J.A. Van Orman, M.J. Walter, Diffusive relaxation of carbon and nitrogen isotope heterogeneity in diamond: a new thermochronometer. Phys. Earth Planet. Inter. (2003). https://doi.org/10.1016/S0031-9201(03)00141-9
440. K.T. Koga, M.J. Walter, E. Nakamura, K. Kobayashi, Carbon self-diffusion in a natural diamond. Phys. Rev. B Condens. Matter. Mater. Phys. (2005). https://doi.org/10.1103/PhysRevB.72.024108
441. B. Harte, T. Taniguchi, S. Chakraborty, Diffusion in diamond. II. High-pressure-temperature experiments. Mineral Mag. (2009). https://doi.org/10.1180/minmag.2009.073.2.201
442. P. Deines, The carbon isotope geochemistry of mantle xenoliths. Earth Sci. Rev. **58**, 247–278 (2002). https://doi.org/10.1016/S0012-8252(02)00064-8
443. P. Cartigny, B. Marty, Nitrogen isotopes and mantle geodynamics: the emergence of life and the atmosphere-crust-mantle connection. Elements (2013). https://doi.org/10.2113/gselements.9.5.359
444. W. Mao, S. Zhong, Slab stagnation due to a reduced viscosity layer beneath the mantle transition zone. Nat. Geosci. (2018). https://doi.org/10.1038/s41561-018-0225-2
445. H. Kárason, R.D. van der Hilst, *Constraints on mantle convection from seismic tomography* (American Geophysical Union, 2000), pp.277–288. https://doi.org/10.1029/GM121p0277
446. K.D. Litasov, E. Ohtani, Effect of water on the phase relations in Earth's mantle and deep water cycle. Spec. Pap. Geol. Soc. Am. (2007). https://doi.org/10.1130/2007.2421(08)
447. B. Harte, S. Richardson, Mineral inclusions in diamonds track the evolution of a Mesozoic subducted slab beneath West Gondwanaland. Gondwana Res. **21**, 236–245 (2012). https://doi.org/10.1016/j.gr.2011.07.001
448. V. Stagno, D.J. Frost, Carbon speciation in the asthenosphere: experimental measurements of the redox conditions at which carbonate-bearing melts coexist with graphite or diamond in peridotite assemblages. Earth Planet Sci. Lett. (2010). https://doi.org/10.1016/j.epsl.2010.09.038
449. T. Stachel, J. Harris, S. Aulbach, P. Deines, Kankan diamonds (Guinea) III: δ13C and nitrogen characteristics of deep diamonds. Contrib. Miner. Petrol. **142**, 465–475 (2002). https://doi.org/10.1007/s004100100297
450. P. Cartigny, Stable isotopes and the origin of diamond. Elements (2005). https://doi.org/10.2113/gselements.1.2.79
451. M. Palot, D.G. Pearson, T. Stachel, R.A. Stern, A. Le Pioufle, J.J. Gurney, J.W. Harris, The transition zone as a host for recycled volatiles: Evidence from nitrogen and carbon isotopes in ultra-deep diamonds from Monastery and Jagersfontein (South Africa). Chem. Geol. (2017). https://doi.org/10.1016/j.chemgeo.2017.07.023
452. D.A. Zedgenizov, H. Kagi, V.S. Shatsky, A.L. Ragozin, Local variations of carbon isotope composition in diamonds from São-Luis (Brazil): evidence for heterogenous carbon reservoir in sub-lithospheric mantle. Chem Geol. **363**, 114–124 (2014). https://doi.org/10.1016/j.chemgeo.2013.10.033
453. F. Nestola, P. Nimis, S. Milani, R. Angel, M. Bruno, J.W. Harris, Anonymous, Crystallographic relationships between diamond and its olivine inclusions; an update, Mineral Mag. **77.** (2013)
454. L. Pasqualetto, F. Nestola, D.E. Jacob, M.G. Pamato, B. Oliveira, S. Perritt, I. Chinn, P. Nimis, S. Milani, J.W. Harris, Protogenetic clinopyroxene inclusions in diamond and Nd diffusion modeling—implications for diamond dating. Geology (2022). https://doi.org/10.1130/G50273.1
455. R. Angel, S. Milani, M. Alvaro, F. Nestola, OrientXplot: a program to analyse and display relative crystal orientations. J. Appl. Crystallogr. **48**, 1330–1334 (2015). https://doi.org/10.1107/S160057671501167X

456. Z.D. Sharp, Nebular ingassing as a source of volatiles to the Terrestrial planets. Chem. Geol. (2017). https://doi.org/10.1016/j.chemgeo.2016.11.018
457. B. Marty, Origins and early evolution of the atmosphere and the oceans. Geochem. Perspect. (2020). https://doi.org/10.7185/GEOCHEMPERSP.9.2
458. C. Dalou, E. Füri, C. Deligny, L. Piani, M.-C. Caumon, M. Laumonier, J. Boulliung, M. Edén, Redox control on nitrogen isotope fractionation during planetary core formation. Proc. Natl. Acad. Sci. **116**, 14485–14494 (2019). https://doi.org/10.1073/pnas.1820719116
459. C.M.O. Alexander, R. Bowden, M.L. Fogel, K.T. Howard, C.D.K. Herd, L.R. Nittler, The provenances of asteroids, and their contributions to the volatile inventories of the terrestrial planets. Science **1979**(337), 721–723 (2012). https://doi.org/10.1126/science.1223474
460. J. Zazula, On Graphite Transformations at High Temperature and Pressure Induced By Absorption of the LHC Beam, Physics - LHC Project Notes. **78**, 1–14 (1997)
461. Z. Zhang, Diamond resorption morphology as a fluid proxy in diamond-bearing environments: constraints from empirical and experimental studies, Ph.D. Thesis, Dalhousie University. (2016)
462. A.F. Khokhryakov, Y.N. Palyanov, Diamond Dissolution Forms in Water-Containing and Water-Free Carbonate Melts, in: No. 91KC-A-00071, 9th International Kimberlite Conference Extended Abstract. (2008)
463. A.D. Kalugina, D.A. Zedgenizov, Micro-Raman spectroscopy assessment of chemical compounds of mantle clinopyroxenes. Minerals. **10**, 1084 (2020). https://doi.org/10.3390/min10121084
464. E.M. Smith, M.Y. Krebs, P.T. Genzel, F.E. Brenker, Raman identification of inclusions in diamond. Rev. Mineral. Geochem. (2023). https://doi.org/10.2138/rmg.2022.88.08